이학박사학위논문

Development of a high resolution GCM with cloud microphysics and its impact on simulation of tropical precipitation

구름물리과정을 도입한 고해상도 기후모형의 개발과 적도지역 강수 모의에 미치는 영향

2014년 2월

서울대학교 대학원

계산과학협동과정

양 영 민

Development of a high resolution GCM with cloud microphysics and its impact on simulation of tropical precipitation

구름물리과정을 도입한 고해상도 기후모형의 개발과 적도지역 강수 모의에 미치는 영향

지도교수 강 인 식

이 논문을 이학박사 학위논문으로 제출함

2014년 2월

서울대학교 대학원

계산과학협동과정

양 영 민

양영민의 이학박사 학위논문을 인준함

2013년 12월

위 원 장 _____ (인)

부위원장 _____ (인)

위 원 _____ (인)

위 원 _____ (인)

위 원 _____ (인)

Development of a high resolution GCM with cloud microphysics and its impact on simulation of tropical precipitation

구름물리과정을 도입한 고해상도 기후모형의 개발과 적도지역 강수 모의에 미치는 영향

지도교수 강 인 식

이 논문을 이학박사 학위논문으로 제출함

2014년 2월

양영민의 이학박사 학위논문을 인준함

2013년 12월

위 원 장 _____ (인)

부위원장 _____ (인)

위 원 _____ (인)

위 원 _____ (인)

위 원 _____ (인)

Abstract

Development of a high resolution GCM with cloud microphysics and its impact on simulation of tropical precipitation

Young-Min Yang
Program of Computational Science and Technology
The Graduate School
Seoul National University

A GCM with cloud microphysics was developed to improve simulated precipitation characteristics at an order of 50-km horizontal resolution. The GCMs with conventional parameterizations tend to produce too much light precipitation, resulting in less heavy precipitation and therefore weak precipitation amount and intra-seasonal variability over tropics. The convective trigger functions and a new mass flux closure were implemented in the convective parameterization to examine its impact on the frequency of precipitation. The results shows that both of them produce light precipitation less and heavy precipitation more than those of the GCM without trigger functions, indicating that the shift of the frequency toward light precipitation is partly result from too frequent deep convection.

A higher resolution GCM simulation without convective parameterization

indicates that the large-scale condensation, which produces grid-scale precipitation depending on relative humidity, is able to capture the large-scale pattern of observed precipitation with increasing the frequency of heavy precipitation. However, the model without convective scheme does not still simulate the extreme precipitation more than 200 mm day^{-1} due to too simple parameterization.

The budget study of rain processes using a cloud resolving model (CRM) shows that heavy precipitation is from not only accretion of cloud water by rain but also the melting of the graupel made from cloud water, whereas light precipitation is from accretion of cloud water by rain water. It is also important that warm and cold cloud processes coexist. However, these processes are not explicitly expressed in the conventional GCM.

In this study, cloud microphysics of the CRM was implemented in the GCM instead of the conventional parameterizations. The GCM simulations with cloud microphysics are not unrealistic and the model produces the extreme precipitation more than 200 mm day^{-1}, although the cloud microphysics may not work properly due to coarse horizontal resolution of the GCM. It is found that the GCM with modified microphysics, increase of condensation and decrease of terminal velocity, improves mean precipitation amount when compared to the GCM with original microphysics, particularly in the western Pacific and mid-

latitude. It is also suggested that the coarse resolution GCM with cloud microphysics need to an additional vertical mixing in order to reduce excessive cloud water amount in the boundary layer and producing realistic eastward propagation of the precipitation with organized convective system. In addition, the model developed in the present study is computationally much less expensive than those of the model with explicit full microphysics, which is called the 'super-parameterization' (Grabowski 2004), because the model does not embeds the CRMs in each grid box of the GCM but explicitly express the CRM physics with GCM state variables.

Keywords

Climate modeling, heavy precipitation, convective scheme, cloud microphysics, cloud resolving model

Student number: 2006-30794

Contents

List of figures

CHAPTER 1

Introduction

A general circulation model (GCM) are useful tool for quantifying and understanding changes in climate. Extreme precipitation events which cause severe sociological, ecological, and economic damages in the region of event (Easterling et al. 2000, USGS 2006), are important phenomena that GCMs are used to study. However, many studies have been reported that the conventional GCMs overestimate frequency of light precipitation and underestimates the frequency of heavy precipitation (Dai 2006, Sun et al. 2006, Lin et al. 2013, DeAngelis et al. 2013). These biases of precipitation frequency are also related to poor parameterization of deep convection (Wilcox and Donner 2007, DeMott et al. 2007, Lin et al 2013, Lorant et al . 2006) and it is also linked to weak intra-seasonal variability (Lee et al. 2003, Lee et al. 2001, Lin et al. 2013).

An important reason for the shift of precipitation frequency toward light precipitation is poor representations of moist physical processes in convectional

GCMs. Many studies suggested that the frequency of heavy precipitation is dependent on the mass flux closure in the convective parameterization (Pan and Randall 1998; Khairoutdinov and Randall 2003; Lin et al. 2000; Scinocca and McFarlane 2004; Lorant et al. 2006). The mass flux closure using convective available potential energy (CAPE), which is popularly used in the Arakawa-Schubert (AS) type convective parameterizations tends to produce too frequent deep convection because the AS scheme sensitively responds to the CAPE that has almost positive values (Pan and Randall 1998, Lin et al. 2008, Xie et al. 2004). Lorant et al. (2006) showed that a prognostic closure produces more intense convective precipitation than that of a closure using the CAPE closure, but the frequency of total precipitation is not much improved because the changes in the frequency of convective precipitation are offset by opposite changes in the frequency of large-scale condensation. This study indicates that in the convectional GCM framework, which has two precipitation processes of sub-grid scale convection (represented by a convective parameterization) and grid scale condensation (represented by the large-scale condensation), the improvement of convective parameterization may have a limited impact to the frequency of total precipitation. On the other hand, it is also well known that arbitrary setting of cloud tops in ensemble cloud parameterization produces deep convective clouds too much frequently, resulting in less accumulation of convective instability, and

therefore light precipitation more but heavy precipitation less than the observed. To remedy this problem, several triggering mechanisms, such as the Tokioka trigger (Tokioka 1988, Lee et al. 2001, Lee et al. 2003) and threshold relative humidity (Wang and Schlesinger 1999), were introduced in the convective parameterizations. Also several studies demonstrated that the entrainment and detrainment formula play an important role for proper simulation of precipitation amount and distribution (Kim and Kang 2012; Gregory 2001). This trigger functions also produce stronger intra-seasonal variability than those of the GCM without trigger functions. However, the parameter of trigger function and entrainment (detrainment) formula is uncertain and the improvement by them is generally accompanied by worsened mean state bias in many GCMs (Kim et al. 2011, Mapes and Neale 2011).

Several studies showed that an increase of horizontal resolution improves the frequency of heavy precipitation by increasing vertical motion, which contributes to increase of heavy precipitation and precipitation amount. Chen and Knutson (2008) and Wehner (2008) showed that low horizontal resolution GCMs with an order of 100km grid size cannot simulate severely heavy precipitation. Boyle and Klein (2010) showed that increases in resolution yield more realistic spatial patterns and probability distributions of precipitation over most continental regions. Oouchi (2006) and Mizuta et. al. (2006) found that

global average of precipitation increases with the horizontal resolution increasing. Mechoso (2006) found the south ITCZ which is penetrated to the eastern Pacific is reduced at higher resolution atmospheric model. On the other hand, Li et al. (2011b) showed in ideal experiments that when a horizontal resolution of a GCM is larger than T170, the frequency of heavy precipitation does not increase. Iorio et al. (2004) found that the GCM with T239 horizontal resolution still underestimates the frequency of heavy precipitation. These results suggested that an increase of horizontal resolution also has a limitation for improvement of the frequency of parameterization. Li et al. (2011b) also argued that the scale separation between convective and large-scale precipitation in a conventional parameterization may be less accurate in high resolution simulations because some of convective cloud can be resolved in a high-resolution model. In order to avoid this scale-separation problem, Knutson and Tuleya (2004) introduced a high resolution GCM without convective parameterization. The model produces not only more precipitation amount but also more heavy precipitation than that of the GCM with conventional parameterization. It is noted that the GCM without convective scheme does not blow up and the results are similar to those of the GCM with Manabe moist convective scheme (Frierson 2007). Lin et al (2008) demonstrated that the GCM without convective scheme produces better signals of intra-seasonal variability than the GCM with convective scheme. These results

shows that the GCM with grid-scale precipitation produce reasonable the frequency of heavy precipitation and intras-seasonal variability. However, the parameters in the large-scale condensation is uncertain, and the model without convective scheme still does not produce extreme precipitation (> 200 mm day^{-1}).

A promising approach to improve frequency of heavy precipitation in a GCM may be explicitly representing the moist physical processes of cloud and rain. Global-scale simulations with explicit full cloud microphysics have been performed in the several studies. One approach is to replace a conventional moist parameterization with a finer horizontal resolution CRM in a GCM. Grabowski (2001) developed the GCM that includes a two-dimensional cloud resolving model (CRM) in place of a conventional parameterization, called multi-scale modeling framework (MMF). The GCM simulations using the MMF showed that the models improve the MJO simulation (Benedict and Randall 2009, Zhu et al. 2009)and the frequency of heavy precipitation (Iorio et al, 2004, DeMott et al 2007, Li et al, 2012) when compared to those of the GCM with a conventional parameterization. Although, the MMF has an explicit representation for moist processes, it has a limitation: there is no interaction between clouds represented by embedded CRM and the adjacent GCM grids. The other approach is to extend a CRM to a global scale. Satoh et al. (2005) conducted a 3.5-km resolution global simulation using the nonhydrostatic icosahedral atmospheric model. The model

successfully reproduces the eastward propagation of the observed MJO (Miura et al. 2007, Liu et al 2009) and typhoon genesis (Oouchi et al. 2009). However, these approach is computationally two or three order of magnitude more expensive than that of a convectional GCM. It is known that the MMF method has intrinsic problems, particularly the cyclic cloud condition within the gird box and no interaction between the clouds in adjacent GCM grids, by embedding the CRM in each grid box.

This study is aimed to develop the GCM with cloud microphysics at an order of 50 km horizontal resolution in order to improve simulated precipitation and reduce computational time. Cloud microphysics is directly implemented in a GCM instead of convective parameterization and large-scale condensation. However, this model has limitations of expressing the CRM processes in a reasonable way due to coarse horizontal resolution. Two main problems are suggested: One is poor representation of cloud microphysics and the other is relatively weak vertical mixing. Many studies demonstrated that cloud microphysics has resolution dependency, particularly at an order of 10km horizontal resolution (Weisman et al. 1997, Yu and Lee 2010, Bryan and Morrison 2012, Arakawa et al. 2011, Bryan et al. 2003, Deng and Stauffer 2006, Pauluis and Garner 2006, Jung and Arakawa 2004). Jung and Arakawa (2004) showed that a lower horizontal resolution CRM produces sub-grid scale turbulence heating

more and microphysical heating less than those of the 1-km horizontal resolution CRM. Pauluis and Garner (2006) showed using CRM simulations with radiative-convective equilibrium (RCE) experiments that the 50-km horizontal resolution CRM has produces less moisture and condensation than those of 1-km horizontal resolution CRM. These results show that the CRM has resolution dependency in microphysical processes and vertical motion, which indicates that modification of cloud microphysics is essential for reducing the resolution dependency of cloud microphysics.

There are several studies to alleviate the resolution dependency of cloud microphysics at the lower horizontal resolution. One of important deficiencies in a coarse resolution CRM is relatively weak vertical motion. In order to increase vertical velocity of a coarse resolution CRM, Pauluis and Garner (2006) derived a formula which is defined as a function of the grid size based on the behavior of an idealized cloud. The lower horizontal resolution CRM with this formula produces probability distribution for vertical velocity closer that of the 1-km CRM. Deng and Stauffer (2006) showed that lower horizontal resolution CRM simulation is improved by increasing vertical mixing in the turbulence scheme. However, an order of 50km grid size, these modifications have a limited impact for reducing the resolution dependency of microphysics. On the other hand, Moncrieff and Liu (2006) improves the simulation of organized convection using

a regional model with cloud microphysics by adding a conventional convective parameterization. Moncrieff and Liu (2006) found that cloud microphysics produces realistic precipitation through enhancing vertical transport of moisture, moist static energy and momentum at lower resolution regional models. These results indicates that proper sub-grid scale vertical mixing may be required for a good simulation of cloud microphysics at coarse resolution. On the other hand, the modification of cloud microphysics adapted for lower horizontal resolution CRM have been hardly studied. Instead, we can obtain the hind for modification of cloud microphysics at coarse resolution from the GCM studies. Several studies developed the climate model with simplified microphysics (Salzmann et al 2010, Morrison et al 2005, Phillips et al 2008, Zhang and Lohmann 2005, Fowler et al 1996). The one of important modification of microphysics is condensation processes. Because the saturation occurs hardly at coarse resolution, sub-grid scale variability of specific humidity or supersaturation with relaxation time scale were used (Fowler et al 1996, Morrison et al 2005) to increase condensation amount. In the present study, not only modification of condensation but also modification of accretion and other processes will be examined to find which processes are domain for resolution dependency. Also, the effect of subgrid-scale vertical mixing will be examined by using various type of convective scheme for better simulation of the GCM with microphysics at an order of 50km horizontal

resolution.

In this study, a GCM with cloud microphysics was developed to improve simulated precipitation at an order of 50 km horizontal resolution. The CRM simulations with the RCE experiments were intensively analyzed in order to find the resolution dependency in the dominant microphysical processes and to reduce the resolution dependency by various modification of cloud microphysical processes. The CRM simulations were intensively analyzed in order to investigate dominant processes of cloud microphysics for heavy precipitation. The GCM simulations with cloud microphysics were compared to those of the GCM with a conventional parameterization. Chapter 2 describes the utilized models and their simulations. Chapter 3 examined the effect of trigger function and mass flux closure in a GCM with conventional parameterization. Chapter 4 examined the effect of increasing horizontal resolution on simulate precipitation. In the Chapter 5, the resolution dependency of cloud microphysics and the effect of modified cloud microphysics was examined using the CRM. In addition, Section 6 presents the impact of cloud microphysics on the simulated precipitation characteristics. The summary and future direction are given in Section 5.

CHAPTER 2

Models

2.1 Cloud resolving model

In order to examine the resolution dependency of cloud microphysics and implement cloud microphysics in a GCM, a CRM is used in this study. The CRM adapted is the Goddard Cumulus Ensemble Model developed at the National Aeronautic Space Administration/Goddard Space Flight Center (Tao et al. 1993). The CRM includes a dynamical core, microphysics, radiation, surface flux and sub-grid turbulence scheme. It uses the compressible equations (Klemp and Wilhelmson, 1978) with periodic lateral boundary conditions. The cloud microphysics includes the Kessler-type two-category liquid water scheme and the three-category ice-phase scheme, developed mainly by Lin et al. (1983). In this study, a two-dimensional version of the model is used, where the domain size is 512 km in the x-axis and the horizontal grid size is 1 km. The vertical resolution is about 80 m near the surface and gradually increases with height up to about

700 m near the 10 km level.

The CRM was integrated from 28 November 1992 to 31 January 1993, which is the duration of the Tropical Ocean and Global Atmosphere-Coupled Ocean–Atmosphere Response Experiment (TOGA-COARE, Webster and Lukas 1992). The initial condition and forcing data are obtained from the Global Energy and Water Cycle Experiment Cloud System Study, which represents an averaged flux of the TOGA-COARE (Ciesielski et al. 2003). Convective scheme is added to increase of vertical mixing in a GCM. The ideal radiative-convective equilibrium (RCE) experiments were performed to investigate resolution dependency of cloud microphysics based on Pauluis and Garmer (2006). In this experiment, a constant surface temperature of 301.5 K is used and the tropospheric cooling is determined from an idealized cooling profile instead of explicit radiative transfer calculation. The cooling rate is -1.5 K day $^{-1}$. It is noted that the RCE experiment does not account for the interactions between cloud and radiation, which play an important role both for the behavior of convective systems. However, this study focused on the interaction between dynamics and thermodynamics in order to clearly identify resolution dependency of cloud microphysics. An investigation of the sensitivity of the cloud radiative feedbacks to horizontal resolution is left to a future study. The RCE experiments were performed for horizontal resolution of 1, 10 and 50km. The 1-km simulation is used as a control run. The CRMs was

integrated for two months and all analysis are performed on last one month of the simulation, because it takes about a month for the CRM with the RCE experiment to reach equilibrium state

2.2 Atmospheric General Circulation Model

The atmospheric general circulation model (AGCM) used in this study is a Seoul National University AGCM (SNUAGCM). It has 20 sigma levels in the vertical, and T42 truncation is used horizontally. The cumulus parameterization is based on the Relaxed Arakawa-Schubert scheme (Moorthi and Suarez, 1992), and it includes downdrafts due to the evaporation of precipitating water. Cumulus cloudiness and cumulus cloud water are simply estimated as a function of cumulus updraft mass flux. Cumulus cloudiness is assumed to be uniform in the vertical. The scheme is modified following Tokioka et al. [1988] for the improvement of tropical ISO simulation in the model. The large-scale condensation scheme is based on Le Treut and Li (1991). This scheme converts the relative humidity exceeding 75% to precipitation with a certain relaxation time scale (3600 seconds). Shallow convection is the diffusion-type of shallow convection scheme suggested by the Tiedtke (1984). This scheme does not produce precipitation and it is turned off when a deep convection occurs. The boundary layer scheme is a nonlocal diffusion scheme of Holtslag and Boville (1993). Radiation processes are parameterized by the two-stream k-distribution scheme implemented by Nakajima et al. (1995). The land surface processes use

the land surface model (Bonan, 1996) developed at the National Center for Atmospheric Research (NCAR). A detailed model description of physical parameterizations in the original model can be found in Lee et al. (2001).

The cloud microphysics of the GCE was directly implemented in the SNUAGCM instead of the conventional parameterization (convective and large-scale condensation parameterization). The GCM has a 50-km horizontal resolution and 20 vertical levels. All cloud hydrometeor (three ice-phase and two warm-phase cloud hydrometeor) are treated as prognostic variables. Because clo ud microphysics requires relatively very small time step (a few seconds) when c ompared to that of a GCM (20-30 minutes), we use sub-time step (300 s) for clou d microphysics. This value is determined by considering both computation reso urces and performance of simulated cloud hydrometeor, although it is relatively larger than that of the CRM. The sensitivity of sub-time step on simulated hydrometeor was examined in the GCM. The various sub-time step are used in the experiments. The details will be discussed in the Chapter 6. The temperature and moisture are updated at every sub cycling and winds are assumed not to be changed during calculating cloud microphysics. In a GCM, fractional cloud cover is generally used due to a large grid size. However, in the CRM, fractional cloud cover is not valid due to small grid size. At the target resolution, It is not sure whether fractional cloud cover concept is appropriate or not. We examined

sensitivity of parameterization of fractional cloud cover on simulated precipitation and cloud microphysics in the Chapter 6. The cloud fraction and cloud water were parameterized on the basis of Le Treut and Li (1991), the calculated variables were used for radiative processes. It is also assumed that other cloud hydrometeors (rain water and graupel) do not affect radiative processes because of poor parameterization of radiative processes. It is noted that correction of excessive precipitation over steep and high mountain areas was added in a GCM (Chao 2012).

CHAPTER 3

Improvement of a convective parameterization

3.1 Description of convective scheme

3.1.1 Cloud model

In this section, we reviewed the convective scheme in the SNU AGCM. The Arakawa-Schubert type of convective parameterization is used in the present study, which is popularly used in the climate model. From this review, we will aim to find out the limitation of the convective parameterization. First, updraft cloud mass flux (M) in cloud is defined as entrainment (E) and detrainment (D) when source or sink term is zero.

$$\frac{\partial M(z)}{\partial z} = E(z) - D(z) \tag{3.1}$$

where, z refers to the height. In order to reduce unknown variables, it is assumed that vertical structure of M, E, D are represented as normalized form (η).

Therefore, unknown variable is diluted updraft mass flux at cloud-base level ($M_B(\lambda)$), where λ refers to the entrainment rate, which controls the cloud structure. It is assumed that entrainment occurs at all vertical level but detrainment occurs only at cloud top. The cloud affects moist static energy (h) and specific humidity (q) of environments by detrainment and updraft mass flux.

$$\frac{\partial \bar{h}}{\partial t} = M\frac{\partial \bar{h}}{\partial z} + D\left(h^t - \bar{h}\right) \tag{3.2}$$

$$\frac{\partial \bar{q}}{\partial t} = M\frac{\partial \bar{q}}{\partial z} + D(q^t + l^t - \bar{q}) \tag{3.3}$$

where, overbar $\left(\bar{}\right)$ and superscritps (^{t}) refer to the grid-mean and cloud top value, respectively. l means liquid water content. The mass flux is the sum of those from individual cloud.

$$\mathrm{M(z)} = \sum_i M_B^i \eta^i(Z) \tag{3.4}$$

In order to determine cloud-base level, the convective scheme uses the lifting condensation level (LCL).

3.1.2 Entrainment

The convective scheme uses cloud-ensemble concept. It assumes that there exist various type of clouds with differently specified cloud tops in a grid box of

a GCM. In this model, cloud top occurs for all vertical level above cloud-base level. Therefore, entrainment rate is determined by the specified cloud top in order to produce all type of cloud. The entrainment rate is defined as vertical change of normalized mass flux and is expressed as

$$\frac{\partial \eta}{\partial z} = \lambda \ (z > z_B) \tag{3.5}$$

where, z_B refers to the height of cloud-base level. Entrainment determines vertical profile of each cloud ensemble and it reduces the buoyancy of cloud (B) by mixing with relatively cold and dry environments. Because the detrainment is assumed as existing at cloud top, we can obtain the entrainment rate from the equation, $B(z_{top}) = 0$. The observation or CRM studies show that entrainment rate is determined by buoyancy of cloud and cloud top is calculated by entrainment rate and the buoyancy (Khairoutdinov and Randall 2001, Khairoutdinov and Randall 2003). When the buoyancy has a relatively large value at cloud-base level, the convective velocity is increased, resulting in less mixing with environment (small entrainment rate) and therefore deep convection occurs. However, the model assumes arbitrarily cloud top and entrainment rate is adjusted to the specified cloud top. Therefore, when the buoyancy is small, the model produces deep convection, which tends to have weak precipitation due to small mass flux. It contributes to production of too much light precipitation.

3.1.3 Mass flux closure

In order to calculate M(z), cloud-base mass flux should be determined using mass flux closure. It is assumed that convection is started from near surface and initiated by turbulent eddy in the planetary boundary layer (PBL), which is produced by large-scale forcing. Also, it is assumed that convective instability produced by large-scale forcing is balanced with stabilization by cumulus convection (quasi-equilibrium, Arakawa and Schubert 1974). The mass flux closure in the convective scheme is based on the method suggested by Lee et al (2003). The closure assumes that cumulus mass fluxes relax the cloud work functions toward neutral stability with a specified adjustment time scale. Specifically, a perturbed cloud work function A′ is computed in response to a small trial mass flux M_0, and then the appropriate amount of cloud-base mass flux is calculated as

$$M_B = M_0 \frac{A}{A - A'} \frac{\Delta t}{\tau} \tag{3.6}$$

where M_B is cloud-base mass flux, Δt is the time step of the model, A is cloud work function (diluted CAPE) and τ adjustment time scale. In the scheme, M_B is dependent on A because Mo is constant parameter and the variability of A′ is relatively small when compared to those of A. The mass flux closure is strongly dependent on the convective instability. In fact, due to the quasi-equilibrium

assumption, convection tends to occurs too frequently to remove convective instability, resulting in less accumulation of convectively instability and therefore light precipitation much more than the observation.

3.2 Modification of convective parameterization

3.2.1 Convective trigger functions

It is known that an Arakawa-Schubert type of convective scheme (AS) tends to produce too much light precipitation because it sensitively responds the convective instability (Dai 2006). This results in less heavy precipitation and therefore weak precipitation amount. Too frequent deep convection also disturbs eastward propagation of the precipitation near the equator. Therefore, proper suppression of convection is required for a good simulation of precipitation. With a GCM, Tokioka et al. (1988) implemented the convective trigger (TOK) in addition to the Convective Available Potential Energy (CAPE) closure, by introducing a minimum entrainment rate which is inversely proportional to the PBL depth. The TOK controls the cloud-base mass flux by removing undiluted deep cumulus updrafts when the PBL depth is relatively shallow. Therefore, the TOK can be considered as one way of determining the cloud-base mass flux by considering the PBL thermal condition. Several recent studies demonstrated that

the TOK improves the tropical precipitation and its intra-seasonal variability (Lee et al. 2001, Lee et al. 2003 and Lin et al. 2008). Following Tokioka et al. (1988), an additional trigger function was added to the standard simplified AS scheme (SAS), which constrains the entrainment rate of convective plumes (μ) as

$$\mu_{min} = -\frac{\alpha}{D} \tag{3.7}$$

where D is the depth of the planetary boundary layer and α is a nonnegative constant. Only convective plumes of $\mu \geq \mu_{min}$ are triggered in the cumulus ensemble. We used the value of constant α, 0.05. On the other hand, AS type of convective schemes tend to produce convection frequently at dry condition because it do not consider in-cloud humidity. In order to apply moisture criteria to the AS type of convective scheme, Wang and Schlesinger (1999) used the relative humidity criteria, which turns convection on when the relative humidity of cloud exceeds 80%.

3.2.2 Mass flux closure

Precipitation simulated by a general circulation model (GCM) is strongly dependent on a deep convective parameterization. A mass flux scheme is popularly used for the convective parameterization because it provides internally consistent treatments in cloud fraction, mass flux, cloud water and moist static energy. In this scheme, a cloud-base mass flux should be parameterized as a

boundary condition of the vertical structure of cloud mass flux, called a mass flux closure. Many previous studies have developed various types of mass flux closures, and found that the simulated precipitation is quite sensitive to a mass flux closure (Neggers et al. 2004, Lorant et al. 2006). One of the most widely used mass flux closures, particularly in the Arakawa-Schubert (AS) type convective parameterizations, is based on the convective available potential energy (CAPE, Arakawa and Schubert 1974, Moorthi and Suarez 1992, Pan and Randall 1998). The CAPE is defined as the vertical integration of buoyancy from cloud base to cloud top. Moorthi and Suarez (1992) and others determined the closure in terms of the rate of change of the CAPE by assuming the quasi-equilibrium between convection and the large-scale variables. However, observational studies showed that cloud-base mass flux and rainfall poorly correlate with the CAPE (Mapes and Houze 1992, Neggers et al. 2004, Xie and Zhang 2000). In particular, Neggers et al. (2004) revealed that the CAPE closure (Zhang and Mcfarlane type of mass flux closure, 1995) incorrectly estimates cloud-base mass flux in the early and final stages of convection, and the cloud-base mass flux is more controlled by the planetary boundary layer (PBL) processes. In this section, we examine the relationships between the cloud-base mass flux and various PBL properties by using the CRM simulations, and formulate the cloud mass flux closure as a function of the GRN. Before examining these relationships, the CRM simulated

precipitation is compared to the observations during the TOGA-COARE period. Figure 3.1 shows the time series of the 6-hour mean observation of TOGA-COARE (bar) and that of the simulated precipitation (blue line). The two periods are shown separately for early December (Fig. 3.1a), the period with gradually increasing precipitation, and the latter part of January (Fig. 3.1b), the period with active precipitation. The CRM simulates the observed weak precipitation for early December and heavy precipitation events in January. In general, the model simulates the temporal variation of observed precipitation reasonably well, although it tends to simulate the precipitation amount slightly more than the observed for most of the periods. Now, using the CRM simulated data, we examine how the precipitation is related to the cloud-base mass flux. Figure 3.2 shows the scatter plot of 1-hour mean simulated precipitation and cloud-base mass flux. As in Fletcher and Bretherton (2010), the cloud base level is defined as the lifting condensation level (LCL) of a surface parcel (which is at the 3-10 vertical levels (200~1000 m) above the surface in the present CRM), where the cloud water exists and the cloud vertical velocity is positive. The results show that the precipitation is closely related to the cloud-base mass flux, as their correlation coefficient is 0.65. It indicates that a realistic expression of the cloud-base mass flux, which is the closure of cloud mass flux parameterizations, is essential for a good simulation of precipitation with a GCM.

We examined the relationship between the cloud-base mass flux and the CAPE. The CAPE is obtained by integrating vertically the positive buoyancy of cloud from the cloud base to the top. The positive buoyancy is defined as the buoyancy at the level where cloud temperature is larger than environment temperature. As in Fletcher and Bretherton (2010), the domain mean temperature is assumed to represent the environment temperature due to small domain size (512km), and the cloud temperature is directly obtained from the CRM simulation. As seen in Fig. 3.3, the cloud-base mass flux has no relationship with the CAPE (Fig. 3.3a), indicating that the closure of the original AS convection scheme should be replaced by some other formula. The relationship between the cloud-base mass flux and the mixed layer Richardson number (MRN) was also examined. The MRN is defined as the bulk Richardson number calculated using the mean variables of the vertical levels between 0.3 and 0.7 of the PBL depth, as in Ridout and Reynolds (1998). Figure 3.3b shows that the cloud-base mass flux is also poorly correlated with the MRN, which has a low correlation coefficient of 0.1.

In this study, we use the gradient Richardson number for better representing the PBL thermal properties. Following Holtslag and Boville (1993), the gradient Richardson number is calculated using the formula:

$$R_i = -\frac{g(\theta_i - \theta_1)(z_i - z_1)}{\theta_i[(u_i - u_1)^2 + (v_i - v_1)^2]}, i = 2,3,4 \dots \text{n} \tag{3.8}$$

where R_i refers to the gradient Richardson number at the ith vertical level, n the level of the PBL top, $\theta_i$the virtual potential temperature at the ith level, g the gra vity, z_i the height at the ith level, u_i the zonal wind at ith level, and v_i the meridional wind at ith level. All variables used for the Ri are horizontally averaged values. As in Moeng and Arakawa (2012), the PBL top is defined as the height where the vertical gradient of potential temperature is positive and largest or where the water mixing ratio decreases fastestly below a height of 2 km. It is generally at the 5-10 vertical level (400~1000 m) above the surface in the CRM simulations. Here in Eq. (3.8), the R_i is calculated from the second vertical level to the PBL top.

We examined the mean vertical profile of the R_i in the PBL by using the CRM simulations. In fact, the R_i values very much depend on the vertical level and the mid-level R_i does not represent the PBL mean of the R_i. Also, the relationship between the cloud-base mass flux and the R_i is worst when the R_i is chosen with the mid-level value (300-600m) (not shown). These results show that the MRN, which is calculated by using variables at the mid-level, has a poor relationship with the cloud-base mass flux. As an alternative parameter, the mean gradient Richardson number (GRN), which is defined as the vertically averaged gradient Richardson number in the PBL, is examined here. The formula of the GRN is:

$$\mathrm{GRN} = \sum_{i=2}^{n} (R_i \Delta P_i) \Big/ \sum_{i=2}^{n} (\Delta P_i) \tag{3.9}$$

where R_i is the gradient Richardson number at the *i*th vertical level defined by Eq. (3.8), *n* the level of PBL top, P_i the pressure at the *i*th vertical level. Fig. 3.3c, which shows the relationship between the cloud-base mass flux and the GRN, clearly demonstrates that the cloud-base mass flux is related to the GRN and the cloud-base mass flux appears to be an exponential function of the GRN. The formula of the mass flux closure can be best expressed as

$$M_b = C_1 \exp(C_2 GRN) \tag{3.10}$$

where M_b denotes the cloud-base mass flux. C_1 = 10^{-4} and C_2 = 1.09 are the constants, obtained by the least square method. The best-fit curve (dotted red line) is shown in Figure 3.3a. The correlation coefficient between the fitted curve and the scattered data is relatively high (0.71). For the GRN larger than 5.5, the value of cloud-base mass flux is scattered and is not represented by the exponential curve. Therefore, for the GRN larger than 5.5, the cloud-base mass flux is set to the constant value (M_b = 0.05 m s^{-1}), which is the value of the fitted curve at GRN=5.5. The Eq. 3.10 will be used as the mass flux closure in the GCM convective parameterization and is referred to as the 'GRN closure'. Because of the exponential function adapted, the cloud-base mass flux is almost zero when the GRN has a relatively small value.

The horizontal distributions of the observed precipitation (shading) and the GRN (contour) for boreal summer are shown in Fig. 3.4. The ERA Interim reanalysis data (Dee et al, 2011) was used to calculate the GRN and the Tropical Rainfall Measuring Mission (TRMM, Huffman et al. 2007) was used for precipitation. In most of the heavy precipitation regions (particularly, the Western Pacific, ITCZ, and equatorial Indian Ocean), the GRN values are also large. One exception appears in the Bay of Bengal, where the GRN has a small value. In this region, the heavy precipitation is not simply controlled by the local PBL properties but more controlled by the meridional heating contrast between Eurasian continent and Indian Ocean (Chou 2003). Although the GRN also has large values in the north and south eastern Pacific, convective precipitation does not occur because of large-scale sinking motion there. The observational studies showed that precipitation is related to relative humidity and a dry atmospheric condition inhibits an organized convection (Brown and Zhang 1997, Holloway and Neelin 2009). It may be interesting to examine the relationship between the GRN and the relative humidity in the PBL by using the CRM simulations. In fact, Figure 3.5 shows that the GRN is related to the relative humidity in the PBL, although the GRN is not a function of relative humidity, indicating that the PBL humidity information is implicitly included in the GRN closure.

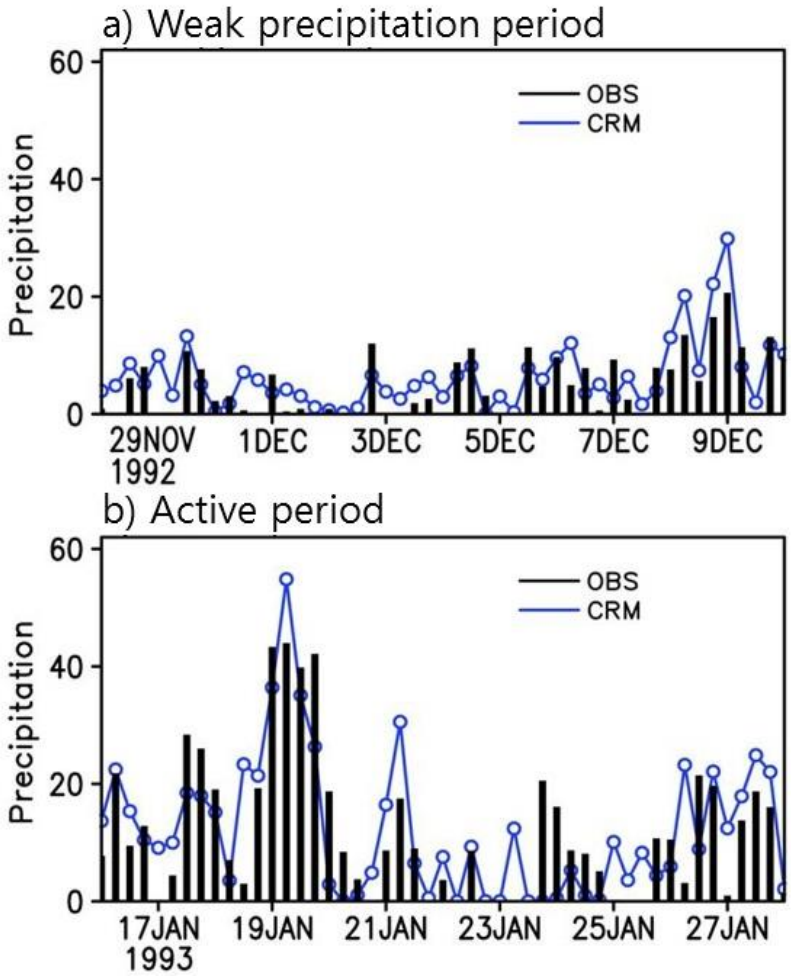

Fig. 3.1. 6-hour mean precipitation (mm day^{-1}) produced by CRM (blue line) and observation (black bar). (a) Weak precipitation period and (b) active period.

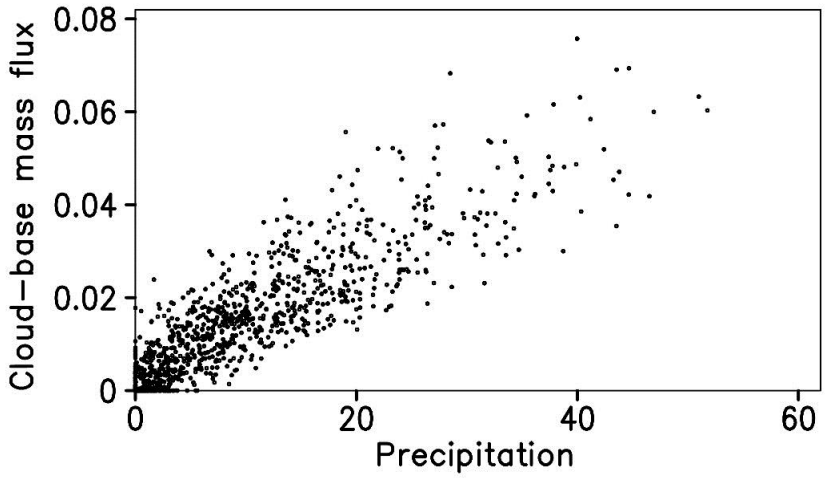

Fig. 3.2. Scatter plots of 1-hour mean cloud-base mass flux (kg m^{-2} s^{-1}) against precipitation (mm day^{-1}) in the CRM simulations.

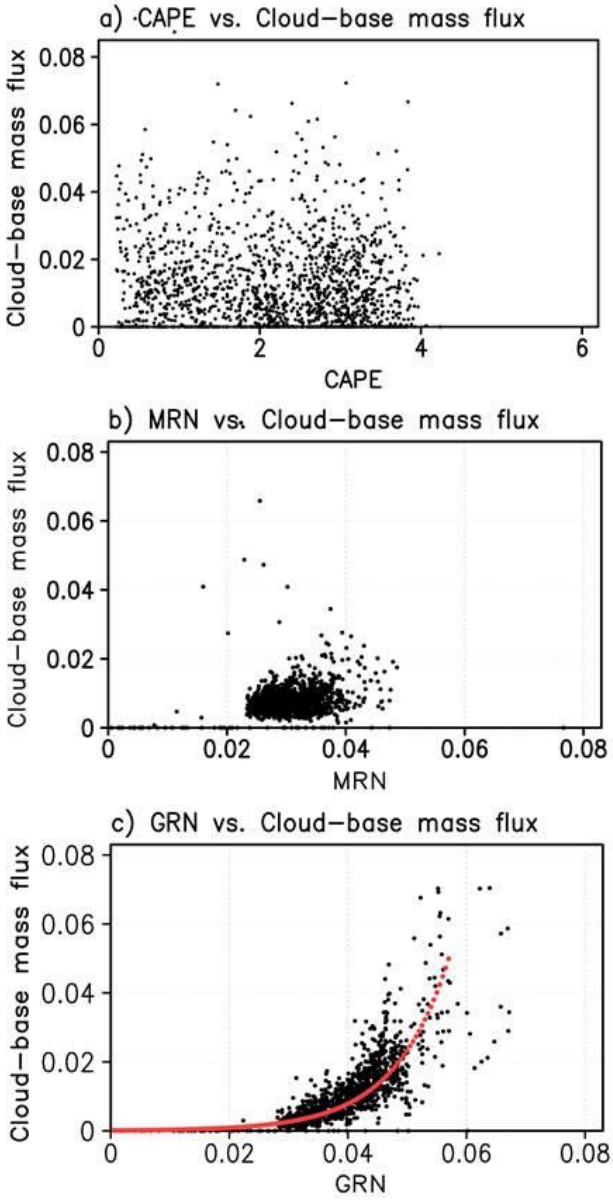

Fig. 3.3. Scatter plots of cloud-base mass flux (kg m^{-2} s^{-1}) against (a) the CAPE (kJ kg^{-1}), (b) the mixed layer Richardson number and (c) the mean gradient Richardson number. The function, best fitted curve to the data in (c), is represented by a dotted red line.

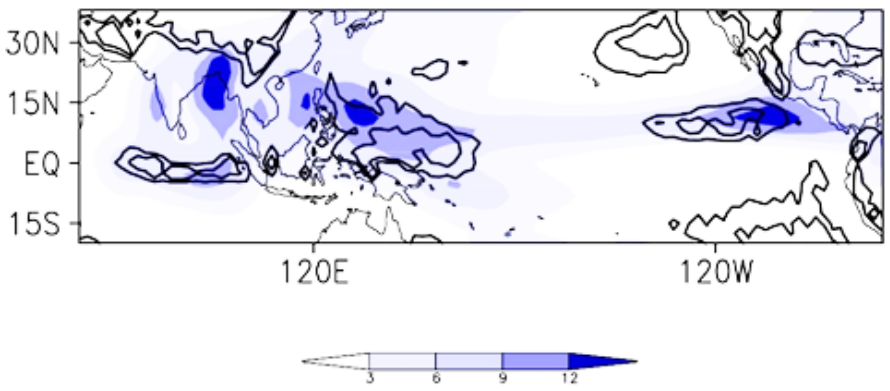

Fig. 3.4. Spatial distribution of the mean gradient Richardson number (GRN, contour) and precipitation climatology (mm day^{-1}, shading) for 10 year boreal summer. The ERA Interim data is used for the GRN and the TRMM data is used for precipitation. The TRMM and the ERA Interim data are from 1998 to 2007. Contour interval of the GRN is 2.

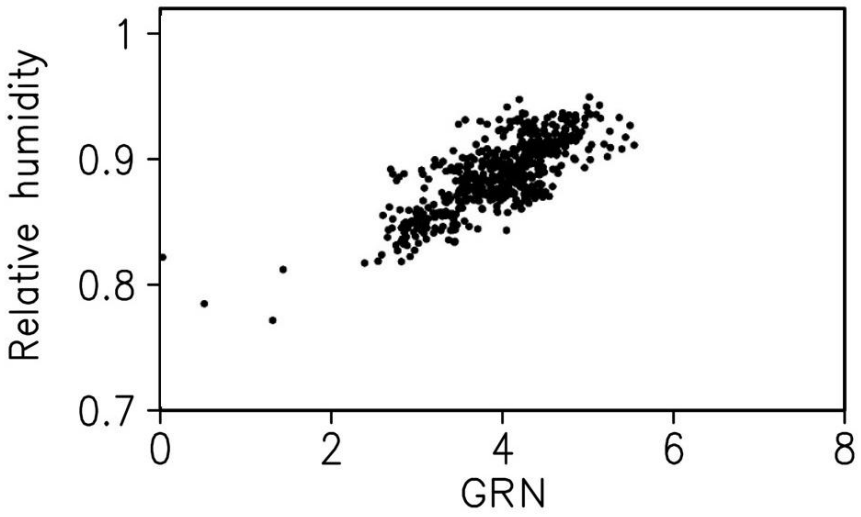

Fig. 3.5. Scatter plots of relative humidity against the mean gradient Richardson number in the CRM simulations

3.3 GCM simulation with modified parameterization

In this section, the effects of the modified convective parameterizations on the simulated precipitation are examined using the SNUGCM. As mentioned in previous section, the original SNUGCM will be referred to as the model of control run (CTL). On the other hand, the GCM with the Tokioka constraint will be referred to as the 'TOK', the GCM with the relative humidity criteria will be referred to as the 'RHC' and the GCM with the new mass flux closure will be referred to as the 'GRN'. All models were integrated using the observed SST for 10 years (1998~2007). The GCM simulations with the modified parameterization were compared to those of the GCM with the original convective scheme.

Figure 3.6 shows that summer-mean precipitation of the model and the observation. 10-year averaged simulated data is used for analysis and the CMAP data is used for the observation (Fig. 3.6a). The CTL captures large-scale patterns of the observation but the heavy rain band in the western Pacific is weaker precipitation amount than the observation (Fig. 3.6b). The TOK produces the precipitation amount more than that of the CTL in western Pacific (Fig. 3.6c). In the RHC, the spatial pattern of precipitation appears not to be similar to the observation (Fig. 3.6d). In particular, the excessive precipitation over the subtropical western Pacific still exists in Fig. 3.6d, particularly to the north of Philippines. The trigger functions produce less light precipitation by suppression

of deep convection, resulting in more heavy precipitation and therefore more precipitation amount than that of the CTL. In the GRN, the spatial patterns of the precipitation is similar to the observation but the precipitation amount is strong in the western Pacific. Generally, the spatial pattern of precipitation are not much improved by convective trigger functions.

The convective trigger function and mass flux closure improve the frequency of heavy precipitation but have a limitation on simulating the extreme precipitation of the three-hour mean precipitation more than 200 mm day-1, as seen in Fig. 3.7. The figure shows the frequency of 3-hr precipitation for each interval of precipitation, which is 1 mm day-1 from 0 to 40 mmday-1 of precipitation and is gradually increased to 20 mmday-1 at 200 mm day-1. The observed frequency is made using the corresponding data of the TRMM. The figure clearly shows that the CTL produces light rain more and heavy precipitation less than the observed. To simulate the extreme precipitation more frequently, triggering mechanisms and mass flux closure using exponential functions are implemented in the convection scheme. When the PBL height has a small value, the trigger function suppresses the convective precipitation and the convective instability is accumulated without precipitation. The accumulated instability tends to be removed by the large-scale heavy precipitation, which increases the heavy precipitation. However, the results show that the heavy

precipitation frequency is still less than the observed, and the model has a limitation for simulating the extreme precipitation more than 120 mm day^{-1}.

To examine the effect of convective trigger functions on the eastward propagation of the precipitation, a space-time power spectral analysis was calculated for boreal winter (Fig. 3.8). This shows the frequency and propagating direction of waves. The NCEP reanalysis date was used for the observation and 10 year data was used for calculating space-time power spectral analysis. The results show that the observation has clear eastward propagation with 20-100 day periods and relatively weak westward propagation with shorter periods (2-8days). The CTL produces the power of eastward propagation less and that of westward propagation more than the observation and the speed of eastward propagation is also slower (60~120 day periods) than the observation. Because too frequent convection produces Rossby wave in the off-equator, which disturbs the eastward propagation of the Kelvin wave in the equator. It is known that too frequent convection suppresses the eastward propagation of the MJO because the convection produces Rossby wave too frequently and it disturbs the eastward propagation (Kang et al. 2013). The CTL produces too much high-cloud by detraining the moisture of frequent deep convection and this reduces long-wave radiative cooling in the upper level but heating in the lower level. This leads to increase of diabatic heating and thus additional convections repeatedly occur.

Small large-scale clouds occur in the upper-level, which move along mean wind (easterly). This contributes to too strong westward propagation. The TOK produces the power of westward propagation less and that of eastward propagation more than those of the CTL, which is closer to the observation. The speed of eastward propagation is increased with faster speed (25-80 days). In the RHC, the power of eastward propagation is more dominant than that of westward propagation but the powers are too stronger than the observation. In the GRN eastward propagation is also more dominant and the speed is slower than the observation (50-100 day). The improvement of eastward propagation by convective trigger and mass flux closure is due to decrease of high-cloud induced positive feedback (Lee et al. 2001). The convective trigger function reduces high-cloud amounts by suppressing convection and thus high-cloud induced positive feedback is reduced. The convective trigger function generally improves the eastward propagation of the MJO simulation by reducing strong cloud-radiative interaction. This leads to increase of eastward propagation and reduction of westward propagation. It is noted that the ratio of convective to total precipitation may be related to eastward propagation and proper suppression of convection is important for a good simulation of the MJO.

As computing resources increases, a high horizontal resolution climate modeling have been studied in order to improve simulation of precipitation. Also,

at higher horizontal resolution, convective parameterization, which remains one of the largest sources of uncertainty in a GCM, may not be needed because high horizontal resolution model may represent convective-scale vertical motion. In the next section, it will be examined the effect of horizontal resolution on simulated precipitation in the GCM.

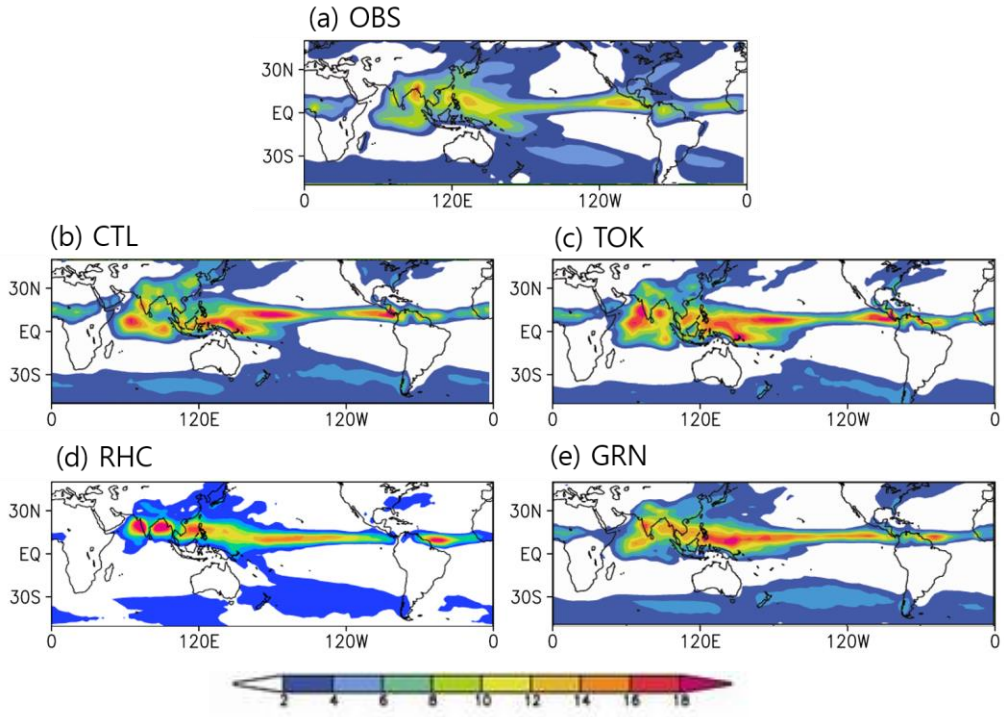

Fig. 3.6. Summer-mean precipitation of the model and observation. (a) CMAP, (b) CTL, (c) TOK and (d) RHC. 10-year averaged data is used and the CMAP data is used for the observation.

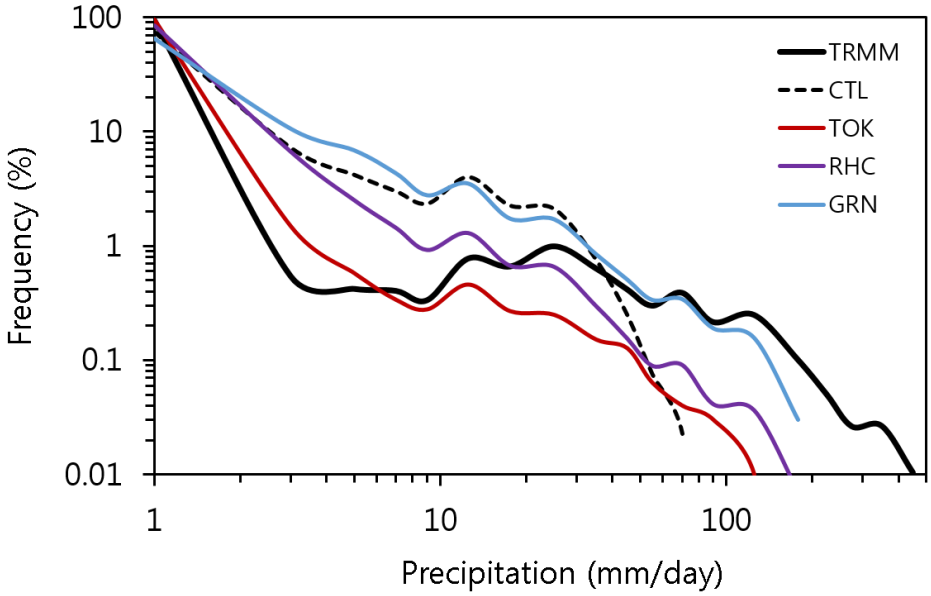

Fig. 3.7 Frequency of 3-hourly precipitation from TRMM (solid black line), GCM with the AS scheme (dashed black line), GCM with Tokioka trigger (solid red line), GCM with relative humidity criteria trigger (solid purple line) and GCM with the GRN mass flux closure (solid blue line) for boreal summer. The interval of each bin is 1 mm day^{-1} below 60 mm day^{-1} precipitation intensity, which gradually increases up to 20 mm day^{-1} near 400 mm day^{-1} precipitation intensity. Figure is on a logarithmic scale.

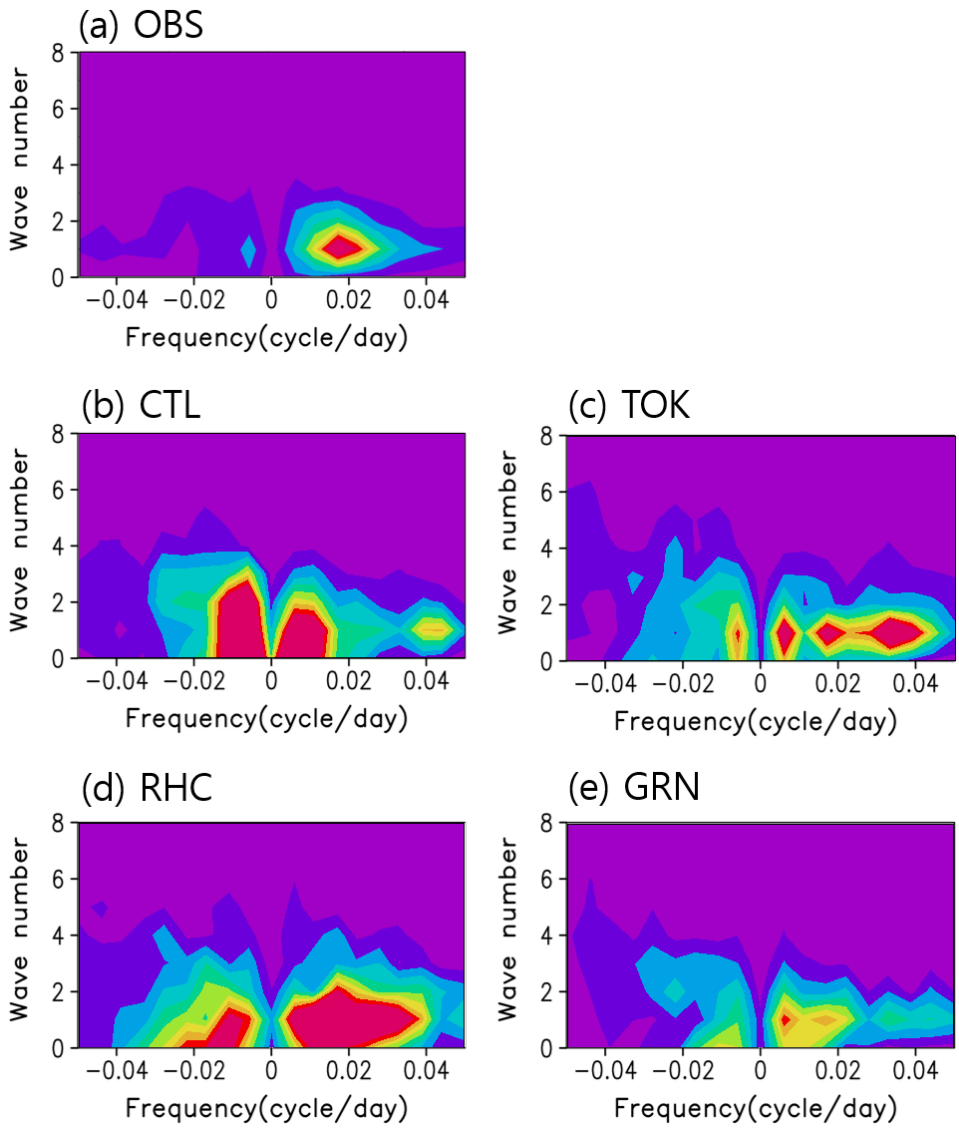

Fig. 3.8. Space-time power spectral analysis of the model and observation. (a) CMAP, (b) CTL, (c) TOK and (d) RHC. 10-year averaged data is used and the NCEPdata is used for the observation.

CHAPTER 4

High resolution GCM simulation

4.1 New dynamical core: finite volume method

4.1.1 Performance of the GCM with spectral GCM.

In this section, a high horizontal resolution GCM was developed in order to examine the impact of increase horizontal resolution on climate simulation and the GCM simulations were compared to those of the GCM with lower horizontal resolution. The three different horizontal resolution GCM (T42, T106 and T512) were integrated using observed SST (1996-1999). All models have identically same physical parameterization except numerical damping, which is increased with the resolution increasing because numerical instability occurs near the pole due to very small grid size. Figure 4.1 shows the snapshot of precipitation of models at June 1 1996. The snapshot can roughly represent an instantaneous state for precipitation. The GCM with the T42 resolution simulates unrealistic features: It does not produce reasonable synoptic disturbance in mid-latitude and

organized convection in the tropics compared to the TRMM shown in Fig. 4.2a. Most precipitation intensity is relatively weak, which is related to too much light precipitation by convective parameterization. The model does not simulate typhoon. There is no distinct different between T106 and T42. The snapshot of precipitation in the T106 are basically similar to those of the T42. The T512 captures synoptic disturbance and tropical typhoon reasonably well. However, the model does not produces organized convection in the tropics and still simulates too much light precipitation. The moisture often negative in a spectral methods since the advection of moisture is calculated as a function of waves, resulting in less organized convection. On the other hand, GCMs with spectral methods tend computationally less effective, particularly at high horizontal resolution. The spectral methods need to both grid and wave domain. Therefore, it requires large physical memory size. Because a parallelization is generally applied for wave domain, the scalability of parallelization is relatively lower than those of other different numerical methods. In addition, as the resolution increases, the time step should be reduced due to numerical instability near the poles. Therefore, computationally efficient dynamical core is required for high horizontal resolution climate modeling.'

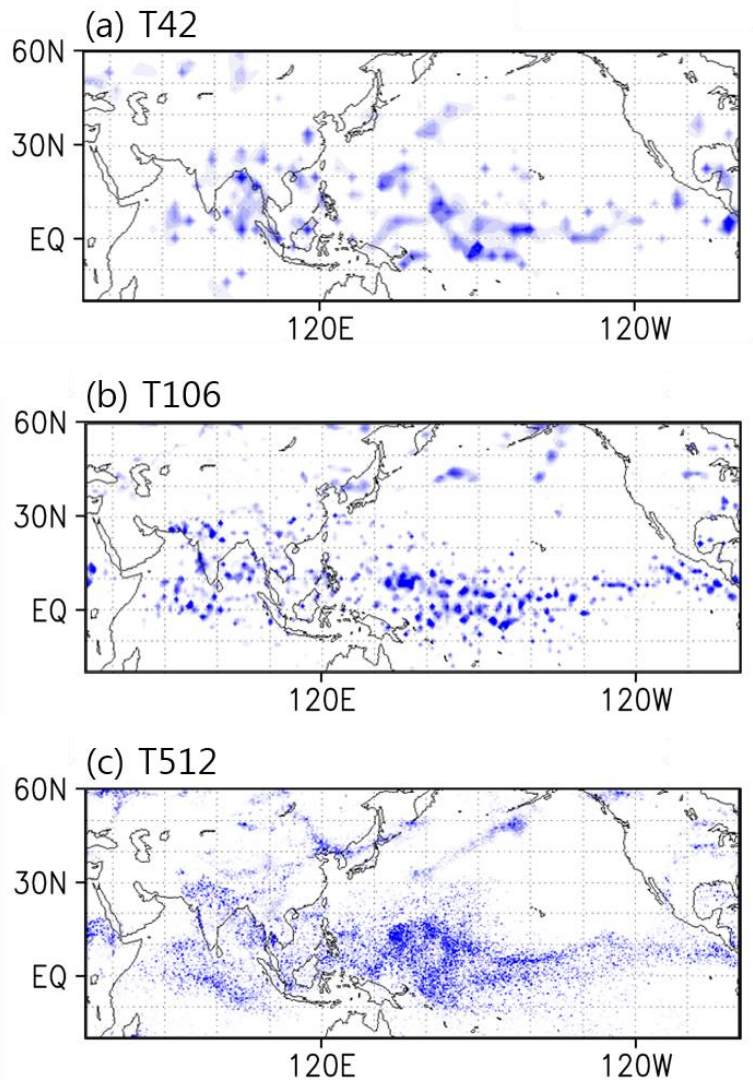

Fig. 4.1. Snapshot of simulated precipitation of Spectral GGM. (a) T42, (b) T106 and (c) T512.

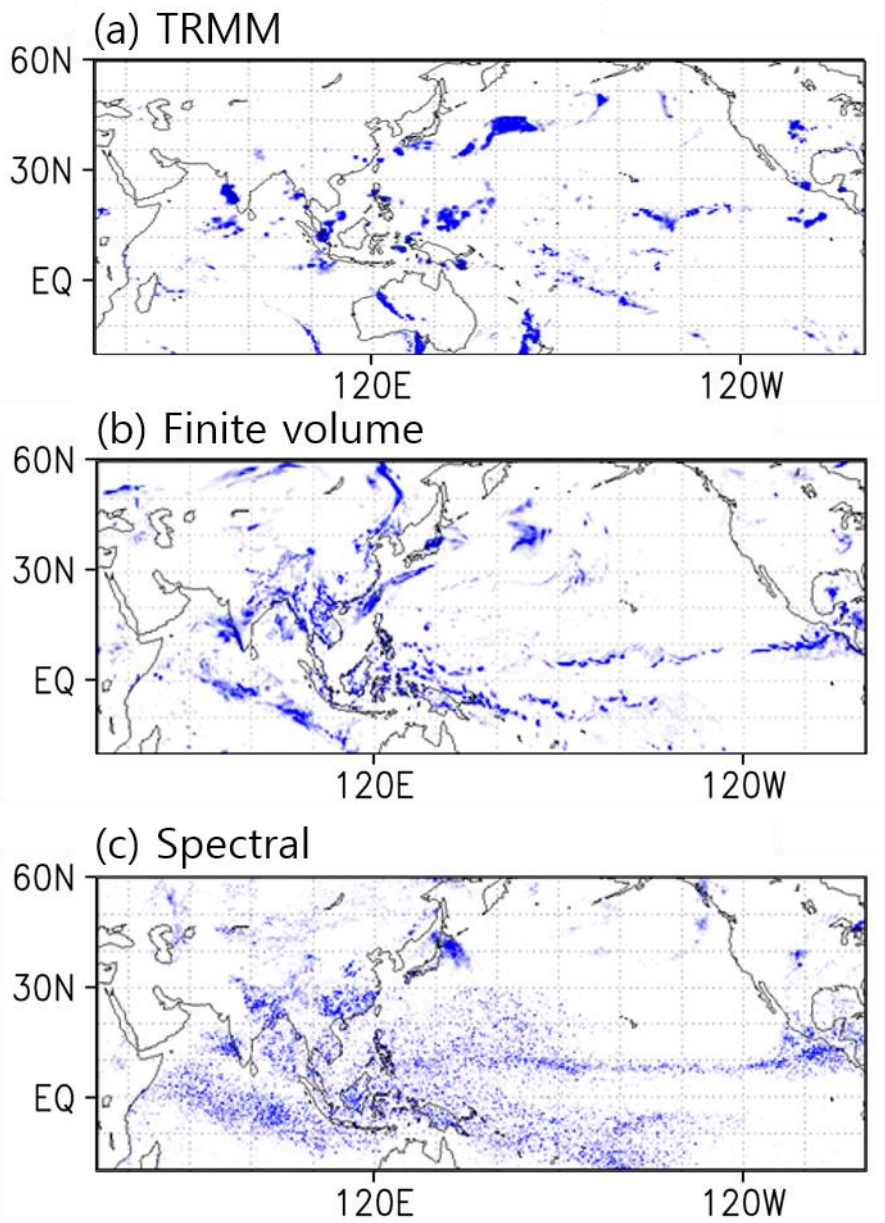

Fig. 4.2. Snapshot of 3-hourly simulated precipitation of (a) TRMM, (b) GCM with finite volume method (25km) and (c) GCM with spectral method (T512).

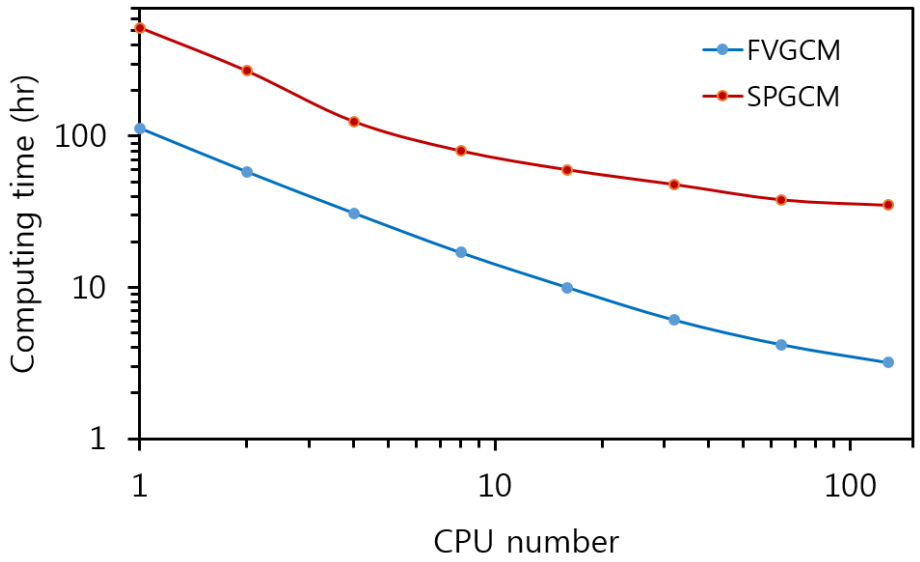

Fig. 4.3. Computing time of the Finite volume GCM (blue) and Spectral GCM (red) with different CPU numbers. The times consuming for month integration are used. The linux cluster machines are used for running the model. The spectral model with T42 and the finite volume model with 300km grid size were used.

4.1.2 Description of finite volume method

A finite volume methods (FV) is used for high horizontal resolution GCM. The FV is based on Lin (2009) and coupler with physical process, mass conservation and divergence coefficient are modified. The finite-volume dynamical core adapted in this study has been successfully implemented into other GCMs, the NASA–NCAR general circulation model (NGCM) and the Community Atmosphere Model (CAM). It is also in the process of being implemented into Geophysical Fluid Dynamics Laboratory's Flexible Modeling System (GFDL FMS) for climate applications. The vertical Lagrangian discretization with the associated remapping conserves the total energy exactly. The governing equations for the hydrostatic atmosphere on the sphere with a general vertical coordinate z (e.g., Kasahara 1974) was represented. Using standard notations, the hydrostatic balance equation is

$$\frac{1}{\rho}\frac{\partial p}{\partial z} + g = 0 \qquad (4.1)$$

where ϱ is the density of the air, p the pressure, and g is the gravitational constant. Introducing the pseudo-density $\pi = \partial p / \partial \zeta$, vertical pressure gradient in the general coordinate, from the hydrostatic balance equation, the pseudo-density and the true density are related as follows:

$$\pi = -\frac{\partial \phi}{\partial \zeta}\rho \tag{4.2}$$

where $\phi = gz$ is the geopotential height. The mass conservation law for tracers (or water vapor) can be written as

$$\frac{\partial}{\partial t}(\pi q) + \nabla \cdot (V\pi q) = 0 \tag{4.3}$$

Let (λ, θ) denote the (longitude, latitude) coordinate, the momentum equations are written in the ''vector-in-variant form'' (e.g., Arakawa and Lamb 1981)

$$\frac{\partial}{\partial t}u = \Omega v - \frac{1}{Acos\theta}\left[\frac{\partial}{\partial \lambda}(\kappa + \phi - \nu D) + \frac{1}{\rho}\frac{\partial}{\partial \lambda}p\right] - \frac{d\zeta}{dt}\frac{\partial u}{\partial \zeta}, \tag{4.4}$$

$$\frac{\partial}{\partial t}v = -\Omega \mathrm{u} - \frac{1}{A}\left[\frac{\partial}{\partial \theta}(\kappa + \phi - \nu D) + \frac{1}{\rho}\frac{\partial}{\partial \theta}p\right] - \frac{d\zeta}{dt}\frac{\partial v}{\partial \zeta}, \tag{4.5}$$

where A is the radius of the earth, ν is the coefficient for the optional divergence damping, D is the horizontal divergence, Ω is the vertical component of the absolute vorticity, κ is the kinetic energy, Φ is the geopotential, and v is the angular velocity of the earth.

Since the vertical transport terms vanish with the Lagrangian control-volume vertical discretization, only the 2D forms of the flux form semi-Lagrangian transport scheme (FFSL) algorithm are represented for the transport of density and mixing ratio–like quantities. The conservation law for the pseudodensity (Eq. 4.3) reduces to

$$\frac{\partial}{\partial t}\pi + \frac{1}{A\cos\theta}\left[\frac{\partial}{\partial \lambda}(u\pi) + \frac{\partial}{\partial \theta}(v\pi\cos\theta)\right] = 0 \qquad (4.6)$$

Integrating Eq. (4.6) analytically in time (for one time step Δt) and around the finite volume, the previous conservation law becomes

$$\tilde{\pi}^{n+1} = \tilde{\pi}^{n} - \frac{1}{A^2\Delta\theta\Delta\lambda\cos\theta}\int_{t}^{t+\Delta t}\left[\oint \pi(\tau;,\lambda,\theta)V\cdot n dl\right]d\tau \qquad (4.7)$$

where $V(t;\lambda,\theta)=(U,V)$, dl is the infinitesimal element along the volume edges, n is the corresponding outward normal vector, $\tilde{\pi}$ is the finite-volume representation of π and the contour integral is taken along the edges of the finite volume centered at (λ, θ). Equation (4.7) is still exact. To carry out the contour integral, certain approximations must be made. Lin and Rood (1996) effectively decomposed the flux integral using two orthogonal 1D flux-form transport operators. Introducing the difference and average operators:

$$\delta_x q = q\left(x+\frac{\Delta x}{2}\right) - q\left(x-\frac{\Delta x}{2}\right), \qquad (4.8)$$

$$\bar{q}^{x} = \frac{1}{2}\left[q\left(x+\frac{\Delta x}{2}\right) + q\left(x-\frac{\Delta x}{2}\right)\right] \qquad (4.9)$$

and assuming (u^*, y^*) is the time-averaged (from time t to time $t+\Delta t$) V on the C grid, the 1-D flux-form transport operator F in the λ direction is

$$\mathrm{F}(u^*,\Delta t,\tilde{\pi}) = -\frac{1}{A\Delta\lambda\cos\theta}\delta_\lambda\left(\int_t^{t+\Delta t}\pi U d\tau\right) = -\frac{\Delta t}{A\Delta\lambda\cos\theta}\delta_\lambda[\chi(u^*,\Delta t,\pi)] \qquad (4.10)$$

$$\chi(u^*, \Delta t, \pi) = \frac{1}{\Delta t}\int_t^{t+\Delta t} \pi U d\tau \equiv u^*\pi^*(u^*, \Delta t, \tilde{\pi}) \approx u^* \frac{1}{\Delta t}\int_t^{t+\Delta t} \pi d\tau \qquad (4.10)$$

where X is the time-accumulated (from t to $t+\Delta t$) mass flux across the cell wall, and π^* can be interpreted as a time-mean (from time t to $t+\Delta t$) pseudodensity value of all material that passed through the cell edge. To be exact, the time integration in Eq. (6) should be carried out along the backward-in-time trajectory of the cell-edge position from $t+\Delta t$ back to time t. The essence of the 1D finite-volume algorithm is to construct, based on the given initial cell-mean values of $\tilde{\pi}$, an approximated subgrid distribution of the true π field, to enable an analytic integration of Eq. (4.10).

For 2D problems, the first step toward reducing the splitting error is to apply the two orthogonal 1D flux-form operators in a symmetric way. After the directional symmetry is achieved (by averaging), the ''inner operators'' are then replaced with corresponding advective-form operators. A consistent advective-form operator (f) in the λ direction can be derived from its flux-form counterpart (F) as follows

$$f(u^*, \Delta t, \tilde{\pi}) = F(u^*, \Delta t, \tilde{\pi}) - \tilde{\pi}F(u^*, \Delta t, \tilde{\pi} \equiv 1) = F(u^*, \Delta t, \tilde{\pi}) + \tilde{\pi}\frac{\Delta t \delta_\lambda u^*}{A\Delta\lambda cos\theta} \qquad (4.11)$$

Analogously, 1D flux-form transport operator G in the latitudinal (θ) direction is derived as follows:

$$G(v^*, \Delta t, \tilde{\pi}) = -\frac{1}{A\Delta\lambda cos\theta}\delta_\theta\left(\int_t^{t+\Delta t} \pi V cos\theta d\tau\right) = -\frac{\Delta t}{A\Delta\theta cos\theta}\delta_\theta[u^*, cos\theta\pi^*] \quad (4.12)$$

The 2D transport algorithm on the sphere can then be written as

$$\tilde{\pi}^{n+1} = \tilde{\pi}^n + \mathrm{F}\left(u^*, \Delta t, \tilde{\pi}^\theta\right) + G\left(v^*, \Delta t, \tilde{\pi}^\lambda\right) \quad (4.13)$$

The fulfillment of the earlier incompressibility condition for constant-density flows is crucial to the accuracy of the 2D flux-form formulation. For transport of mixing ratio–like quantities ($\tilde{q}$) the mass fluxes (X, Y) as defined previously should be used as follows

$$\tilde{q}^{n+1} = \frac{1}{\tilde{\pi}^{n+1}}\left[\tilde{\pi}^n\tilde{q}^n + \mathrm{F}\left(\chi, \Delta t, \tilde{q}^\theta\right) + G\left(Y, \Delta t, \tilde{q}^\lambda\right)\right] \quad (4.14)$$

The preceding form of the tracer transport equation consistently degenerates to Eq. (15) if q˜ 5 constant, which is another important condition for a flux-form transport algorithm to be able to avoid generation of artificial gradients and to maintain mass conservation.

The update of ''pressure thickness'' dp, using the fractional time step Dt 5 Dt/m, can be written for fractional step i = 1, . . . , m

$$\delta p^{n+(\frac{i}{m})} = \delta p^{n+(\frac{i=1}{m})} - \frac{\Delta\tau}{Acos\theta} \times \left\{ \begin{array}{c} \frac{1}{\Delta\lambda}\delta_\lambda\left[x^*\left(u^*, \Delta\tau;\ \delta p^\theta\right)\right] \\ +\frac{1}{\Delta\theta}\delta_\theta\left[cos\theta y^*\left(v^*, \Delta\tau;\ \delta p^\lambda\right)\right] \end{array} \right\} \quad (4.15)$$

4.1.3 Computational efficiency

The finite volume dynamical core was implemented in a GCM instead of a spectral dynamical core. The performance and computational efficiency of the FV were compared to those of the GCM with spectral method. The 25km horizontal resolution and T512 are used for the GCM with finite volume and spectral methods, respectively. The FV has several benefits for high horizontal resolution GCM. One is that the FV used only grid domain, resulting in less required computing memory. Another is that the parallelization of the FV is more convenient than that of the spectral method because the FV is grid-based numerical methods. The other is that the FV include Flux-Form Semi-Lagrangian Methods (FFSL, Lin and Rood 1997) for zonal advection. It allows large model time step because the model is still stable for Courant-Friedrichs-Lewy (CFL) condition > 1. Therefore, the computing time in the FV is much less than that of the spectral method. The snapshot of 3-hourly precipitation from the model and observation is shown in Figure 4.2. The TRMM data is used for the observation. The results show that the GCM with spectral method do not produce organized convection but the GCM with finite volume method produces realistic organized precipitation, which is closer to the observation. Because the tracer is also treated as a wave in a spectral method, the advected tracer sometimes becomes negative, which disturb convergence of moisture. In contrast, a finite volume methods uses

a semi-Lagrangian methods, resulting in more accumulated moisture from many adjacent grids and therefore more organized convection. We also examined the computational efficiency of two dynamical cores. Figure 4.3 shows the required computing time for a month integration of models with different number of CPUs. The 25km and T512 horizontal resolution are used. For single CPU, the computational time of GCM with finite volume method is much smaller (about 5 times more) than that of the GCM with spectral method due to large time step by FFSL. In spectral GCM, the computing time linearly decrease with the number of the CPU but does not decrease when the number of the CPU is larger than 32, indicating that the efficiency of parallelization is poor for the CPU number > 32. In contrast, computing time of the finite volume GCM is linearly reduce even if the number of the CPU is 128. These results indicates that finite volume GCM has better computational efficiency then and produces good simulation of 3-hourly precipitation. The finite volume GCM will be used as the control GCM.

4.2 High resolution GCM simulation

4.2.1 AGCM simulation

In this section, the effects of increasing horizontal resolution on simulated precipitation are examined in a GCM. Figure 4.4 shows summer-mean precipitation of the GCM with different horizontal resolutions. Three different

grid size (25km, 100km and 300km) were used. 10-year averaged data is used. The results show that there is no distinct difference in large-scale pattern of simulated precipitation among the GCMs. It is noted that the precipitation amount in the eastern Pacific is increased with the resolution increasing. Because of higher relative humidity in the small grid size, saturation occurs more frequently than that at large grid size, resulting in more large-scale condensation and therefore less deep convection. This weakens Walker circulation and then precipitation amount is increased in the eastern Pacific. On the other hands, there are improvement for regional details of precipitation with the resolution increasing. High horizontal resolution is able to represent realistic steep topography and therefore precipitation amount is increase near steep mountain area, particularly west of India and Himalaya mountain area, as seen Figure 4.5. The corresponding precipitation amount of the TRMM is also heavy in those area. Therefore, topographic precipitation is improved at higher horizontal resolution. It is noted that the precipitation in the Bay of Bengal is not improve with increasing resolution. In this region, the heavy precipitation is not simply controlled by the local convection but more controlled by the meridional heating contrast between Eurasian continent and Indian Ocean (Chou 2003). Higher resolution model resolves complicate land-sea contrast and there it contributes to improving the precipitation over east Asia. Figure 4.6 shows summer-mean

precipitation of the models over East Asia. The TRMM shows heavy precipitation over Korea Peninsula and Japan. The GCM with 300km grid size produce less precipitation than the observation. As the resolution increases, precipitation tends to be increased over Korea and Japan, which is closer to the observation.

The frequency distribution as a function of precipitation intensity is shown in Fig. 4.7 (the counterpart of Fig. 3.8). The figure is made by using the three-hourly precipitation data for the grid points in the tropics between 30°S and 30°N. The purple, blue and red lines indicate the frequency distribution of the GCM with the 300km, 100km and 25km horizontal resolution, respectively. The figure clearly indicates that the increasing horizontal resolution leads to increasing the frequency of heavy precipitation. The vertical motion increases with resolution increasing, which contributes to production of heavy precipitation. However, the GCM with 25km grid size does not still produce the extreme precipitation over 200 mm day-1. These results show that the increase of horizontal resolution has a limitation for improving the frequency of heavy precipitation. In order to improve the frequency substantially, better representation of physical processes will be required.

We examined diurnal cycle of precipitation for models and observation for boreal summer (Fig. 4.8). The GCM with 300 km horizontal resolution produces the diurnal peak of the precipitation in the late night, which is 2-4 hours earlier

than that of the TRMM. The convective parameterization is sensitively responds to convective instability and therefore the diurnal cycle of precipitation mainly follows the convective instability that often has a peak at late afternoon. In the GCM with 35km horizontal resolution, the diurnal cycle of precipitation is almost same as that of the GCM with 300km grid size. Increase of horizontal resolution does not improve diurnal cycle of precipitation. It suggests that poor simulation of diurnal cycle for precipitation in the GCM results from deficit of physical parameterization rather than model horizontal resolution.

4.2.2 AGCM simulation without convective scheme

As mentioned in the previous section, the poor GCM simulation is mainly due to poor convective parameterization. In the higher horizontal resolution, precipitation may be represented by using only large-scale condensation due to increased vertical motion. In this section, the GCM without convective scheme (NOCONV) was integrated and the simulations were compared to the GCM with a conventional convective parameterization (CTL). The models have a 35km horizontal resolution and 20 levels vertically. The precipitation of the models and observation for June is shown in the Fig. 4.9. The CTL captures large-scale patterns of observation but underestimate precipitation in the western Pacific. The NOCONV also captures large-scale patterns of observation reasonably well

although precipitation amount is larger than the observation. It suggests that in the high resolution model, the large-scale condensation scheme (large-scale precipitation) produces reasonable mean precipitation. It is examined how the GCM without convective scheme simulates the eastward propagation of the daily precipitation over equator.

Figure 4.10 shows Hovmuller diagram of daily precipitation averaged over 10S~10N. The GPCP data was used for observation. The CTL shows clear and slow westward propagation and relatively weak eastward propagation with relatively faster speed, which is far from observation. Many studies shows that strong westward propagation due to too frequent light precipitation. Lee et al. (2001, 2003) suggested that too frequency convection make humid condition in the upper level and it produces small cloud. These clouds move along mean easterly wind in the upper level, which disturbs the eastward propagation of precipitation, called as to 'high cloud induced positive feedabck, as discussed in the section 3. The NOCONV shows clear and regular eastward propagation of the precipitation. Because of the absence of the convective parameterization, high cloud is reduced and therefore high cloud induced positive feedback is weaken. It indicates that large-scale condensation produces realistic eastward propagation and convective parameterization is an important factor for poor simulation of intra-seasonal variability scheme at high resolution. Moreover, the NOCONV

produce more heavy precipitation than that of the GCM with convective parameterization (Fig. 4.11). This result is consistent with that of the GCM with convective trigger function that suppress the convection. Increasing horizontal resolution and suppression (or removal) increases the frequency of heavy precipitation. However, they do not simulated extreme precipitation more than 200 mm day^{-1}. The NOCONV also produces too much grid-scale precipitation (Fig. 4.12). The large-scale condensation accumulates convective instability too much and releases the instability at once. The relatively simple parameterization for precipitation may cause these problems. A possible solution is to represent explicitly cloud and rain processes. The present stud implemented cloud microphysics of the CRM in a GCM with an order of 50km horizontal resolution. However, cloud microphysics does not work properly due to the coarse resolution. In the next section, it will be introduced cloud microphysics and investigate important processes for heavy and light precipitation. It will be examined the resolution dependency of cloud microphysics and how to modify cloud microphysics in order to reduce the dependency.

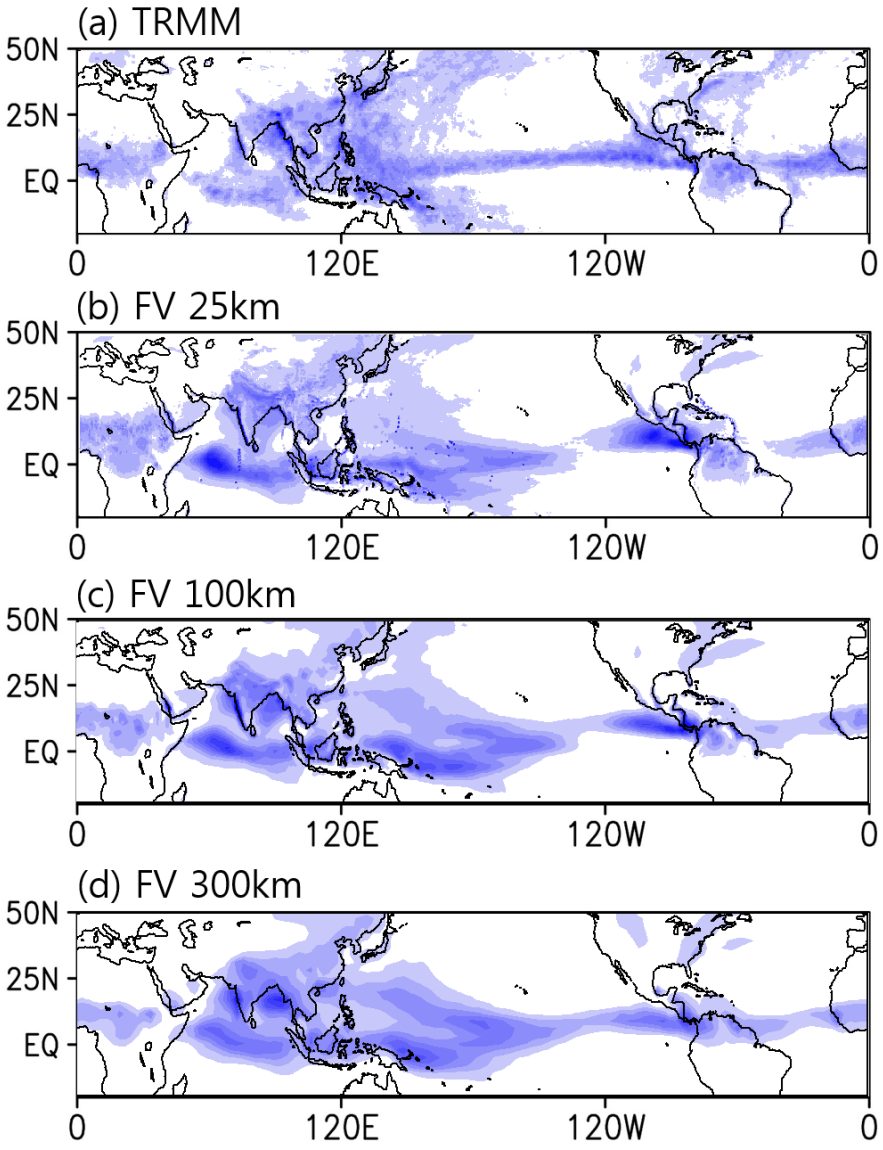

Fig. 4.4. Summer-mean precipitation of the FVSNUAGCM with different horizontal resolution and observation. The TRM data is used

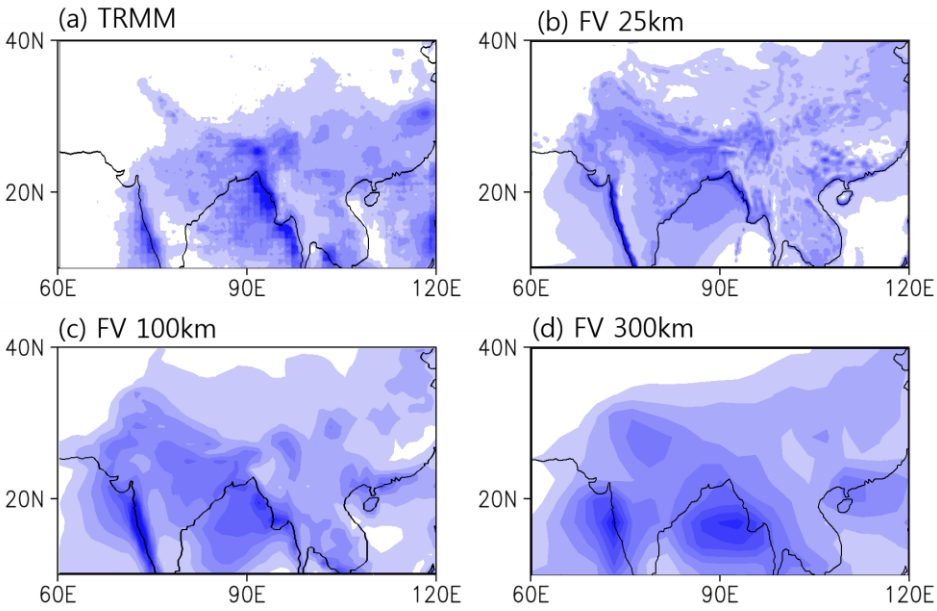

Fig. 4.5. Summer-mean precipitation of the FVSNUAGCM with different horizontal resolutions and the TRMM in the India region.

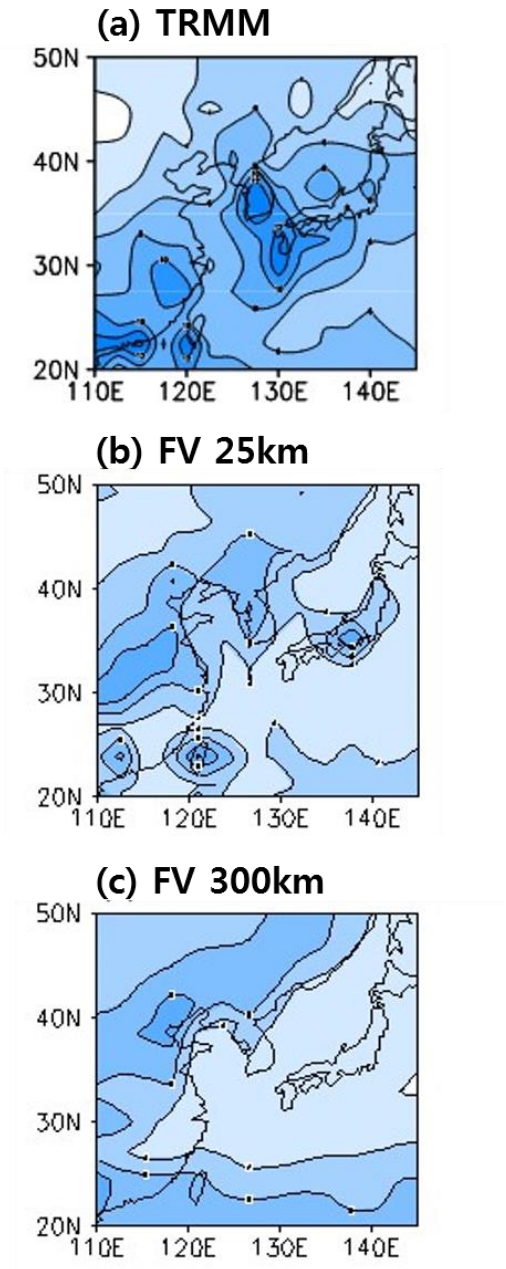

Fig. 4.6. Summer-mean precipitation of the FVSNUAGCM with different horizontal resolutions and the TRMM in East Asia.

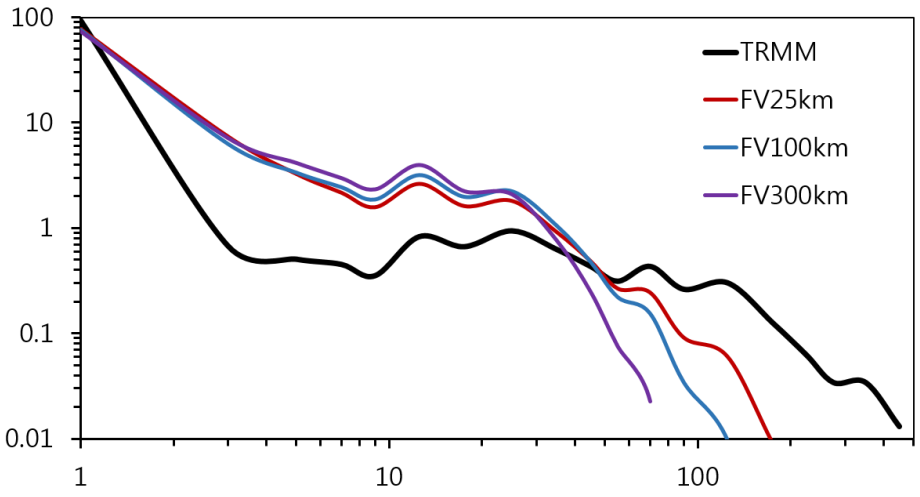

Fig. 4.7. Frequency of 3-hourly precipitation from TRMM (black), FVSNUAGCM with the 300 km (purple), 100 km (blue) and 25km (red) horizontal resolution for boreal summer. The interval of each bin is 1 mm day^{-1} below 60 mm day^{-1} precipitation intensity, which gradually increases up to 20 mm day^{-1} near 400 mm day^{-1} precipitation intensity. Figure is on a logarithmic scale.

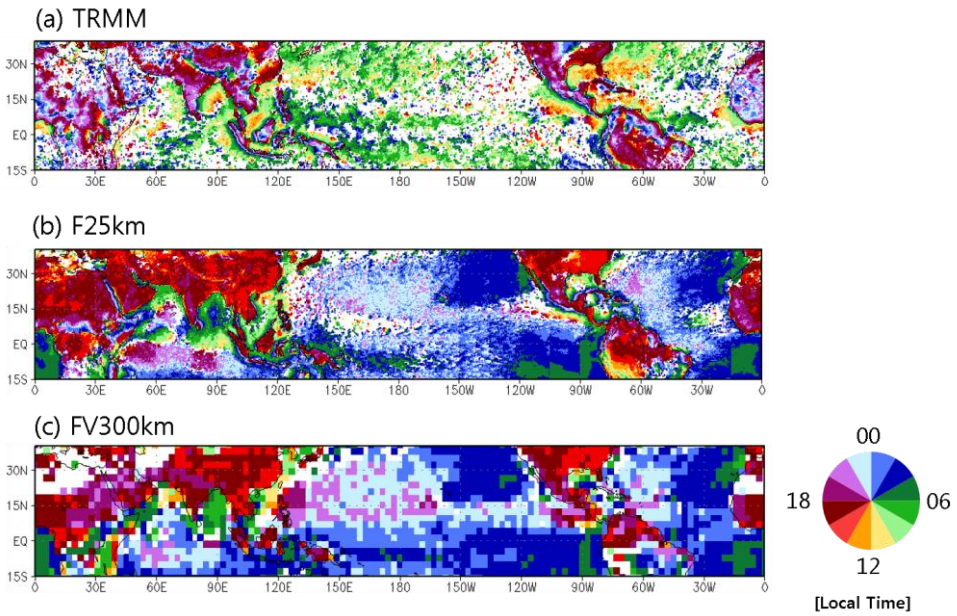

Fig. 4.8. Color maps of local solar time of the maximum of the diurnal harmonic of JJA precipitation from (a) TRMM, FVSNUAGCM with (b) 25km and (c) 300km horizontal resolution. The color represents local solar time.

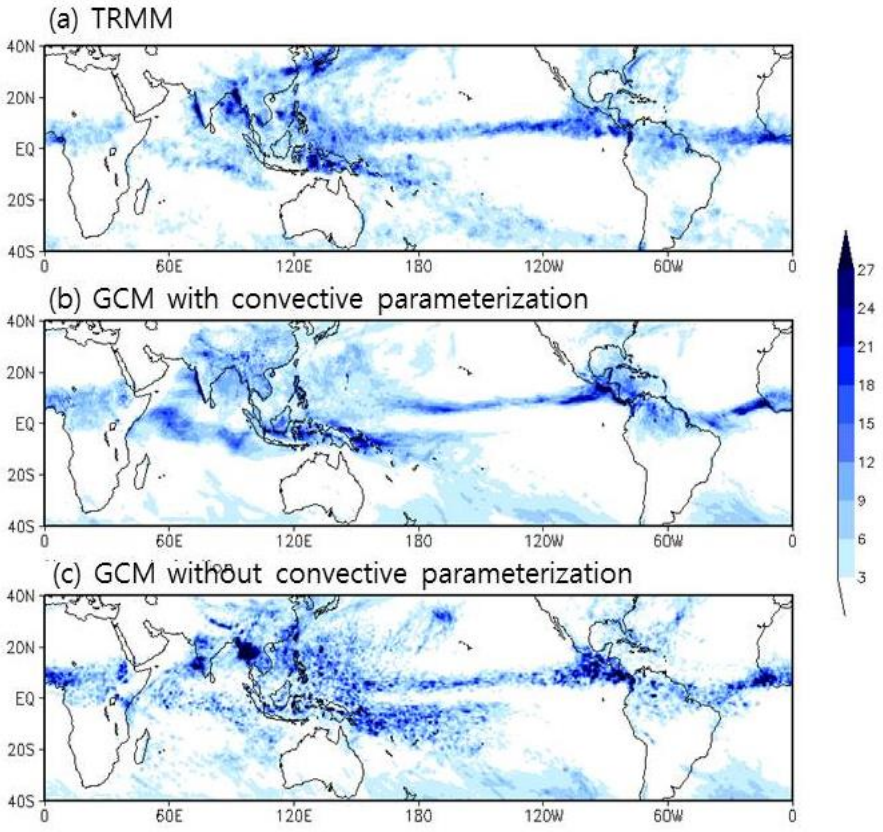

Fig. 4.9. Summer-mean precipitation of the models and observation. (a) TRMM and GCM (a) with and (b) without convective parameterization

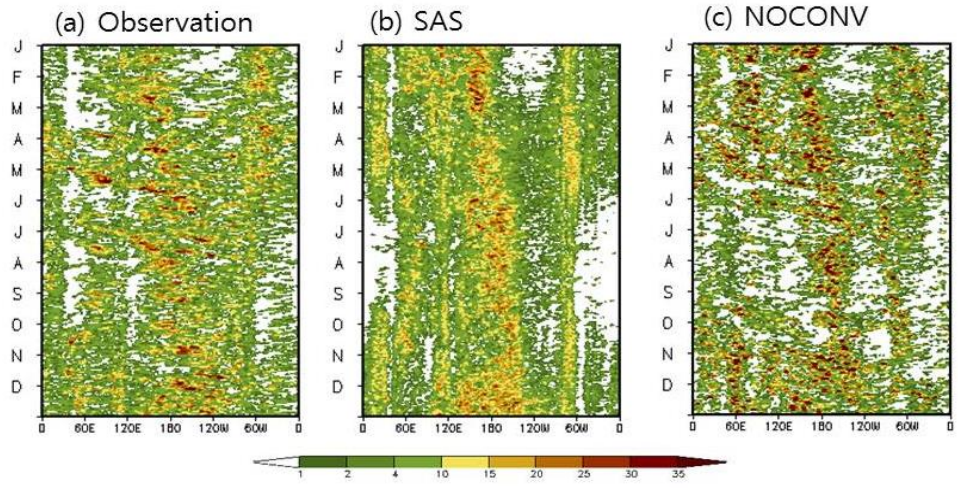

Fig. 4.10. Hovmuller diagram of daily mean precipitation of models and observation. (a) TRMM, (b) GCM with convective scheme and (c) GCM without convective scheme.

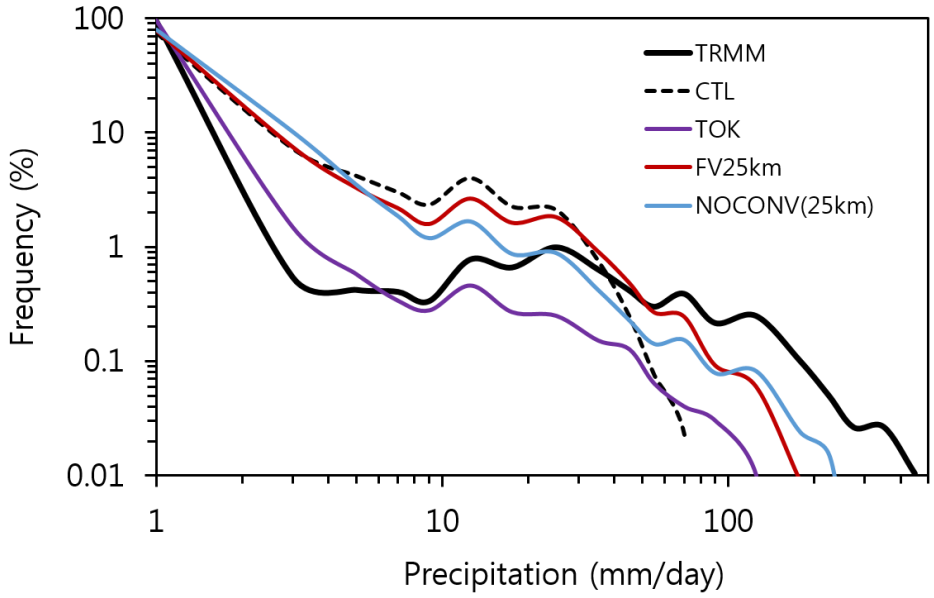

Fig. 4.11. Frequency of 3-hourly precipitation from TRMM (black), 300km horizontal resolution GCM (dashed black), the 300km GCM with trigger function (purple), the 25km GCM (red) and the 25km GCM without convective parameterization (blue) for boreal summer. The interval of each bin is 1 mm day^{-1} below 60 mm day^{-1} precipitation intensity, which gradually increases up to 20 mm day^{-1} near 400 mm day^{-1} precipitation intensity. Figure is on a logarithmic scale.

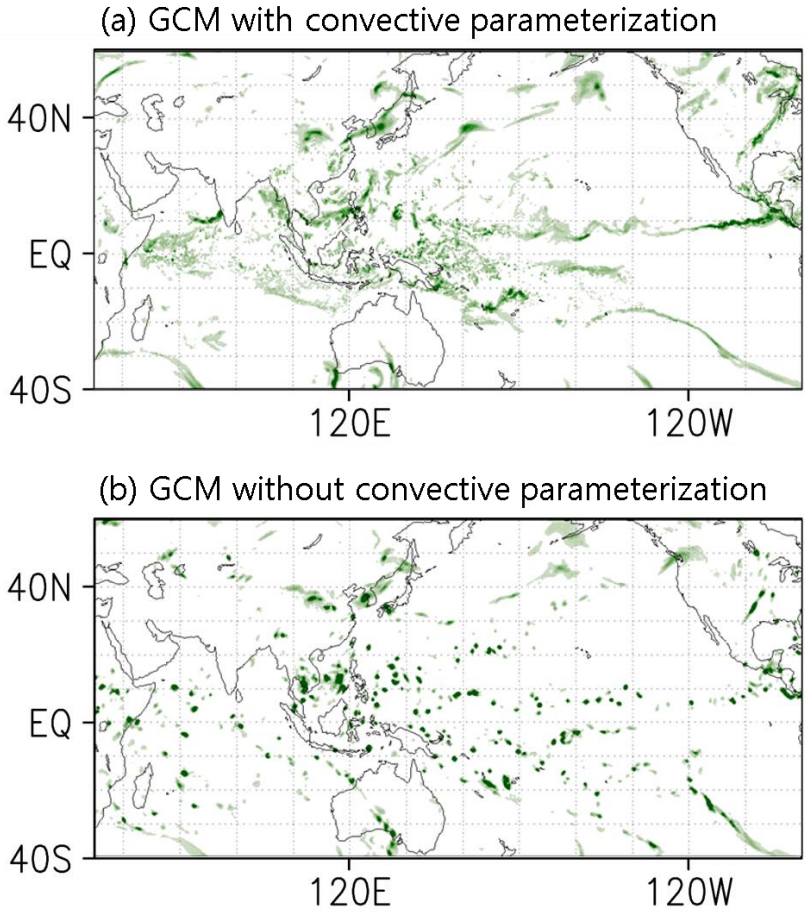

Fig. 4.12. Snapshot of 3-hourly precipitation of GCM (a) with and (b) without convective scheme.

CHAPTER 5

Modification of cloud microphysics

5.1 Cloud microphysics

5.1.1 Dominant microphysics processes

In this section, we examined the important process for heavy precipitation the resolution dependency of cloud microphysics and investigated how to reduce the resolution dependency. Before examining resolution dependency of cloud microphysics, we analyzed the budget of cloud microphysics in order to find dominant processes because it is difficult to examine the resolution dependency for all microphysics processes. Figure 5.1 shows the budget of the microphysics of 1-km CRM simulation. The vertically integrated values are used for budget analysis. Condensation, accretion of cloud water by rain water (graupel) and

melting of graupel are dominant processes in the microphysics. Also, graupel amount is mainly made by accretion of cloud water and relatively small portion of accretion of snow. Rain water is from not only accretion of cloud water made by condensation but also the melting of graupel. In the present study, these dominant processes are mainly used to examine resolution dependency and modify microphysics.

5.1.2 Microphysics process related to light and heavy precipitation

Using the CRM simulation data, the budget of the microphysics of precipitation processes is examined to identify important cloud and rain processes for the light and heavy precipitation. The light and heavy precipitations are defined here as the precipitation less than 10 mm day-1 and that more than 60 mm day-1. As seen in Fig. 5.2a, the rain water of light precipitation is mainly from accretion of cloud water made by the condensation of water vapor. The portion of auto-conversion is relatively small (not shown). On the other hand, the major portion of rain water of heavy precipitation is not only from the cloud water but also from graupel, and a relatively small portion from snow (Fig. 5.2b). The graupel is made mainly by the accretion process of cloud water, and the graupel is converted to the rain water by melting process. A part of graupel is also made by the accretion of snow.

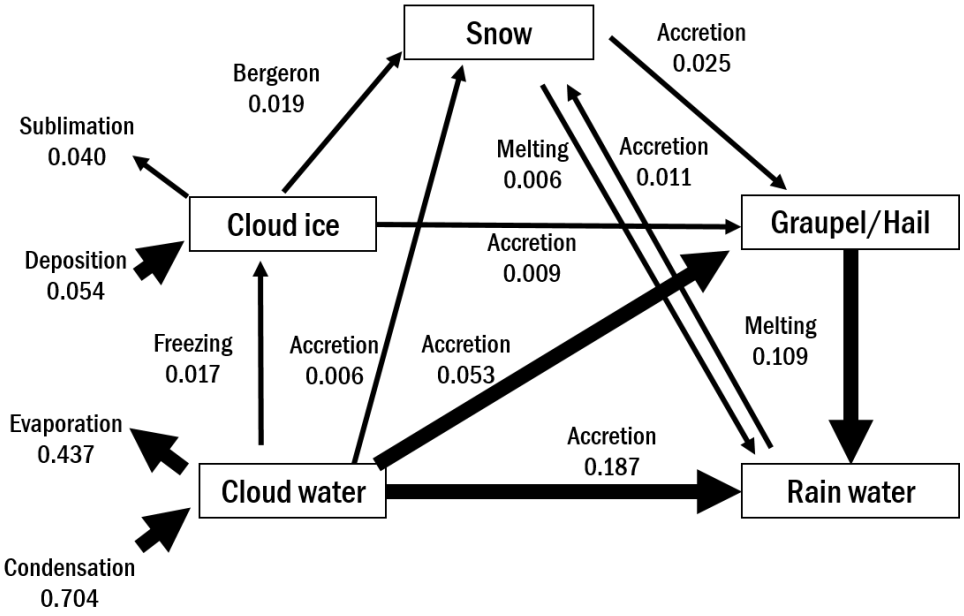

Fig. 5.1. Budget of cloud microphysical processes of the CRM averaged for one month. Thick (thin) arrow represents major (minor) microphysical processes. Units for cloud hydrometeors and microphysical processes are g g^{-1} and g g^{-1} hr^{-1}, respectively. The vertically integrated values are averaged for all domain.

In the GCM, the rain water is made mainly by the cloud water with an auto-conversion time scale of 3600 seconds and partly by the cloud ice without any delayed time scale. Therefore, this GCM rain processes mimic the microphysical process for the light precipitation, however, it does not represent one of the major rain processes, growth of graupel and its melting process, for the heavy precipitation. In order wards, the GCM needs to include the microphysical processes associated with ice phases of cloud water, such as snow and graupel for simulating heavy precipitation realistically.

The importance of the role of graupel in simulating heavy precipitation is clearly demonstrated by Fig. 5.3a., which shows the relationship between the rainfall intensity and the graupel amount vertically integrated within the cloud column. The figure shows that the graupel amount is negligible for light rain unto 10 mm day^{-1} but it increases almost linearly with the increase of rain intensity unto 150 $mmday^{-1}$ and appears to saturate for the heavy precipitation more than 150$mmday^{-1}$. Similar relationship appears between the accretion of cloud water for the graupel and the rainfall intensity as seen in Fig. 5.3b. The two figures clearly indicate that the accretion of cloud water is an importance source of the graupel and a large amount of graupel is required to produce heavy precipitation. But, the accretion and the graupel amount is negligible for the light precipitation unto 10 mm day^{-1}, and therefore the light rain is mostly produced by the warm

rain process without ice species, as demonstrated by Fig. 5.2a. The vertical profiles of various cloud and rain species for the light and heavy precipitation cases are shown in Figs. 5.4a and 5.4b, respectively. As expected, for the light precipitation case, the cloud water and rain water are confined in the lower troposphere and no water and ice species exist in the mid and upper levels. In contrast, for the heavy precipitation case, a large amount of graupel appears in the mid and upper levels above 700 hPa. Even in the upper-level, where the air temperature is much below the freezing temperature, the graupel amount is larger than that of cloud ice. The upper-level graupel appears not to be generated locally but to be transported from the mid tropospheric level associated with deep convection. Fig. 5.4b also shows that the cloud ice, which is generated locally by the decomposition, appears in the upper-troposphere with much less amount than that of the graupel. Large amounts of cloud and rain water are located in the lower level, whose maximum appear near 700 hPa. This cloud and rain water amounts and their maximum heights for the heavy precipitation are much more and higher, respectively, than those for the light precipitation. However, the large difference between the light and heavy precipitation appears in the vertical distributions of graupel and cloud ice.

(a)Light precipitation (0 – 10 mm day^{-1})

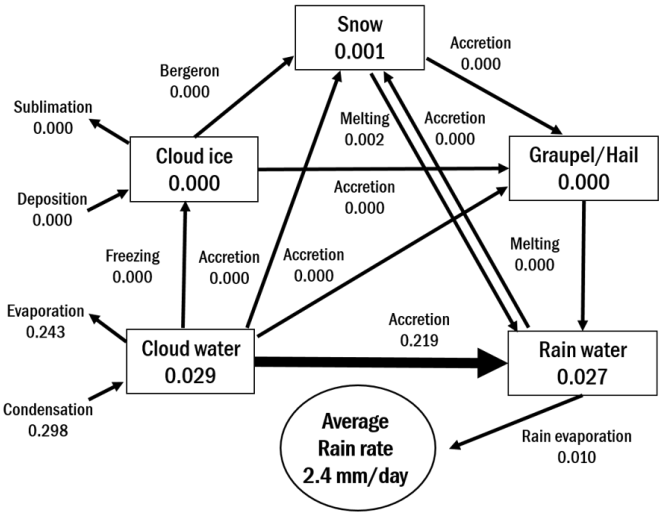

(b) Heavy precipitation (> 60 mm day^{-1})

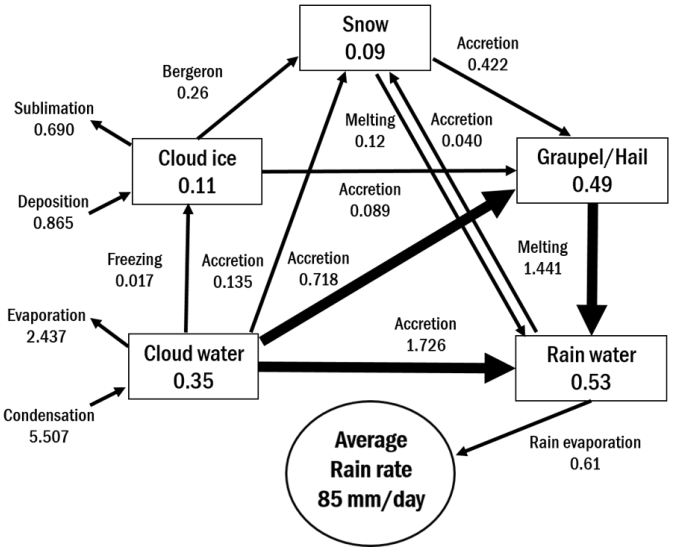

Fig. 5.2. Budget of cloud microphysical processes of the CRM for (a) light and (b) heavy precipitation, respectively. Thick (thin) arrow represents major (minor) microphysical processes.

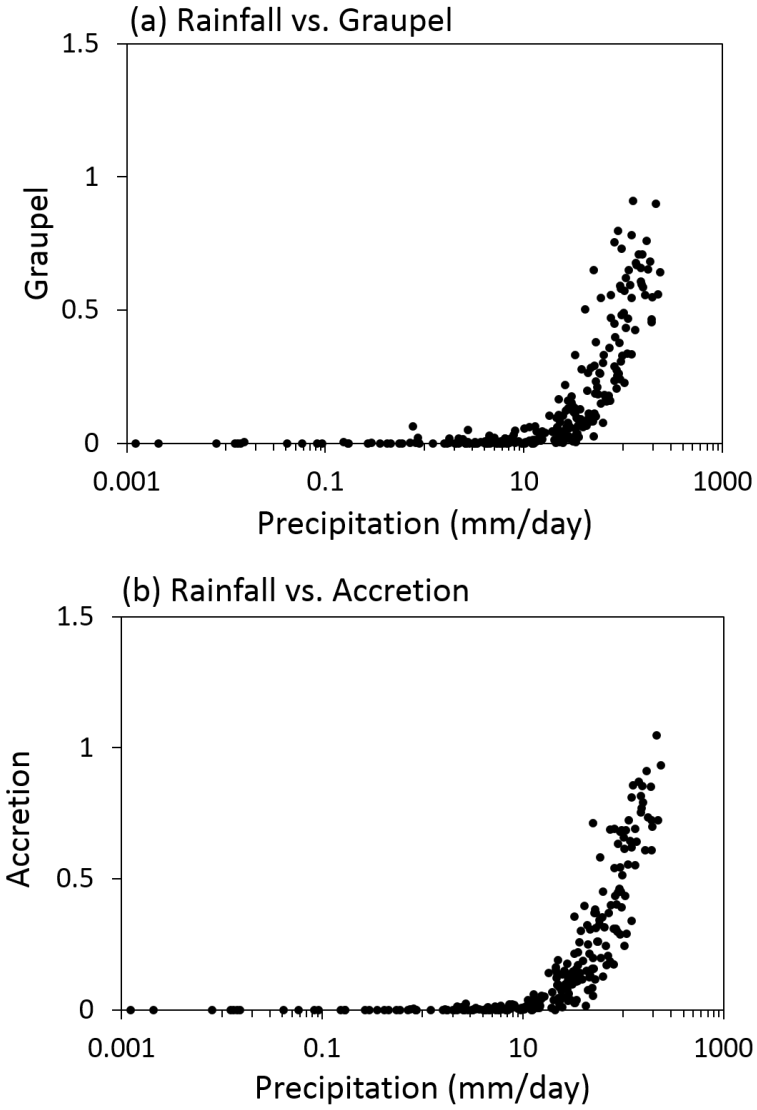

Fig. 5.3. (a) Scatter plot of graupel (g g^{-1}) and precipitation (mm day^{-1}). (b) Scatter plot of accretion of cloud water by graupel (g g^{-1} s^{-1}) and precipitation in the CRM simulation. The graupel and the accretion are vertically averaged within the cloud column.

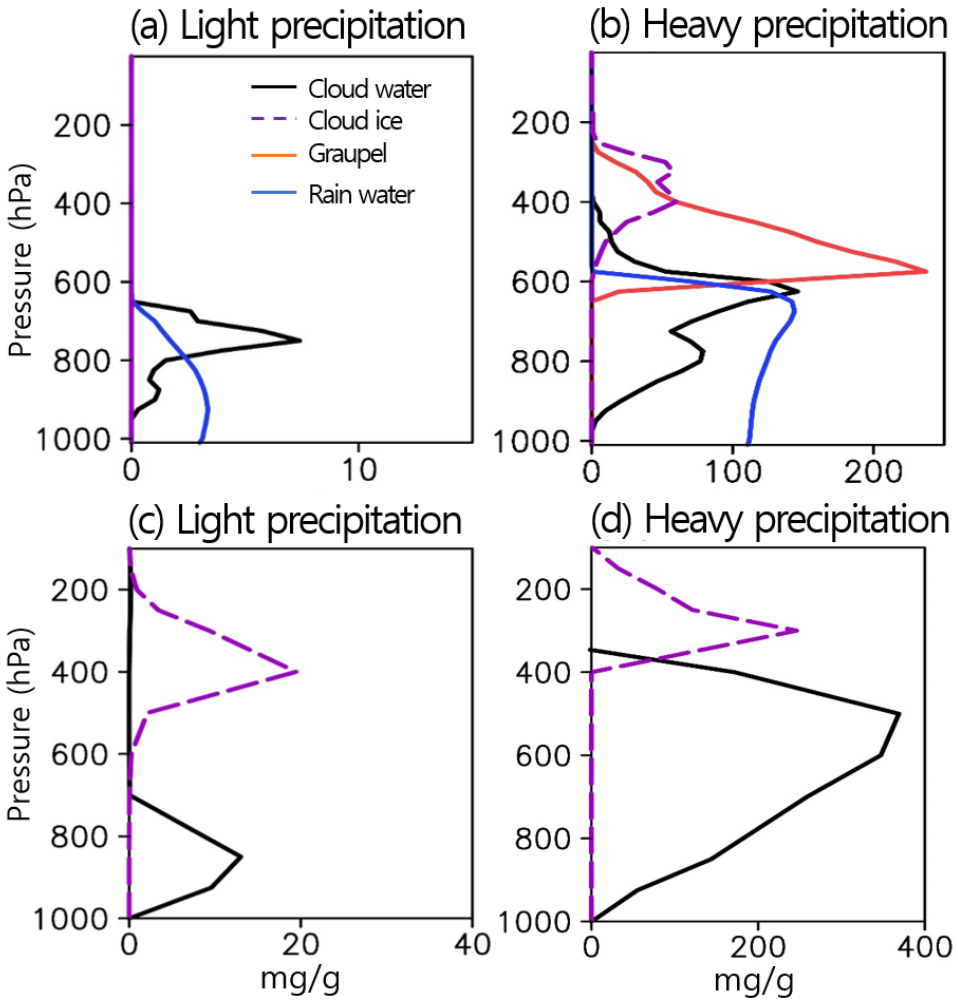

Fig. 5.4. Composite of cloud hydrometeors (mg g^{-1}) of the CRM (a, b) and GCM with parameterizations (c, d) for light (left) and heavy (right) precipitation events.

The corresponding vertical distributions of the hydrometeors for the GCM with the conventional parameterization are shown in Figs. 5.4c and 6d for the light and heavy precipitation, respectively. It is noted that the hydrometeors in the present GCM are confined to the cloud water and ice. As seen in Fig. 5.4c, the GCM light rain is made from cloud ice in the deep cloud as well as from the cloud water in the lower layer. This result confirms that the GCM produces too much light rain because of too frequent generation of deep cloud, and this appears to be a problem of the GCM rain process. For the heavy precipitation, the GCM rainfall is mainly resulted from the cloud water, which is 50% more than that of the CRM. In the CRM, this 50% cloud rain is contributed from the graupel. The cloud ice is located above 400 hPa, which is higher than that of the CRM, and the cloud ice content is also much more (about 3 times more) than that of the CRM. A part of GCM cloud ice is contributed from the graupel in the CRM. Those results combined with the results of Fig. 5.1 indicate that the graupel play an important role for the rain process but is a missing hydrometeor in the GCM.

5.2 Resolution dependency of cloud microphysics

We examined the resolution dependency of cloud microphysics using the CRM simulations with different horizontal resolutions. Figure 5.5 shows vertical structure of domain-mean specific humidity, temperature and vertical velocity

from the CRMs. The domain-mean temperature and specific humidity are averaged for all grids of the domain but the domain-mean vertical velocity is averaged by using grids where vertical velocity is positive. The domain-mean vertical motion is weakened with horizontal resolution decreasing. The coarse resolution CRMs produce moisture less and temperature warmer than those of the CRM with 1-km resolution. The big dry bias in the lower troposphere is related to relatively small moisture from the boundary layer level to the free atmosphere. The small vertical transport is due to the relatively small vertical wind associated with the raw horizontal resolution (50 km) of the CRM, compared to that of the CRM with a resolution of 1 km. Figure 5.6 and 5.7 shows the vertical profile of cloud hydrometeor and dominant microphysical processes from the CRMs. The domain-averaged values are used in these figures. The CRM with 50-km resolution produces not only condensation, accretion and melting processes but also rain water and graupel amount less than those of 1-km CRM. It is noted that cloud water is not changed because both condensation and associated accretion processes are reduced. Two reasons for reduction of condensation were suggested. One is due to less saturation by large grid size. Saturation occurs hardly at the 50 km grid size and therefore condensation is decreased. The other is due to dry and warm condition in the lower troposphere by relatively weak vertical motion and thus condensation amount is reduce at the

50-km CRM. On the other hand, two reasons for reduction of accretion of cloud water by rain water (or graupel) were suggested. One is due to too strong falling effect of rain water (or graupel). Because of relatively vertical motion, rain water or graupel tends to fall down to the surface, resulting in decrease of rain water or graupel and therefore less accretion of cloud water processes. A poor representation of terminal velocity contributes to strong falling effect of cloud hydrometeor. The magnitude of terminal velocity is proportional to size of cloud hydrometeor. The microphysics used in the present study assumed that size distribution is fixed due to single momentum approach. However, the size distribution is dependent on model horizontal resolution. For example, at coarse resolution the sub-grid variability of cloud hydrometeor contents in each grid box is large. In other word, some portion of cloud hydrometeor contents is much larger or smaller than grid-mean value in a grid. Because of logarithmic relationship between cloud hydrometeor and terminal velocity (Lin et al. 1983), the modified grid-mean terminal velocity considering sub-grid variability is smaller than the original grid-mean terminal velocity. Therefore, at coarse resolution the terminal velocity should by reduced compared to that of the 1-km CRM. The other is due to decrease of cloud water by less condensation. In the next section, various modifications of cloud microphysics were suggested for coarse resolution and examined their impact.

5.3 Modification of cloud microphysics

The effects of the modification in cloud microphysics were examined using the 50-km CRM. Various modifications in the cloud microphysics were suggested to reduce the resolution dependency: increase of condensation, decrease of terminal velocity, increase of accretion processes. As discussed above, saturation tends to hardly occur at large grid size. However, some part of a grid may be saturated due to sub-grid scale variability of specific humidity at coarse resolution, although grid-mean relative humidity is less than 100%. In order to consider the sub-grid scale variability of specific humidity, we implemented the GCM parameterization used in the large-scale condensation scheme (Le Treut and Li (1991) instead of the original condensation process of the CRM. The parameterization assumes a uniform distribution of specific humidity between a certain value from grid-mean value. The formula of cloud fraction is as follows :

$$C_{frc} = \begin{matrix} 0 & ,(1+b)\bar{q} \le \overline{q^*} \\ \dfrac{(1+b)\bar{q} - \overline{q^*}}{2b\bar{q}} & ,(1-b)\bar{q} < \overline{q^*} < (1+b)\bar{q} — \\ 1 & ,(1-b)\bar{q} \ge \overline{q^*} \end{matrix} \tag{5.1}$$

where $\bar{q}$ refers grid-mean specific humidity, $\overline{q^*}$ saturation of grid-mean specific humidity and b is determined by mixing length,

$$\mathrm{b} = \varepsilon\lambda^{-1}\left(\frac{\kappa z}{1+kz/\lambda}\right) \tag{5.2}$$

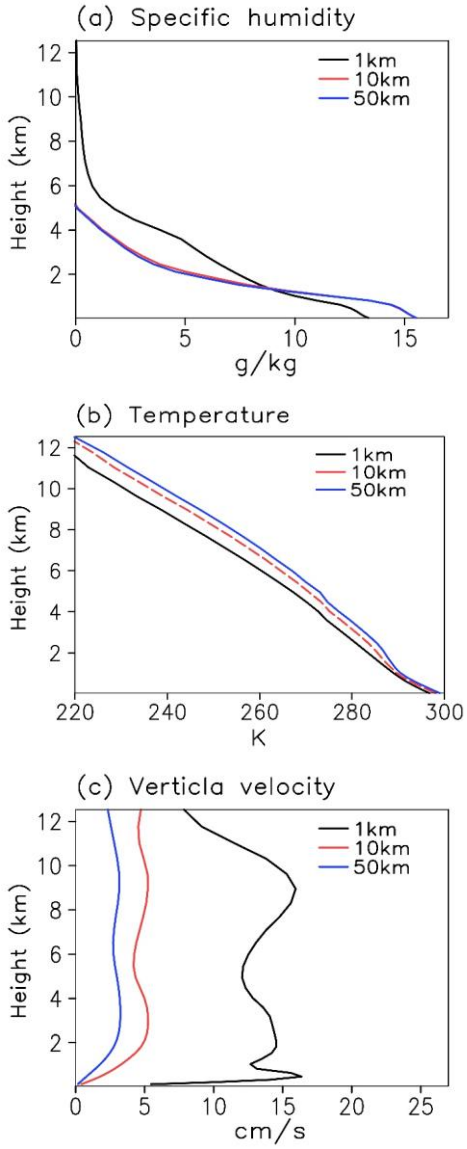

Fig. 5.5. Vertical profile of domain-mean specific humidity, temperature and vertical velocity from the CRMs with different horizontal resolutions. The vertical velocity is averaged by using the grid where vertical velocity is positive.

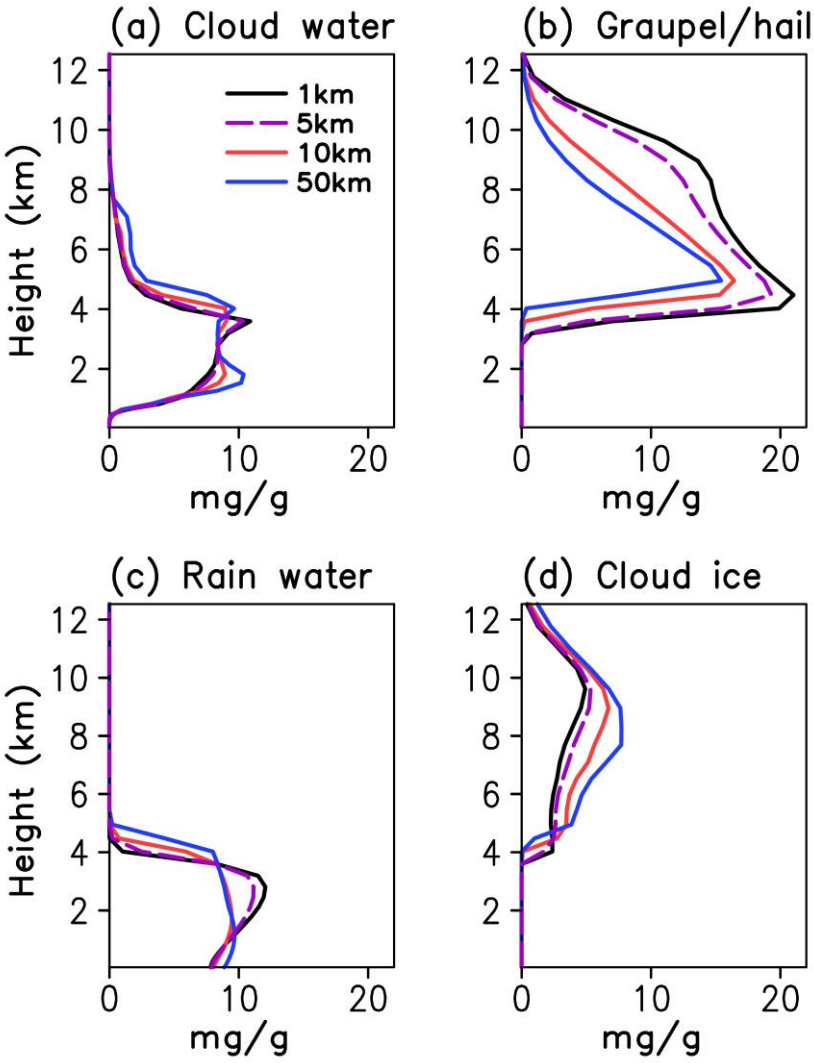

Fig. 5.6. Vertical profile of domain-mean cloud hydrometeors in the CRMs with different resolutions.

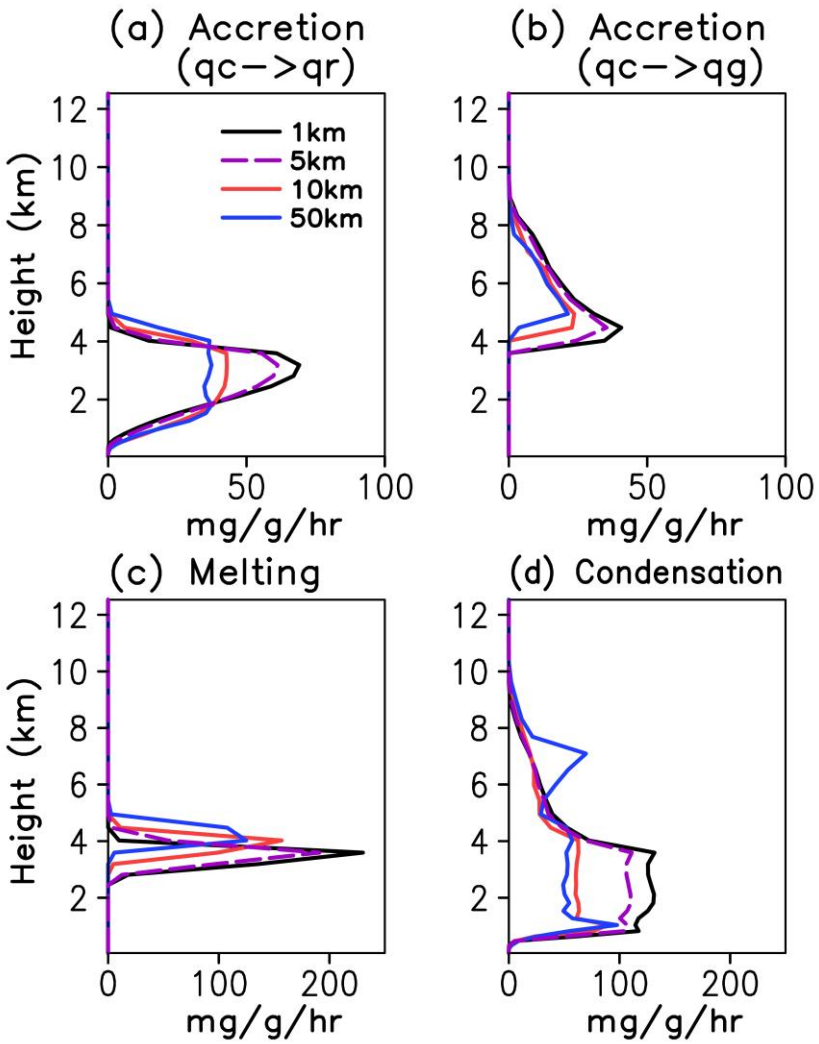

Fig. 5.7. Vertical profile of domain-mean cloud microphysical processes in the CRMs with different resolutions. (a) accretion of cloud water by rain water, (b) accretion of cloud water by graupel, (c) melting of graupel and (d) condensation process.

where λ refers neutral mixing length, 300 m, κ von Karman constant, z height. The range of grid-mean specific humidity is determined by an empirical constant, ε. The original value of ε in Le Treut and Li (1991) is 0.25 for 300km grid size. Because the grid size used in the present study is much smaller than 300km, we use 0.15 of ε in the 50-km CRM. The formula of condensation amount is as follows:

$$q_c = \begin{matrix} 0 \\ \dfrac{((1+b)\bar{q} - \overline{q^*})^2}{4b\bar{q}} \\ \overline{q^*} - \bar{q} \end{matrix} \quad \begin{matrix} ,(1+b)\bar{q} \le \overline{q^*} \\ ,(1-b)\bar{q} < \overline{q^*} < (1+b)\bar{q} — \\ ,(1-b)\bar{q} \ge \overline{q^*} \end{matrix} \qquad (5.3)$$

In the 50-km, it is assumed that condensation and evaporation occurs concurrently within a grid box due to large grid size. The fraction of condensation in a grid is C_{frc} and therefore the fraction of evaporation is $\left(1 - C_{frc}\right)$. The formula of evaporation is as follows:

$$q_{evap} = \begin{matrix} \overline{q^*} - \bar{q} \\ \dfrac{(\overline{q^*} - (1-b))^2}{4b\bar{q}} \\ 0 \end{matrix} \quad \begin{matrix} ,(1+b)\bar{q} \le \overline{q^*} \\ ,(1-b)\bar{q} < \overline{q^*} < (1+b)\bar{q} — \\ ,(1-b)\bar{q} \ge \overline{q^*} \end{matrix} \qquad (5.4)$$

The 50-km CRM simulation with the modification of condensation is called as to 'COND'. Second, we modified terminal velocity because the accretion processes depends on terminal velocity. Vertical motion in the 50-km CRM is weaker than that of the 1-km CRM and therefore the cloud hydrometeors fall to the surface

more quickly compared to that of the 1-km CRM. Also, the subgrid variability of cloud hydrometeor contents is relatively large at the coarse resolution, terminal velocity using grid-mean cloud hydrometeor content is overestimated. When terminal velocity has a relatively small value, the duration time is increased, which leads to increase of accretion. The original formulation of the terminal velocity is as follows (Lin et al, 1983):

$$U_R = \frac{a\Gamma(4+b)}{6\lambda_R^b}\left(\frac{\rho_0}{\rho}\right)^{1/2}, \qquad \lambda_R = \left(\frac{\pi\rho_w n_{oR}}{\rho q_R}\right)^{0.25} \tag{5.5}$$

$$U_S = \frac{\mathrm{c}\Gamma(4+d)}{6\lambda_S^d}\left(\frac{\rho_0}{\rho}\right)^{1/2}, \qquad \lambda_S = \left(\frac{\pi\rho_S n_{oS}}{\rho q_S}\right)^{0.25} \tag{5.6}$$

$$U_G = \frac{\mathrm{e}\Gamma(4,5)}{6\lambda_G^{0.5}}\left(\frac{4g\rho_G}{3C_D\rho}\right)^{1/2}, \qquad \lambda_G = \left(\frac{\pi\rho_G n_{oG}}{\rho q_G}\right)^{0.25} \tag{5.7}$$

where n_{oR}, n_{oS} and n_{oG} refer to the intercept parameters of the rain, snow and graupel size distributions, respectively. q_R, q_S and q_G refer to mixing ratio of water, snow and graupel, respectively. ρ_{oR}, ρ_{oS} and ρ_{oG} refer to densities of rain, snow and graupel particles of size distribution, respectively. λ_{oR}, λ_{oS} and λ_{oG} refer to slop parameters of rain, snow and graupel particles of size distribution, respectively and a, b, c, d, e is empirical constants. In the present study, we used 75% of original values for a, c, and e and their effects are examined using the 50-

km CRM. It is noted that the CRM produces too much accretion processes for very small terminal velocity, because the cloud hydrometeors stay for too long time in the atmosphere. Therefore, it is important to find proper value of the constants. The CRM simulation with the modification of terminal velocity is called as to 'FVEL'. Third, we examined the effect of increased accretion processes on the resolution exponentially as particle size increases. Ladino et al. (2011) and Wang et al. (2010) showed that the collection efficiency decreases linearly particle size. Therefore, when the collection efficiency is calculated by considering the sub-grid variability of particle size, its value is larger than that of grid-mean particle size. The formula of the original accretion process of cloud water by rain water is as following :

$$P_{RACW} = \frac{\pi}{4} q_c E_{RW} n_{oR} \left(\frac{\rho_0}{\rho}\right) \left[\frac{a_0 \Gamma(3)}{\lambda_R^3} + \frac{a_0 \Gamma(4)}{\lambda_R^3} + \frac{a_0 \Gamma(5)}{\lambda_R^3} + \frac{a_0 \Gamma(6)}{\lambda_R^3}\right] \qquad (5.6)$$

where, q_c refers to mixing ratio of cloud water, E_{RW} collection efficiency of graupel for cloud water (approximate to 1), a_0 empirical constant. At coarse resolution, particle size is relatively small, resulting in large collection efficiency and therefore more accretion. In the present study, we simply use two times as the original value of the collection efficiency, in order to increase accretion process. On the other hand, the collection efficiency of graupel for cloud water should be increased at coarse resolution, as discussed above. The formula of the

original accretion process of cloud water by graupel is as following :

$$P_{GACW} = \frac{\pi q_c E_{GW} n_{oG} f_0 \Gamma(3+\mathrm{f})}{4\lambda_G^{3+f}} \left(\frac{\rho_0}{\rho}\right) \tag{5.9}$$

where, E_{GW} refers to collection efficiency of graupel for cloud water (approximate to 1), f_0 and f empirical constants. We use two times as the original value, in order to increase the accretion amount. The CRM simulations with the modification of accretion of cloud water by and rain water and graupel are called as to the 'RACW' and 'GACW', respectively. Figure 5.9 shows vertical structure of domain-mean specific humidity and temperature from the CRMs with various modification of cloud microphysical processes. The temperature and specific humidity are averaged for all grids of the domain. All modification does not improve the dry bias; moisture less in the lower troposphere and moisture more than in the boundary layer. The increase of condensation only improves the warm bias. The results indicates that modifications of cloud microphysics do not reduce the resolution dependency. Figure 5.10 shows the budget of dominant cloud microphysical processes and cloud hydrometeors from the 50-km CRM with various modification of cloud microphysics. The all values are vertically integrated. The COND produces much more saturation amount than that of the original 50-km CRM, which is closer to that of 1km CRM. Since condensation

process is one of major sources in the microphysical system (see Fig. 5.1), increase of condensation increases cloud water and accretion of cloud water by rain water and graupel, and therefore rain water and graupel is increased closer to those of the 1-km CRM. The FVEL increases not only graupel and rain water amount but also accretion processes due to decrease of terminal velocity. However, the RACW does not increase rain water and graupel. The RACW contributes to increasing accretion of cloud water by rain water, whereas it reduces the accretion of cloud water by graupel, resulting in decrease of graupel and therefore less melting of graupel. As a result, the increase of accretion of cloud water by rain water is cancel by decrease of melting of graupel. Because of these opposite effects, the RACW does not reduce the resolution dependency. Similarly, the GACW also has no effect to reduce resolution dependency.

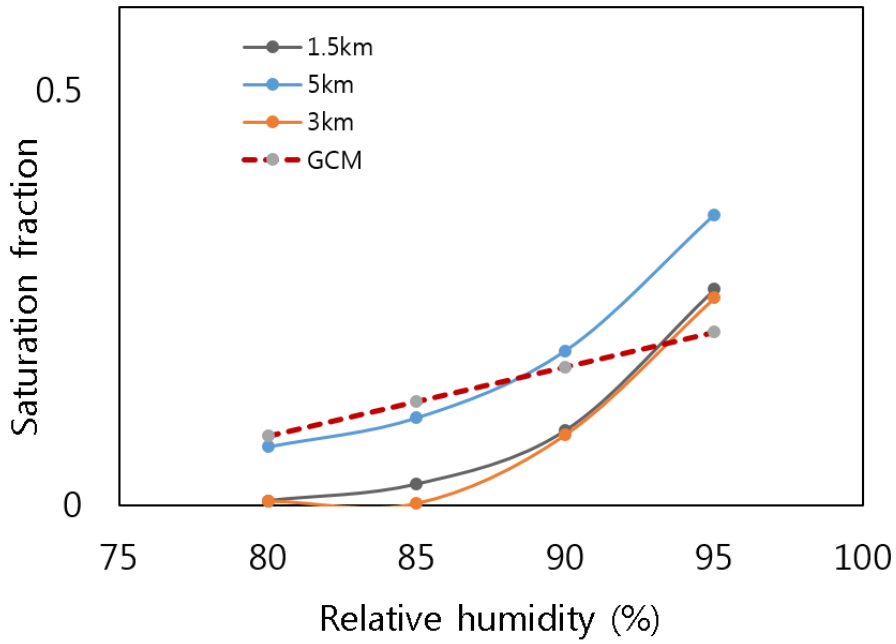

Fig. 5.8. Saturation fraction as a function of relative humidity for each vertical level. 1km horizontal resolution CRM is used for calculating saturation fraction at 50km horizontal resolution.

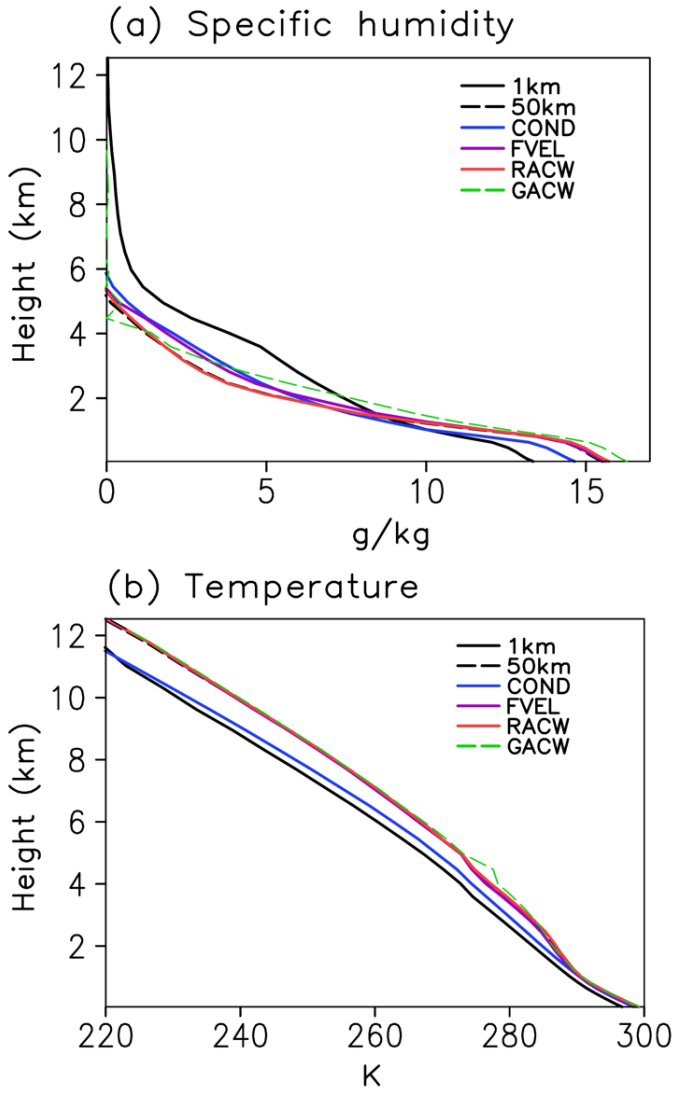

Fig. 5.9. Vertical profile of (a) specific humidity and (b) temperature from 50km CRMs with different modifications and 1km CRM. The solid black line is 1km CRM, dashed black line is 50km CRM, solid blue line is 50km CRM with modified condensation, solid purple line is 50km CRM with modified terminal velocity, solid red line is 50km CRM with modified accretion of cloud water by rain water and dashed green line is 50km CRM with modified accretion of cloud water by graupel.

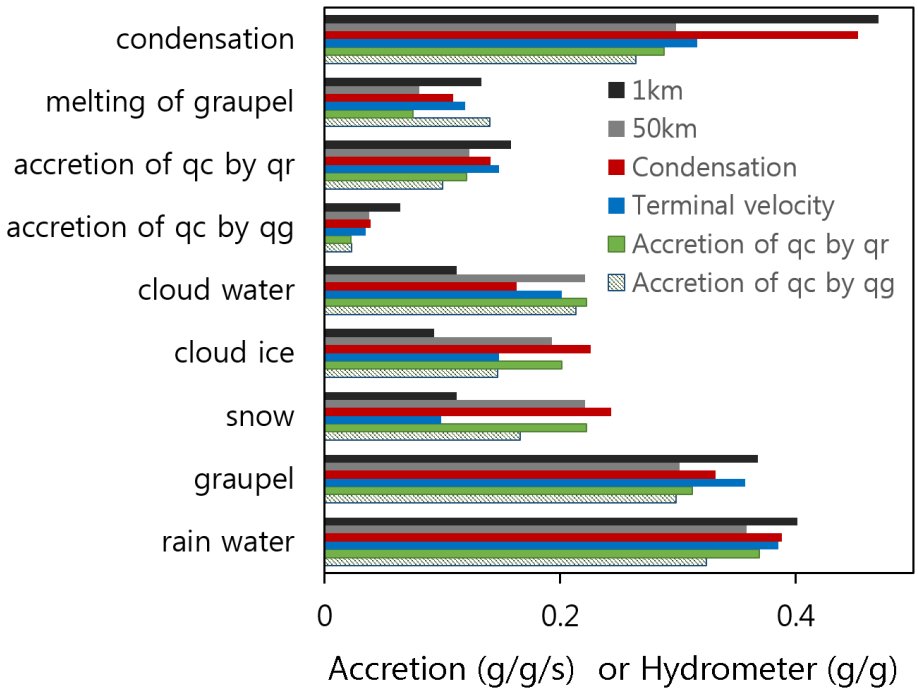

Fig. 5.10. Vertical integrated values of microphysical processes and hydrometeors of 50km CRMs with different modifications and 1km CRM. The black is 1km CRM, gray is 50km CRM, red is 50km CRM with modified condensation, blue is 50km CRM with modified terminal velocity, green is 50km CRM with modified accretion of cloud water by rain water and dashed purple is 50km CRM with modified accretion of cloud water by graupel.

5.4 Convective scheme for increase of vertical mixing

5.4.1 Diffusion type of shallow convective scheme

As discussed in the previous section, in order to increase insufficient vertical transport of moisture between boundary layer and free atmosphere, a diffusion type of convective scheme based on Tiedke (1984) was implemented in the CRM to increase vertical mixing. The formula is as follows:

$$\left(\frac{\partial \bar{s}}{\partial t}\right) = \frac{1}{\bar{\rho}}\frac{\partial}{\partial z}\left\{\bar{\rho}K\frac{\partial}{\partial z}\left(\bar{s} - L\bar{l}\right)\right\} \tag{5.10}$$

$$\left(\frac{\partial \bar{q}}{\partial t}\right) = \frac{1}{\bar{\rho}}\frac{\partial}{\partial z}\left\{\bar{\rho}K\frac{\partial}{\partial z}\left(\bar{q} + \bar{l}\right)\right\} \tag{5.11}$$

where s refers to dry static energy, l cloud water, K coefficient of diffusion. The dry bias in the 50-km CRM exists in the lower troposphere, coefficients of diffusion are modified. The coefficients have relatively large values (1.5) in the PBL and they gradually decrease with the height and then become 0 at cloud top, which generally is located at middle level. The CRM simulation with the convective scheme is called as to the 'CONV_DIFF'.

5.4.2 Modified BULK scheme

A conventional parameterization was used in order to increase vertical transport of moisture. In the present study, the BULK scheme developed by Kim and Kang (2012) was modified for cloud microphysics. First, the two cloud hydrometeors, cloud water and water vapor are vertically transported by cloud model in the original scheme, whereas all cloud hydrometeors are included in the cloud model. Second, as ice-phase cloud hydrometeors are included, a frozen moist static energy is used for buoyancy and vertical velocity. Third, rain process in the cloud is calculated by cloud microphysics of the CRM. It is noted that condensation amount is determined by the method of Arakawa and Schubert (1974). The cloud model determines in-cloud properties, such as, the normalized mass flux profile, temperature. We employed an entraining-detraining plume model equations

$$\frac{\partial \eta}{\partial z} = (\varepsilon - \delta)\eta \tag{5.12}$$

$$\frac{\partial h_u}{\partial z} = -\varepsilon\left(h_u - \bar{h}\right) \tag{5.13}$$

where η refers to the normalized mass flux, ε and δ fractional entrainment and detrainment rates respectively. In Eq. 5.13, h_u represent frozen moist static energy in the convective updraft, which is the sum of the liquid/ice water static

energy and the total condensate amount times the latent heat of vaporization. At cloud-base level, it is assumed that h_u equals frozen moist static energy in the environment, $\bar{h}$. The frozen moist static energy in the environment is defined as followes:

$$\bar{h} = \bar{s} + L_c\overline{q_v} - L_f\left(\overline{q_i} + \overline{q_s} + \overline{q_g}\right) \tag{5.14}$$

where, L_c and L_f refer to the latent heat of condensation and fusion, respectively, $\overline{q_v}$, $\overline{q_c}$, $\overline{q_i}$, $\overline{q_r}$, $\overline{q_s}$ and $\overline{q_g}$ water vapor, cloud water, cloud ice, rain water, snow and graupel in the environment, respectively, $\bar{s}$ is dry static energy; that is,

$$\bar{s} = c_p\bar{T} + gz \tag{5.15}$$

where, g refers to the gravitational constant, z the height, $\bar{T}$ the temperature in the environment, c_p the heat content constant. For cloud hydrometeors, plume model equations considering source or sink of cloud hydrometeor by microphysical processes are adapted. Cloud base and cloud top is determined by cloud vertical velocity. Cloud base is defined as the level where cloud water exist and cloud vertical velocity is positive. Cloud top is defined as the level where cloud vertical velocity is negative. The vertical velocity equation of the updraft parcel is given by (Simpson and Wiggert 1969, Gregory 2001)

$$\frac{1}{2}\frac{\partial w_u^2}{\partial z} = a(1 - C_\varepsilon b)B_u \tag{5.16}$$

where a and b are constants which are specified here as a = 1/6 and b = 2. C_ε is the conversion factor of the kinetic energy generated by buoyancy to entrained air (Gregory 2001). Kim and Kang (2012) assumed a simple dependency of C_ε on environmental humidity, such that

$$C_\varepsilon = \left(\frac{1}{\overline{RH}} - 1\right) \tag{5.17}$$

where $\overline{RH}$ refers to the relative humidity in the environment. B_u is the buoyancy of the updraft parcel, defined as

$$B_u = \frac{g}{\overline{T_v}}(T_{vu} - \overline{T_v}) \tag{5.18}$$

where, and $\overline{T_v}$ the virtual temperature in the environment, T_{vu} virtual temperature of convective updraft. For a parcel in the updraft, virtual temperature of convective updraft is given by

$$T_{vu} = T_u\left(1 + 0.608q_{vu} - q_{iu} - q_{ru} - q_{su} - q_{gu} - q_{cu}\right) \tag{5.19}$$

which includes the loading of condensation water in form of cloud water, cloud ice, rain water, snow and graupel. T_u is diagnosed using the definition of h_u

$$T_u = \frac{\left(h_u - gz - L_c q_{vu} + L_f\left(\overline{q_\iota} + \overline{q_s} + \overline{q_g}\right)\right)}{c_p} \tag{5.20}$$

Similarly, $\overline{T_v}$ is defined as

$$\overline{T_v} \quad = \bar{T}\left(1 + 0.608\overline{q_v} - \overline{q_\iota} - \overline{q_r} - \overline{q_s} - \overline{q_g} - \overline{q_c}\right) \tag{5.21}$$

Gregory (2001) suggested fractional entrainment rate parameterization based on budgets of cumulus vertical velocity as

$$\varepsilon = \frac{C_\varepsilon a g}{w_u^2} B_u \tag{5.22}$$

where a refers a constant. A value of 0.25 is used in Gregory (2001). It is assumed that the detrainment occurs when parcel buoyancy decreases with height (Bretherton and Smolarkiewicz 1989)

$$\delta = \varepsilon + \frac{1}{z_t - z},\ z_{Bmax} \le z \le z_t \tag{5.23}$$

where z_{Bmax}, z_t refers to the maximum buoyancy height, respectively.

For cloud hydrometeors, entraining-detraining plume model equations is as follows:

$$\frac{\partial q_{vu}}{\partial z} = -\varepsilon(q_{vu} - \bar{q}) + S_{vu} \tag{5.24}$$

$$\frac{\partial q_{cu}}{\partial z} = -\varepsilon(q_{cu} - \bar{q}) + S_{cu} \tag{5.25}$$

$$\frac{\partial q_{iu}}{\partial z} = -\varepsilon(q_{iu} - \bar{q}) + S_{iu} \tag{5.27}$$

$$\frac{\partial q_{ru}}{\partial z} = -\varepsilon(q_{ru} - \bar{q}) + S_{ru} \tag{5.29}$$

$$\frac{\partial q_{su}}{\partial z} = -\varepsilon(q_{su} - \bar{q}) + S_{su} \tag{5.30}$$

$$\frac{\partial q_{gu}}{\partial z} = -\varepsilon\left(q_{gu} - \bar{q}\right) + S_{gu} \tag{5.31}$$

Where q_{vu}, q_{cu}, q_{iu}, q_{ru}, q_{su} and q_{gu} refers to water vapor, cloud water, cloud ice, rain water, snow and graupel in the updraft, respectively, S_{vu}, S_{cu}, S_{iu}, S_{ru}, S_{su} and S_{gu} is source/sink term for water vapor, cloud water, cloud ice, rain water, snow and graupel in the in-cloud, respectively. Now, we focused on source or sink term, S_{iu} (i refers to cloud hydrometeors). It is defined as changed amount due to microphysical processes. Because the air is saturated in the clouds (Arakawa and Schubert 1974), water vapor amount (q_{vu}) raised from the cloud bottom is reduced to saturation water vapor (q_{vs}) and the rest of water vapor of the updraft is converted to cloud water or ice; that is :

$$q_{vs} = \overline{q_{vs}} + \frac{\gamma}{1+\gamma}\frac{1}{L_c}\left[h_u - \overline{h_s} + L_f\left(q_{iu} + q_{su} + q_{gu}\right)\right] \tag{5.32}$$

where $\overline{q_{vs}}$ refers to saturation water vapor in the environment, $\overline{h_s}$ saturation moist static energy, γ the rate of change of $\overline{q_{vs}}$ as a function of $\bar{T}$ on a constant pressure surfrace. $\overline{h_s}$ is defined as

$$\overline{h_s} = \bar{s} + L\overline{q_{vs}} \tag{5.33}$$

The changed amount of water vapor is converted to cloud water or ice dependent on the temperature. It is assumed that condensation occurs if the in-cloud temperature is warmer than 0°C, deposition takes place if the temperature is

colder than -20°C. The cloud water and ice are allowed to coexist between -20°C and 0°C. Rain water, snow and graupel is updated by microphysical process using the changed cloud water and ice. The changed amount for cloud hydrometeors is defined as

$$dq_{vu} = (M(q_{vu}) - q_{vu}) \tag{5.34}$$

$$dq_{cu} = (M(q_{cu}) - q_{cu}) \tag{5.35}$$

$$dq_{iu} = (M(q_{iu}) - q_{iu}) \tag{5.36}$$

$$dq_{su} = (M(q_{su}) - q_{su}) \tag{5.37}$$

$$dq_{ru} = (M(q_{ru}) - q_{ru}) \tag{5.38}$$

$$dq_{gu} = \left(M(q_{gu}) - q_{gu}\right) \tag{5.39}$$

Where $M(q_{xu})$ refers to the updated q_{xu} by microphysical processes and x represents water vapor, cloud water, cloud ice, rain water, snow and graupel in the updraft, respectively, dq_{xu} changed cloud hydrometeors amount by microphysics. The sink/sour term S_{iu} is define as dq_{iu} divided by Δz. In cloud, because air is saturated, evaporation and sublimination At cloud-base, in-cloud temperature and cloud microphysics is defined as sum of grid-mean value and excesses from the surface layer.

$$\emptyset_c = \overline{\emptyset} + b\frac{\overline{w'\emptyset'_s}}{\sigma_w} \tag{5.40}$$

where, $\emptyset$ refers to the temperature and cloud hydrometeors and $\overline{w'\emptyset_s'}$ the surface flux.

Figure 5.12 shows vertical structure of domain-mean specific humidity and temperature from the CRMs with different convective schemes. The temperature and specific humidity are averaged for all grids of the domain. Both convective schemes improve the vertical distribution of moisture. The vertical profiles of the CRM with convective schemes are similar to that of the 1km CRM. The warm bias of temperature is also reduced. Figure 5.13 shows the budget of dominant cloud microphysical processes and cloud hydrometeors from the 50-km CRM with various convective schemes. The all values are vertically integrated. Both of convective schemes increase produces saturation and accretion amount much more than that of the original 50-km CRM, which is closer to that of 1km CRM. The dry and warm bias that is simulated in the original 50-km CRM is reduced because the convection scheme mixes the moisture and temperature between the PBL and free atmosphere. Increase of moisture leads to increase of condensation. The accretion processes is also increased by increase of condensation and accretion by increased vertical motion. These results indicates that modification of condensation, terminal velocity and increase of sub-grid scale vertical mixing are effective to reduce resolution dependency and produce realistic simulation in the 50-km CRM.

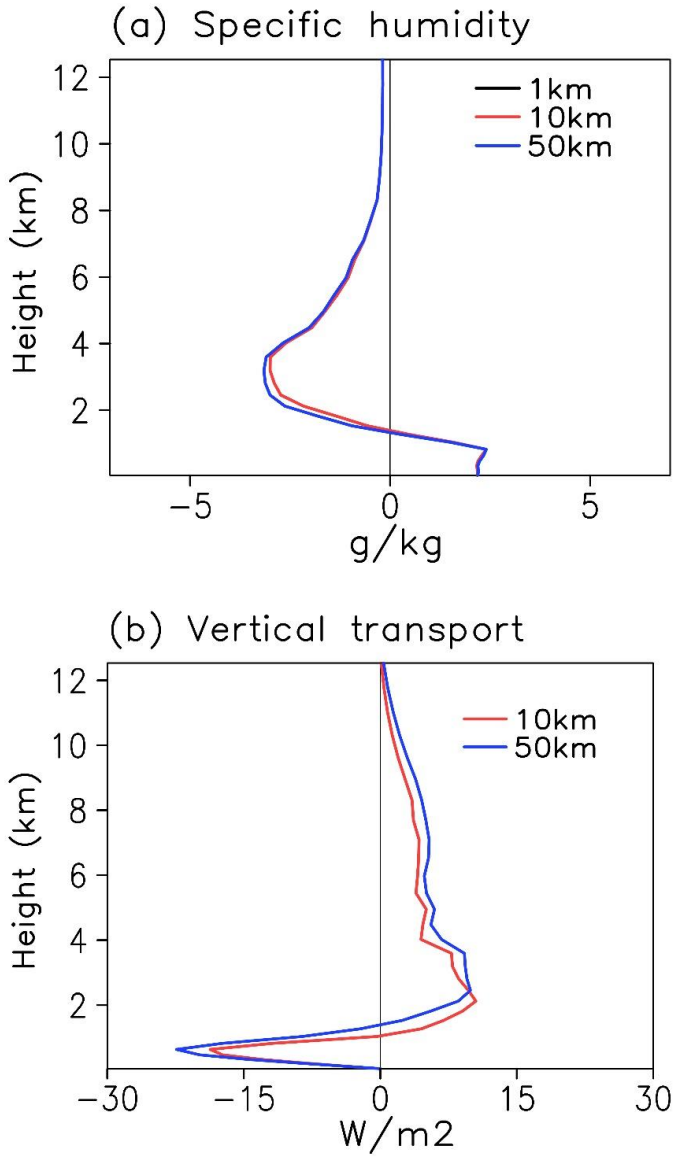

Fig. 5.11. Difference of specific humidity (q) and vertical transport of specific humidity ($\rho L\overline{wq}$) between 1km and other horizontal resolutions (10km and 50km) CRM.

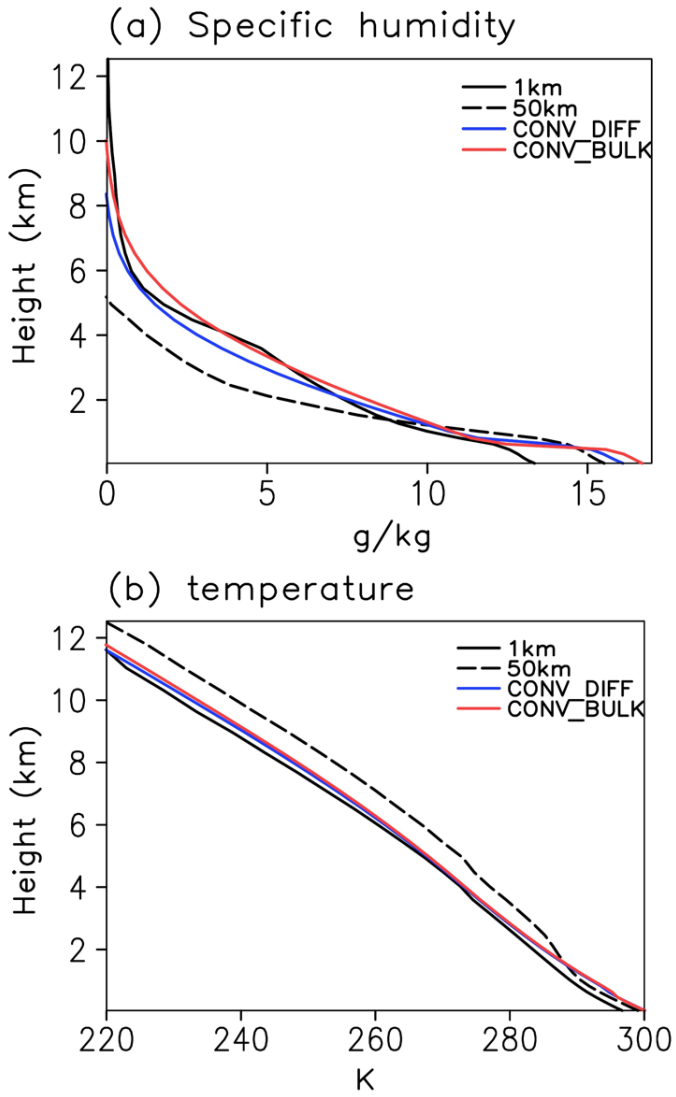

Fig. 5.12. Vertical profile of (a) specific humidity and (b) temperature from 50km CRMs with different modifications and 1km CRM. The solid black line is 1km CRM, dashed black line is 50km CRM, solid blue line is 50km CRM with diffusion type of shallow convection, solid red line is 50km CRM with the modified BULK scheme.

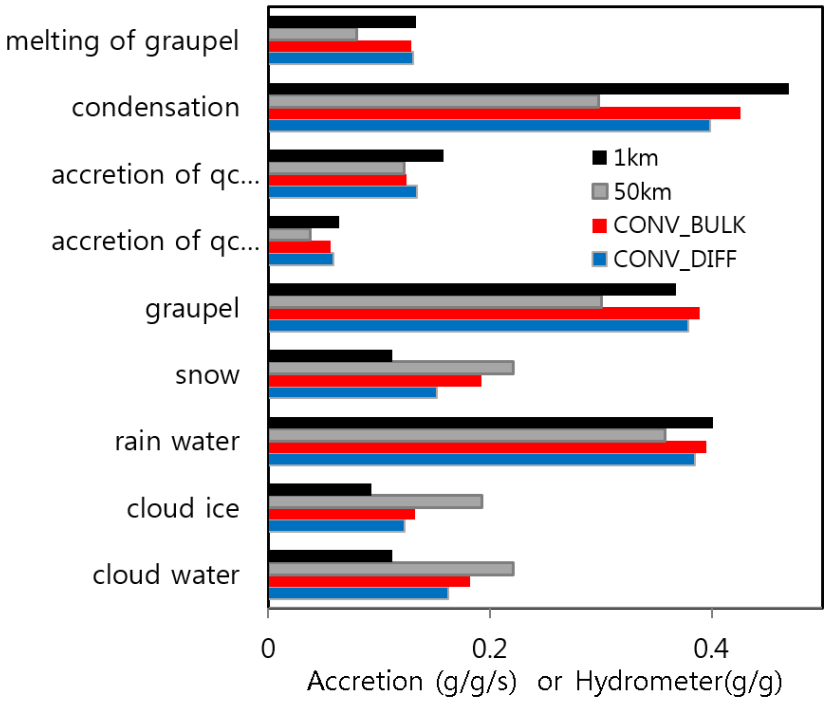

Fig. 5.13. Vertical integrated values of microphysical processes and hydrometeors of 50km CRMs with different modifications and 1km CRM. The black is 1km CRM, gray is 50km CRM, blue is 50km CRM with diffusion type of shallow convection, red is 50km CRM with the modified BULK scheme.

CHAPTER 6

High resolution GCM with cloud microphysics

6.1 Time step dependency of cloud microphysics in a GCM

To examine the effect of time step on cloud microphysics, sensitivity of GCM with different time step is performed. The time step for a conventional GCM is generally 20-30 minutes, whereas the time step for cloud microphysics is a few seconds. It is noted that Satoh and Matsuda (2009) suggested that 30 second of time step is acceptable for 14km horizontal resolution global CRM. Cloud microphysics is developed based on a few second time step, while other parameterization is based on 30 minutes. Therefore, sub-time step is used for cloud microphysics. Because of limitation of computing resources, the simulations of the GCM with cloud microphysics were examined different sub-time steps. Figure 6.1 shows vertical structure of cloud hydrometeor of GCM with different sub-time step for cloud microphysics. When relatively large sub time step is used, all cloud hydrometeor are significantly overestimated. Cloud

water in the model is far larger than the observation. Particularly, the model produces snow and graupel largely at lower level, which is unrealistic feature compared to the CRM because most of graupel and snow is melted in middle level (600 hPa).

Because of adapted large time step for cloud microphysics, most of graupel and snow falls down without melting processes due to their large terminal velocity. When 300 s of time step is used, the vertical profile of cloud water is reduced and similar to that of the observation. The graupel and snow is melted at middle level and they are not found at lower level. When time step is reduced up to 30s, all cloud hydrometeor exception rain water are similar to that of 300s of time step. We also eximined the relationship between sub-time step and computing time of the GCM. With the sub-time step decreasing, the number of sub-cycle, which is defiend as the ratio of model time step (1800s) to sub time step, is increased and computing time is incrased. The results shwo that as sub-time step is reduced, the computing time gradually increases unto 300s and then it increases rapidly due to large number of sub-cycling. The relationship between sub-time step and the Root-Mean-Square-Error (RMSE) of annual mean precipitation from the GCM with cloud microphysics. The TRMM data is used for observation.

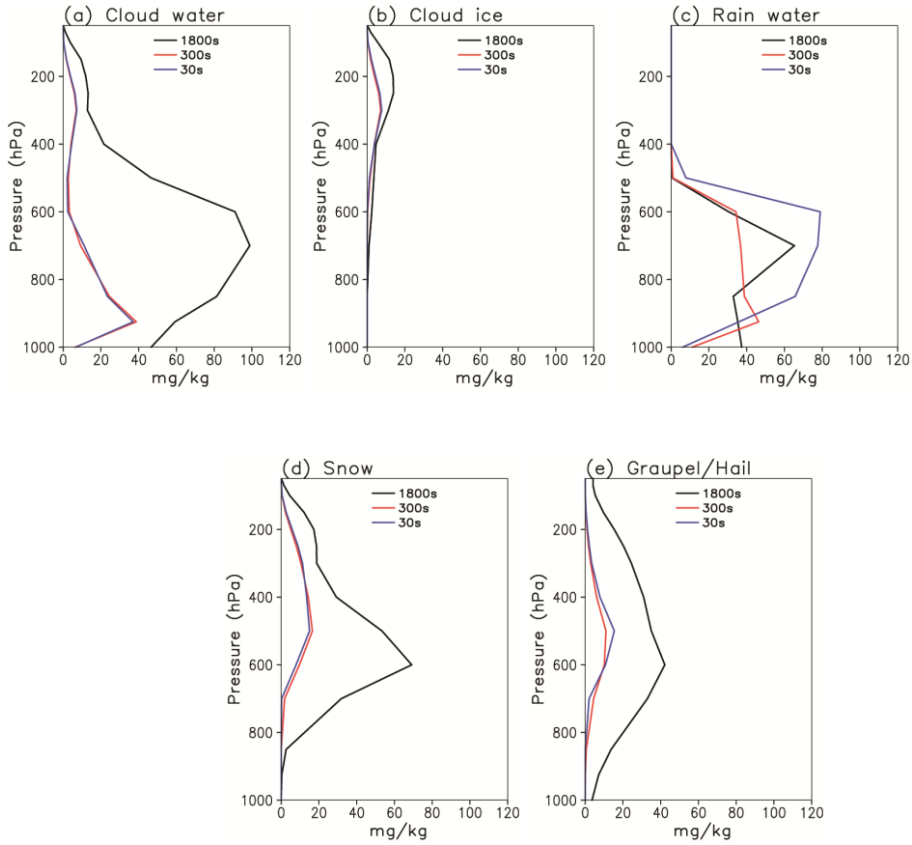

Fig. 6.1 Sensitivity of different sub time step on cloud hydrometeors in the GCM with cloud microphysics and convective scheme

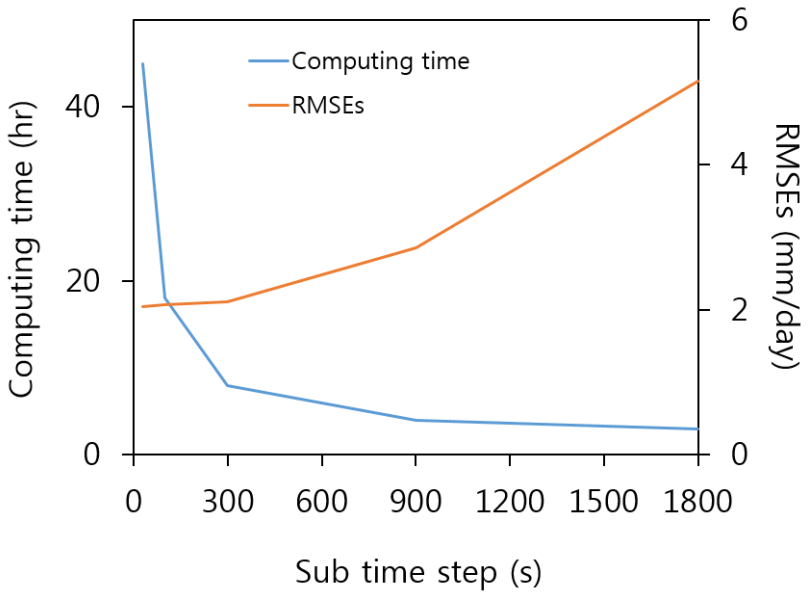

Fig. 6.2 Computing time and RMSE as a function of sub-time step for cloud microphysics. RMSE is calculated over global region and computing time is based on 1month integration of the GCM with 50km horizontal resolution when 128 CPUs are used.

When large time step is used for cloud microphysics, most of cloud hydrometeors is not increased but decayed by falling down the surface due to fast terminal velocity. Therefore, mean precipitation is much less than the observation and the RMSEs have large values. The Fig. 6.2 (red) shows that the RMSEs is reduced rapidly unto 300s of sub-time step and then it is slowly decreased. When the 300s of sub-time step is used, the GCM with cloud microphysics produce the computing time (8 hour)larger and the RMSE (2.11 mm/day) smaller than those of the GCM with the conventional parameterization, respectively (2 hour and 2.62 mm/day). From those results, when the 300s of sub-time step is used for cloud microphysics, the model produces reasonable simulated precipitation with an acceptable computing time.

6.2 Global simulation of the high resolution GCM

6.2.1 The precipitation climatology

The cloud microphysics of the CRM was implemented in a GCM instead of a conventional parameterization (convective and large-scale scheme). In other words, the convective parameterization and large-scale precipitation is removed in a GCM and moist physical processes is only represented by cloud microphysics. The GCM simulations with microphysics were compared to the GCM with a conventional parameterization, the BULK scheme (Kim and Kang 2012), which

modify entrainment and detrainment formula from Tiedtke et al (1988). This GCM will be referred to as the model of control run (BULK). On the other hand, the GCM with the microphysics will be referred to as the 'MPS'. The MPS and BULK were integrated using the climatological SST for 4 and 2years, respectively.

Before examining the mean precipitation, the snapshot of 3-hourly precipitation of the observation and models (Fig. 6.2). The TRMM shows organized convection system with heavy precipitation and relatively small cloud with light precipitation in the tropics, and synoptic disturbance in the mid-latitude. The BULK produces too much light precipitation and simulates organized convection much less than the observation, since the convective scheme responses convective instability. The NOCONV produces strong precipitation over the tropics but it is not organized; It seems to be a "grid-scale storms". In the NOCONV, condensation occur when grid-mean RH exceeds 75% and it is converted quickly precipitation. It leads to production of strong and unorganized precipitation.In the MPS, light precipitation is reduced and heavy precipitation is increased. However, the model still produces organized convective system less than the observation. The organized convective system is simulated reasonably well when the convective scheme is added in the cloud microphysics. This shows that cloud microphysics reproduces organized convective system.

Annual-mean precipitation of the observation and models is show in Fig. 6.4. The Tropical Rainfall Measuring Mission (TRMM, Huffman et al. 2007) is used for observation. Although the GCM state variables with 50km horizontal resolution may be not suitable to calculate cloud microphysical process, the GCM simulations with microphysics are not unrealistic and its precipitation characteristics appears to be better than that of the original GCM with the BULK scheme. The original GCM produces precipitation much more than the observation over the tropics and the South Pacific Convergence Zone (SPCZ) in Fig. 6.4a is too much penetrated to the eastern Pacific in Fig. 6.4b. The GCM with microphysics reduces the excessive precipitation amount that is simulated too much in the GCM with the BULK scheme and its spatial pattern is similar to observation. However, the precipitation intensity is relatively weak compared to the observation, particularly in the heavy rain region of the western Pacific and ITCZ, and Northern Pacific. These weak precipitation amount results from two important problems, insufficient condensation and too fast terminal velocity, as discussed in the Section 5. Two important modifications, increase of condensation and decrease of terminal velocity as described in the Section 5, are incorporated in the cloud microphysics and the GCM simulations with the modified microphysics are integrated for two year (it is called as to the 'MMPS'. As seen in Fig. 6.6a, the model produces the precipitation amount much more than that of

the MPS over tropics and the mid-latitude and horizontal pattern appears to be improved compared to those of the GCM with original cloud microphysics. We examined the biases of temperature, specific humidity and cloud water contents (sum of cloud water and cloud ice) from the BULK and the MMPS averaged over tropics (30°S-30°N) and their vertical profiles are showed in Fig. 6.5. The ERA Interim data (Dee et al, 2011) and CloudSat cloud water content Radar data (Su et al. 2008) are used for the observation. The black and red lines, respectively, indicate the biases of the BULK and the MMPS. The MMPS produces specific humidity less in the lower troposphere and more in the PBL compared to those of the BULK. Because of weak sub-grid scale vertical mixing, moisture is often trapped beneath the top of the PBL and therefore moisture is too much in the PBL but insufficient in the lower troposphere. This bias of moisture is associated with the bias of cloud water content. The MMPS produces cloud water much more than the observation and that of the BULK, although the bias of cloud water is much less than that of the BULK over 850 hPa. This bias is related to weak vertical transport of moisture between the PBL and free atmosphere, as seen in Fig. 6.5b. In order to increase vertical mixing in the PBL, the diffusion type of shallow convective scheme was added in the MMPS (it is called as to the 'MMPSC'). In the MMPSC, the bias of specific humidity and cloud water content that are simulated in the MMPS is reduced below 850 hPa. The figure 6.6c shows the 2-

year annual mean precipitation of the MMPSC. The MMPSC produces realistic horizontal pattern of observed precipitation. The south Inter-Tropical Convergence Zone (ITCZ) that is extended to the eastern Pacific in Fig. 6.6a is shifted to the west in Fig 6.6c, which is closer to the observation. Fig. 6.6b shows the 2-year annual mean precipitation of the GCM with modified microphysics and the modified BULK convective scheme (as discussed in the Section 5) also improve the spatial pattern of mean precipitation compared to that of the MMPS but the precipitation intensity is relatively weak in the Northern Pacific and Indian Ocean. In summary, the GCM with cloud microphysics produce reasonable precipitation at coarse resolution of 50km and its spatial pattern and vertical profile of cloud water are much improved by adding vertical mixing.

6.2.2 Intra-seasonal variability

To examine the effect of cloud microphysics on eastward propagation of the MJO, the hovmoller diagram of daily mean precipitation from model and observation averaged over 10°S~10°N (Fig. 6.7). The TRMM data is used for observation. The observation shows clear eastward propagation of intense precipitation with 20~100 day periods and relatively weak westward propagation of light precipitation with short period

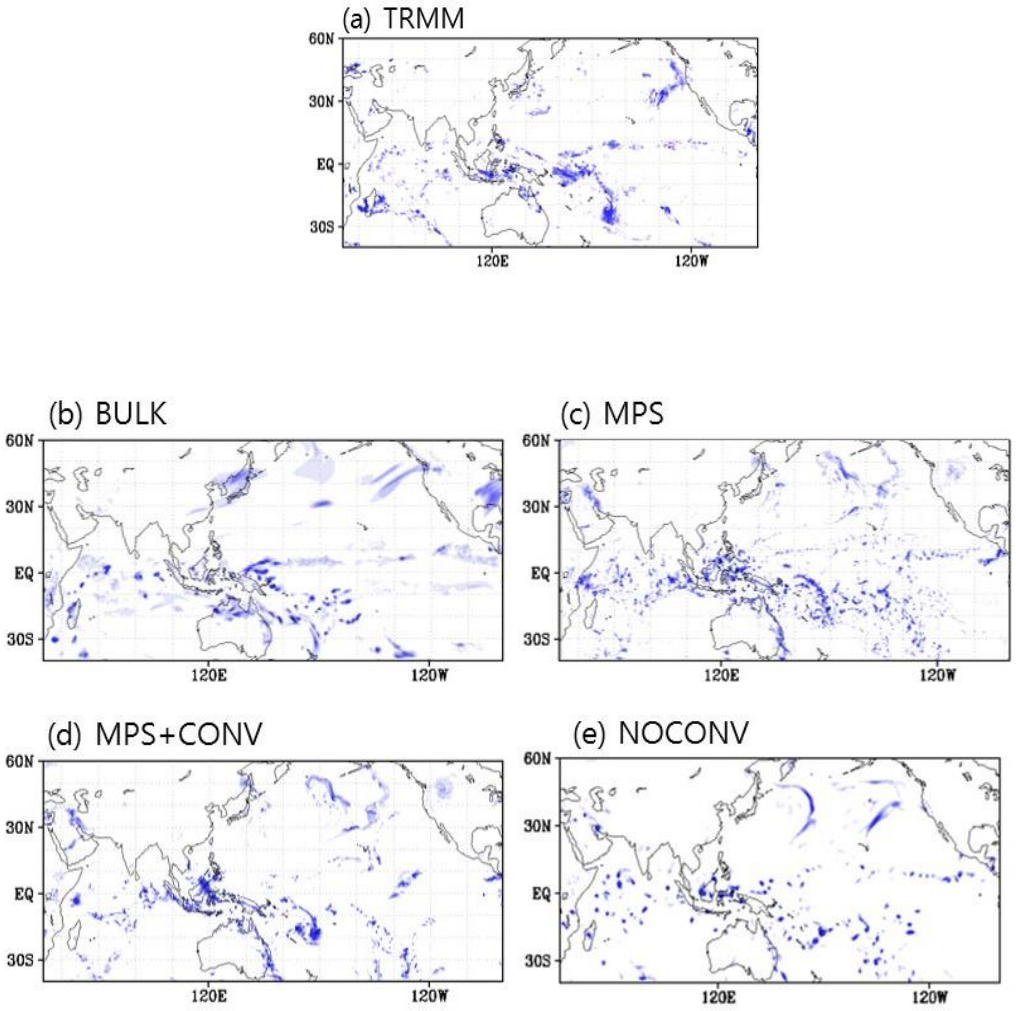

Figure 6.3 Snapshot of 3hourly precipitation. (a) TRMM, (b) a GCM with conventional convective parameterization (BULK scheme), (c) a GCM with cloud microphysics, (d) a GCM with cloud microphysics and the BULK scheme and (e) a GCM without convective parameterization

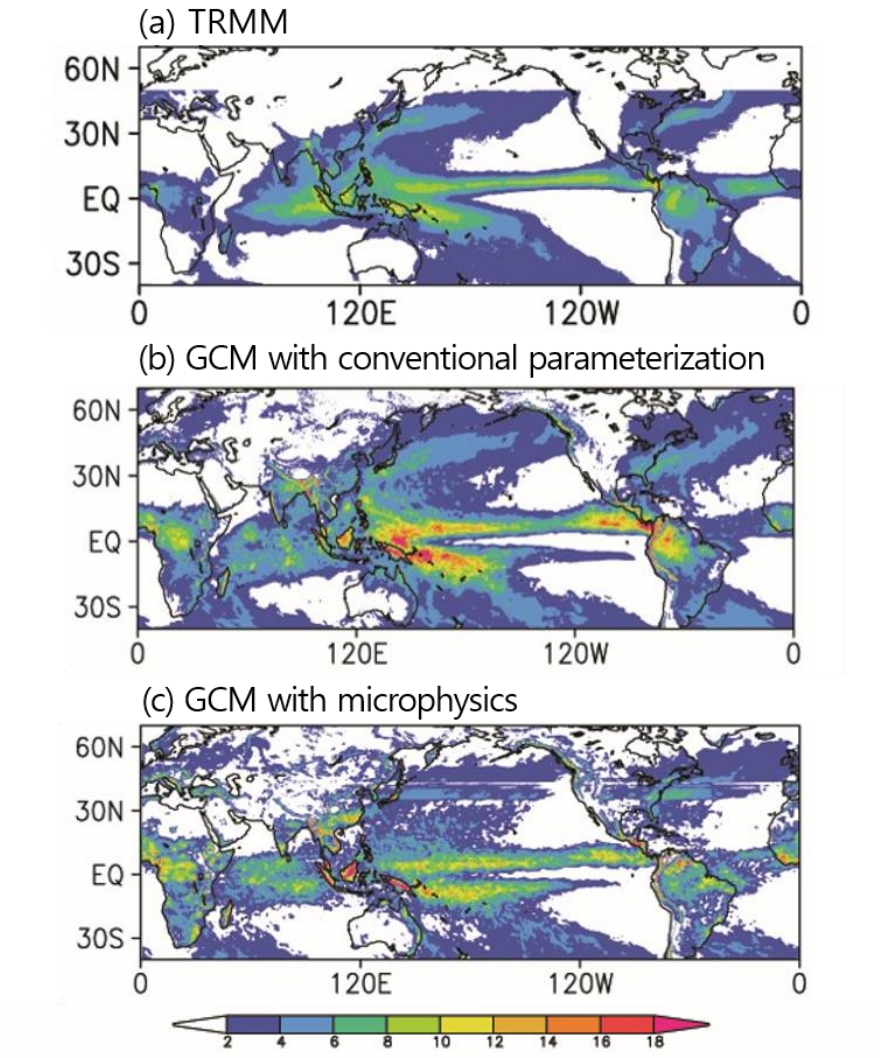

Fig. 6.4. Annual mean precipitation (mm day^{-1}) from (a) TRMM, (b) GCM with the parameterization (BULK scheme) and (c) GCM with the original cloud microphysics. The TRMM and the model data are from 1998 to 2002. The TRMM data was interpolated to model horizontal resolution.

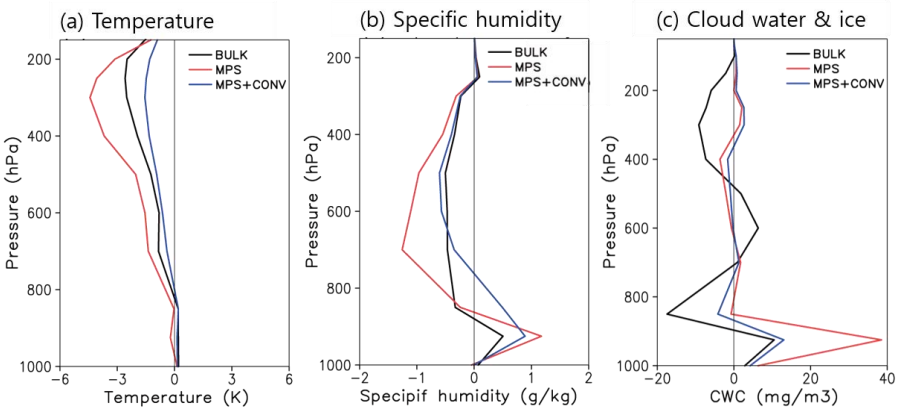

Fig. 6.5. Bias of 5-year annual-mean specific humidity, temperature and cloud water content (cloud water and cloud ice) from the models and observation averaged over tropics (20°S-20°N). The black represents GCM with parameterization (BULK scheme), the red is GCM with modified microphysics and the blue is GCM with modified microphysics and convection. The ERA Interim data is used for observed temperature and specific humidity and the Cloud Sat radar data (Su et al. 2008) is used for observed cloud water content. The ERA interim and the model data are from 1998 to 2002 and the CloudSat data is used for 2007.

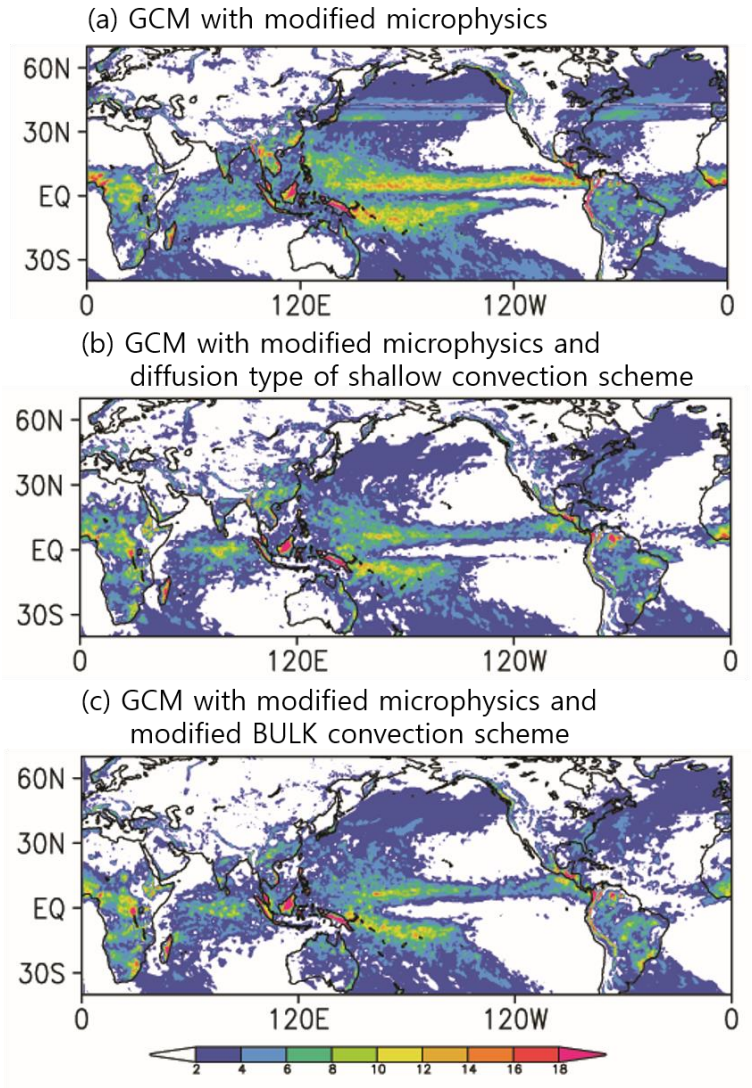

Fig. 6.6. Annual mean precipitation climatology (mm day^{-1}) from (a) GCM with the modified cloud microphysics, (b) GCM with the modified cloud microphysics and diffusion type of shallow convective scheme and (c) GCM with the modified cloud microphysics and the BULK convective scheme. The 2-year GCM simulations using climatology SST are used. The TRMM data was interpolated to model horizontal resolution.

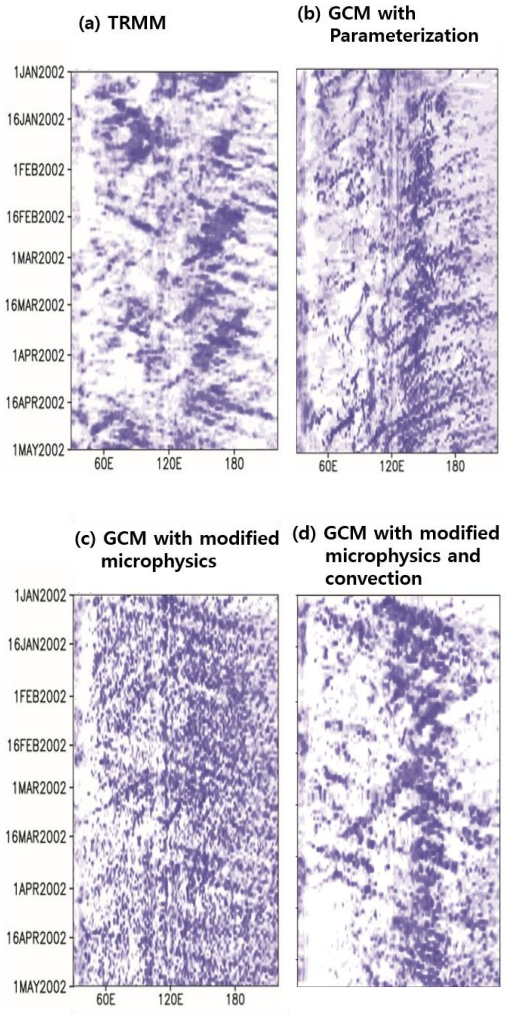

Fig. 6.7. Hovmuller diagram of daily mean precipitation from TRMM and model averaged over (30°S~30N°). (a) TRMM, (b) GCM with parameterization, (c) GCM with original cloud microphysics and (d) GCM with the modified cloud microphysics and shallow convection. The model data are from January 2002 to April 2002. The TRMM data was interpolated to model horizontal resolution (50km).

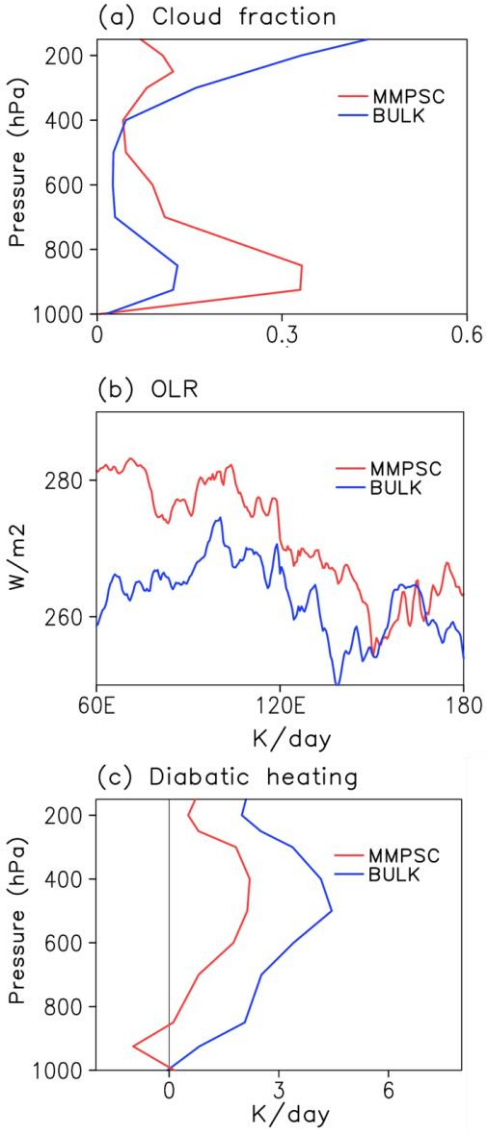

Fig. 6.8. (a) Cloud fraction, (b) out-going long wave radiation (OLR) and (c) total diabatic heating averaged over 60°E-180°E and 10°S-10°Nfrom the GCM with the modified microphysics and the convective scheme (MMPSC) and the GCM with a conventional parameterization (BULK). The OLR simulations averaged for 10°S-10°N are used in (b).

The BULK produces eastward propagation weaker and westward propagation stronger than those of the observation and most precipitation consists of light precipitation and heavy precipitation hardly occurs as seen Fig. 6.8. In contrast, the MPS produces very clear eastward propagation and weak westward propagation compared to those of the BULK. When the diffusion type of shallow convection is added, the model produces slower eastward propagation with organized supercloud cluster. There are two reasons for improvement of eastward propagation in precipitation.

In the coarse horizontal resolution GCM, thermals and moisture is often trapped beneath the top of the PBL due to relatively weak vertical wind and therefore the clouds mainly occur near the PBL top or lower troposphere by condensation process. These clouds move eastward along zonal mean wind, which contributes to clear eastward propagation. The other is due to decrease of high-cloud induced positive feedback (Lee et al. 2001). Figure 6.8 shows summer-mean vertical profile of cloud fraction, out-going longwave radiation (OLR) and totoal diabatic heating from the models averaged over the tropics (10°S-10°N). The BULK produce too much high-clouds by detraining moisture of convection (Fig. 6.8a) and these high clouds induces stronger large-scale diabatic heating (Fig. 6.8c) by increase of long-wave radiative cooling in the upper-level but warming in the lower-level (Fig. 6.8b). This repeatedly generates an additional convection

and persistent high-cloud, which appears to suppress the large-scale Kelvin wave propagating eastward. In the MMPSC, high-cloud is significantly reduced (Fig. 6.8a) and out-going longwave radiation is increased (Fig. 6.8b). Thus, total diabatic heating is reduced (Fig. 6.8c) and it appears to suppress the high cloud positive feedback. This contributes to enhancing eastward propagation of the precipitation.

6.2.3 Heavy precipitation

Figs. 6.9a, 6.9c, and 6.9e, show the distributions of the light precipitation amount (average of the cases of 3-hour precipitation less than 10 mm day-1), the heavy precipitation amount (average of the cases of 3-hour precipitation more than 60 mm day-1), and the mean of total precipitation during boreal summer, respectively, obtained from the TRMM observed data, and Figs 6.9b, 6.9d, and 6.9f are the simulated counterparts of the model. Here the model results are based on four year simulations with climatological varying SST condition. The TRMM data shows that the summer mean precipitation (Fig. 6.9c) is mainly contributed from the heavy precipitation (Fig. 6.9b) over the large precipitation regions of the Inter-Tropical Convergence Zone (ITCZ) and the western Pacific, where the light precipitation is less contributed compared to those of other tropical regions (Fig.

6.9a). On the other hand, the simulated precipitation shows that the light precipitation amount is almost uniformly distributed in the tropics and much more than the observed (Fig. 6.9b), but the heavy precipitation amount is much less than the observed counterpart, particularly in the western Pacific (Fig. 6.9d). As a result, the mean of total precipitation (Fig. 6.9f) has a big bias in the western Pacific. The observed rainband in the western Pacific is shifted to the south in the simulated precipitation pattern. The model produces precipitation much more than the observation in the south ITCZ, where the light precipitation is mainly contributed. It indicates that the too much light precipitation contributes to excessive mean precipitation in the south ITCZ. The climatological distribution of precipitation during boreal summer simulated by MMPSC is shown in Fig. 6.10c. The four year simulation is used to obtain the climatology. The spatial distributions of light and heavy precipitation are also shown in Figs. 6.10a and 6.10b, respectively. Comparison of those figures with those in Fig. 6.9 clearly indicates that the MMPSC reduces the light precipitation and enhances the heavy precipitation of the original GCM with parameterizations, and the patterns of the MMPSC become similar to the counterparts of the TRMM observation. We examined the precipitation spectrums simulated. The precipitation amount for each bin of precipitation intensity is obtained by using the 3-hourly precipitation data. The interval of each bin is 1 mm day^{-1} from 0 to 60 mm day^{-1} precipitation

intensity, which gradually increases up to 20 mm day^{-1} near 400 mm day^{-1} precipitation. The precipitation amount of each bin is divided by the total precipitation amount and the percentage of the precipitation of each bin is shown in Fig. 6.10. The figure shows that the frequency of very light precipitation less than 1 mm day^{-1} covers more than 45%, 37% and 28% of total precipitation for the BULK, MPS and MMPSC, respectively. The corresponding percentage of the TRMM data is 26%. Therefore, the bias of too much light precipitation in the BULK is improved by the MMPS and MMPSC. The Arakawa and Schubert convective scheme of the BULK is sensitively responded to the convective instability because the mass flux is determined by the Convective Available Potential Energy (CAPE). Therefore, the convective precipitation is generated too frequently. In the light precipitation range (2-20 mm day^{-1}), the MMPS and MMPSC produces less precipitation than that of the BULK, which is closer to the observation. The frequency of moderate precipitation (20-100 mm day^{-1}) from MPS and MMPSC is larger than that of the BULK. In the heavy precipitation more than 100 mm day^{-1} the MMPS produces much more precipitation than the BULK does. In fact, the BULK has a limitation in simulating the extreme precipitation more than 250 mm day^{-1}, whereas the MMPS is able to produce the extreme precipitation more than 250 mm day^{-1}. When the convective scheme is added, the frequency of MMPSC is much improved compared to those of the MMPS. The

distinct different physical processes between cloud microphysics and a conventional parameterization are cold cloud processes. The cloud microphysics includes accretion processes of cloud water by graupel and the melting process of graupel, which may be important processes for the heavy precipitation. These results show that the GCM with cloud microphysics improves the frequency of precipitation, particularly for heavy precipitation.

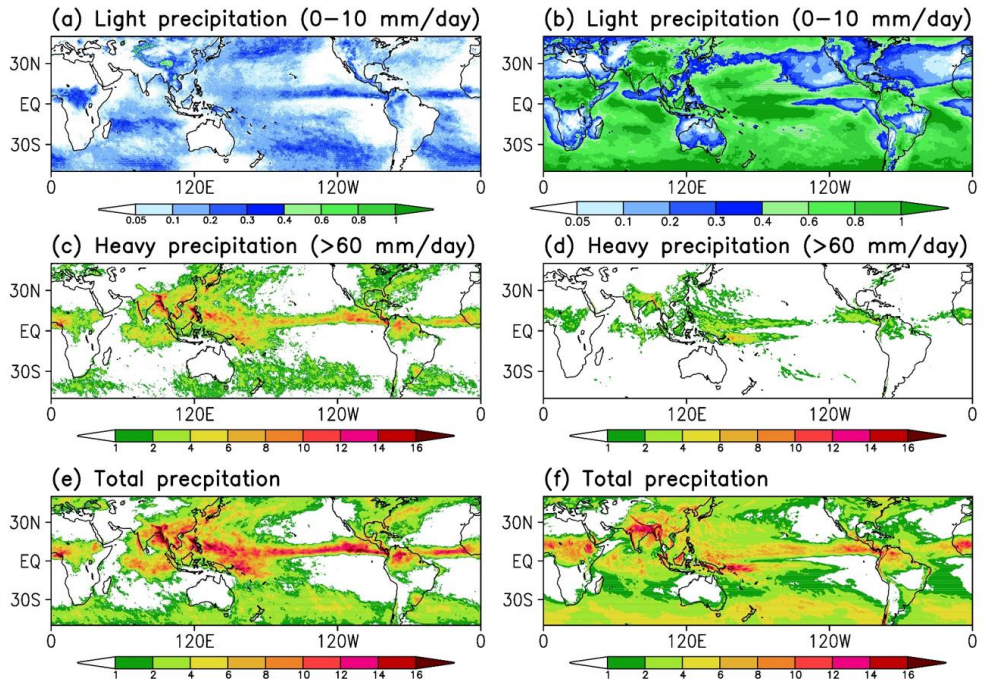

Fig. 6.9. Global distribution of light (upper), heavy (middle) and total mean precipitation (lower) from TRMM (a, c and e), GCM with the BULK scheme (b, d and f) for boreal summer. 3-hourly precipitation data is used.

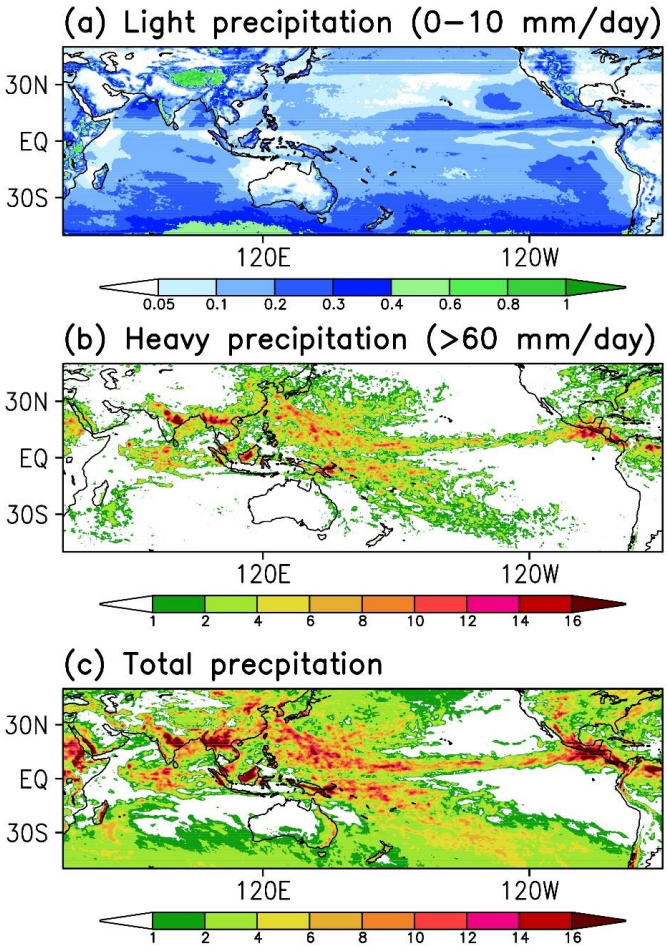

Fig. 6.10. Global distribution of (a) light, (b) heavy and (c) total mean precipitation from GCM with the modified microphysics and the diffusion type of shallow convective scheme for boreal summer. 3-hourly precipitation data is used.

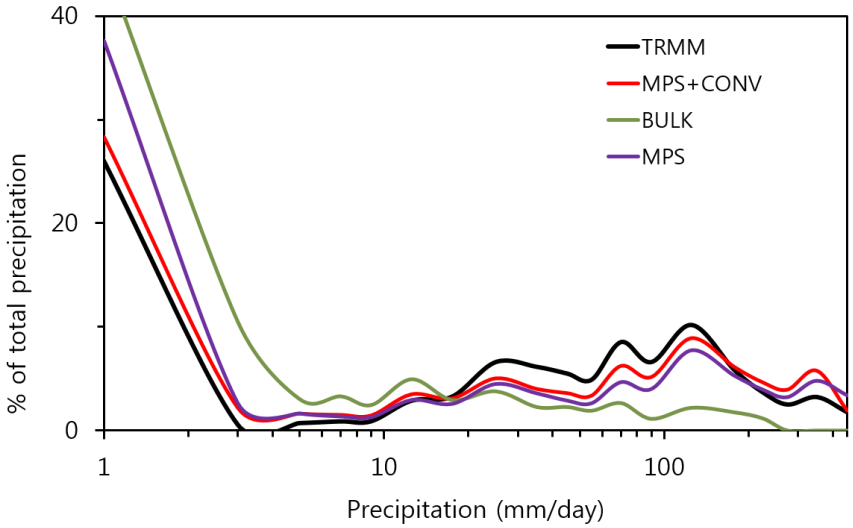

Fig. 6.10 The precipitation amount for each bin of precipitation intensity (mm day^{-1}) from the models and the TRMM over tropics (30°S~30N°). The 3-hourly TRMM and the model data are from 1998 to 2002. The interval of each bin is 1 mm day^{-1} below 60 mm day^{-1} precipitation intensity, which gradually increases up to 20 m m day^{-1} near 400 mm day^{-1} precipitation intensity.

CHAPTER 7

Summary and Future directions

A high resolution GCM with cloud microphysics was developed to improve simulated precipitation at 50km horizontal resolution. The GCMs with conventional parameterizations capture large-scale patterns of observed precipitation but produces many biases in precipitation characteristics: poor spatial pattern in the rain band, weak precipitation amount and intra-seasonal variability, too much light precipitation and too early diurnal cycle. These problems of the GCM simulations may be due to poor simulation of convective parameterization and relatively coarse horizontal resolutions. The convection occurs too frequently due to arbitrary setting of cloud top in ensemble cloud and sensitive mass flux closure sensitive to convective instability. The Tokioka constraints, relative humidity criteria and the mass flux closure based on the Richardson number were implemented in the convective parameterization and its impact on simulated precipitation were examined at coarse resolution. The

results show that when convective scheme is suppressed properly, the models improve intra-seasonal variability and precipitation frequency with scarifying climatology. It indicates that the one of large source for poor simulation of precipitation is convective parameterization. The effect of model horizontal resolution was also examined using the GCMs with different horizontal resolutions. The results show that although the features of 3-hourly precipitation in the higher horizontal resolution GCM appear to be more closer to the observation, increasing resolution generally does not improve precipitation characteristics except regional details of mean precipitation and heavy precipitation frequency (< 200 mm day^{-1}). The additional experiment using the GCM without convective scheme (only grid-scale precipitation) indicates that the large-scale condensation using the GCM state variables produces reasonable simulated precipitation without convection but has a limitation on the frequency of heavy precipitation more than 200 mm day^{-1} due to too simple parameterization. The budget study of rain processes using a cloud resolving model (CRM) shows that heavy precipitation is from not only accretion of cloud water by rain but also the melting of the graupel made from cloud water, whereas light precipitation is from accretion of cloud water by rain water. It is also important that warm and cold cloud processes coexist to represent the interaction between warm and cold processes. However, these processes are not explicitly

expressed in the conventional GCM. In this study, cloud microphysics of the cloud resolving model (CRM) was implemented in an order of 50km horizontal resolution GCM instead of a conventional parameterization. The GCM simulations with cloud microphysics are not unrealistic and the model produces the extreme precipitation more than 200 mm day^{-1}, although the cloud microphysics may not work properly due to coarse horizontal resolution of the GCM. However, the model underestimates the mean precipitation amount, particularly in the western Pacific and mid-latitude, indicating that the modification of cloud microphysics is required for better simulation of precipitation due to coarse resolution. The resolution dependency of cloud microphysics was examined using the CRM with different horizontal resolution. In the 50km horizontal resolution the CRM produces dry and warm biases compared to those of the 1km CRM. The rain water and graupel amount and associated accretion processes are less than those of 1km CRM. In order to reduce these resolution dependency, various modifications of cloud microphysics were suggested and their impacts were examined using the CRM with 50km grid size. The results show that the increase of condensation and decrease of terminal velocity of graupel and rain water are important for simulating reasonable rain water. The modified microphysics was implemented in the GCM and the GCM simulation shows that the model produces mean precipitation amount closer to

the observation but overestimates cloud water too much in the PBL due to relatively vertical mixing. In order to increase vertical transport of moisture between the PBL and free atmosphere, various type of convective schemes were implemented and the CRM simulations were compared to those of original CRM with the resolution of 50km. The results shows that an increase of vertical transport by convective scheme is essential for not only reducing moisture biases but also an increase of rain water. When the convective scheme was added in the GCM with microphysics, the model produces realistic cloud water in the PBL with improvement of climatology. The GCM with microphysics improves the eastward propagation of the daily precipitation over the equator compared to those of the GCM with conventional parameterization. However, the propagation speed is faster than observation and the speed is reduced by adding the convective scheme. This improvement of intra-seasonal variability is very interesting and the reasons will be analyzed in the further studies.

The GCM with cloud microphysics used in the present study is computationally less expensive than those of the global simulations used in the previous studies, the multi-scale modeling framework (MMF, Li et al, 2012) and global-scale CRM because this model calculates cloud microphysical processes not using the CRM embedded in each GCM grid but using the GCM state variables directly. On the other hand, the regular (longitude-latitude) grid

coordinate may be not computationally suitable for very high horizontal resolution more than 25km because it has numerical instability near the Poles. Recently, cubed-sphere finite volume dynamical core was developed and implemented in several models (e.g. NASA/GSFC, GFDL). Because this uses quasi-homogeneous grid size, total number of grid is smaller than that of original dynamical core and therefore more efficient computationally. The new dynamical core will be implemented in the GCM to reduce integration time.

It may be necessary to examine the effect of the cloud microphysics in a coupled GCM, since tropical precipitation is very much controlled by the ocean-atmosphere interaction. The atmospheric GCM used in this study may produce big biases of precipitation in the tropical oceans. For example, in the western Pacific, AGCMs tend to overestimate precipitation due to the fixed SST prescribed in the model. However, the precipitation tends to be reduced in a coupled GCM by coupled processes (Martin and Schumacher, 2012). Another interesting topic for a further study may be a sensitivity of the parameterization of cloud microphysics because the GCM simulations may be more dependent on the type of parameterization of cloud microphysics.

Reference

Arakawa, A., and W. H. Schubert. 1974. Interaction of a cumulus cloud ensemble with the large-scale environment, Part I. J. Atmos. sci 31: 674-701.

Basu, S., J.-F.Vinuesa, and A. Swift. 2008. Dynamic LES modeling of a diurnal cycle. Journal of Applied Meteorology and Climatology 47: 1156-1174.

Biasutti, M., A. Sobel, and Y. Kushnir. 2006. AGCM precipitation biases in the tropical Atlantic. Journal of Climate 19: 935-958.

Biasutti, M., S. E. Yuter, C. D. Burleyson, and A. H. Sobel. 2012. Very high resolution rainfall patterns measured by TRMM precipitation radar: seasonal and diurnal cycles. Climate dynamics 39: 239-258.

Bonan, G. B. 1996. Land surface model (LSM version 1.0) for ecological, hydrological, and atmospheric studies: Technical description and users guide. Technical note. National Center for Atmospheric Research, Boulder, CO (United States). Climate and Global Dynamics Div.

Brown, R. G., and C. Zhang. 1997. Variability of midtropospheric moisture and its effect on cloud-top height distribution during TOGA COARE*. Journal of the atmospheric sciences 54: 2760-2774.

Ciesielski, P. E., R. H. Johnson, P. T. Haertel, and J. Wang. 2003. Corrected TOGA COARE sounding humidity data: Impact on diagnosed properties of convection and climate over the warm pool. Journal of climate 16: 2370-2384.

Dai, A. 2006. Precipitation characteristics in eighteen coupled climate models. Journal of Climate 19: 4605-4630.

Dai, A., F. Giorgi, and K. E. Trenberth. 1999. Observed and model‐simulated diurnal cycles of precipitation over the contiguous United States. Journal of Geophysical Research: Atmospheres (1984‐2012) 104: 6377-6402.

DeMott, C. A., D. A. Randall, and M. Khairoutdinov. 2007. Convective precipitation variability as a tool for general circulation model analysis. Journal of Climate 20: 91-112.

Derbyshire, S., I. Beau, P. Bechtold, J. Y. Grandpeix, J. M. Piriou, J. L. Redelsperger, and P. Soares. 2004. Sensitivity of moist convection to environmental

humidity. Quarterly Journal of the Royal Meteorological Society 130: 3055-3079.

Evans, J. S., and C. A. Doswell III. 2001. Examination of derecho environments using proximity soundings. Weather and Forecasting 16: 329-342.

Grabowski, W., P. Bechtold, A. Cheng, R. Forbes, C. Halliwell, M. Khairoutdinov, S. Lang, T. Nasuno, J. Petch, and W. K. Tao. 2006. Daytime convective development over land: A model intercomparison based on LBA observations. Quarterly Journal of the Royal Meteorological Society 132: 317-344.

Holloway, C. E., and J. D. Neelin. 2009. Moisture vertical structure, column water vapor, and tropical deep convection. Journal of the atmospheric sciences 66: 1665-1683.

Holtslag, A., and B. Boville. 1993. Local versus nonlocal boundary-layer diffusion in a global climate model. Journal of Climate 6: 1825-1825.

Khairoutdinov, M. F., and D. A. Randall. 2001. A cloud resolving model as a cloud parameterization in the NCAR Community Climate System Model: Preliminary results. Geophysical Research Letters 28: 3617-3620.

Khairoutdinov, M. F., and D. A. Randall. 2003. Cloud resolving modeling of the ARM summer 1997 IOP: Model formulation, results, uncertainties, and sensitivities. Journal of the atmospheric sciences 60: 607-625.

Kim, D., and I.-S.Kang. 2012. A bulk mass flux convection scheme for climate model: description and moisture sensitivity. Climate dynamics 38: 411-429.

Klemp, J. B., and R. B. Wilhelmson. 1978. The simulation of three-dimensional convective storm dynamics. Journal of the Atmospheric Sciences 35: 1070-1096.

Kuang, Z., and C. S. Bretherton. 2006. A mass-flux scheme view of a high-resolution simulation of a transition from shallow to deep cumulus convection. Journal of the atmospheric sciences 63: 1895-1909.

Le Trent, H., and Z.-X. Li. 1991. Sensitivity of an atmospheric general circulation model to prescribed SST changes: feedback effects associated with the simulation of cloud optical properties. Climate Dynamics 5: 175-187.

Lee, M.-I., I.-S.Kang, and B. E. Mapes. 2003. Impacts of cumulus convection parameterization on aqua-planet AGCM simulations of tropical intraseasonal variability. Journal of the Meteorological Society of Japan. Ser. II 81: 963-992.

Lee, M. I., I. S. Kang, J. K. Kim, and B. E. Mapes. 2001. Influence of cloud -

radiation interaction on simulating tropical intraseasonal oscillation with an atmospheric general circulation model. Journal of Geophysical Research: Atmospheres (1984‐2012) 106: 14219-14233.

Lee, M. I., S. D. Schubert, M. J. Suarez, J. K. E. Schemm, H. L. Pan, J. Han, and S. H. Yoo. 2008. Role of convection triggers in the simulation of the diurnal cycle of precipitation over the United States Great Plains in a general circulation model. Journal of Geophysical Research: Atmospheres (1984–2012) 113.

Lin, J.-L. 2007. The double-ITCZ problem in IPCC AR4 coupled GCMs: Ocean-atmosphere feedback analysis. Journal of Climate 20: 4497-4525.

Lin, X., D. A. Randall, and L. D. Fowler. 2000. Diurnal variability of the hydrologic cycle and radiative fluxes: Comparisons between observations and a GCM. Journal of Climate 13: 4159-4179.

Lin, Y.-L., R. D. Farley, and H. D. Orville. 1983. Bulk parameterization of the snow field in a cloud model. Journal of Climate and Applied Meteorology 22: 1065-1092.

Lorant, V., N. A. McFarlane, and J. F. Scinocca. 2006. Variability of precipitation intensity: sensitivity to treatment of moist convection in an RCM and a GCM. Climate dynamics 26: 183-200.

Mapes, B., and R. A. Houze. 1992. An integrated view of the 1987 Australian monsoon and its mesoscale convective systems. I: Horizontal structure. Quarterly Journal of the Royal Meteorological Society 118: 927-963.

Mapes, B. E. 2000. Convective inhibition, subgrid-scale triggering energy, and stratiform instability in a toy tropical wave model. Journal of the atmospheric sciences 57: 1515-1535.

Martin, E. R., and C. Schumacher. 2012. The relationship between tropical warm pool precipitation, sea surface temperature, and large-scale vertical motion in IPCC AR4 models. Journal of the atmospheric sciences 69: 185-194.

Moeng, C.-H., and A. Arakawa. 2012. Representation of Boundary Layer Moisture Transport in Cloud-Resolving Models. Monthly Weather Review 140: 3682-3698.

Moorthi, S., and M. J. Suarez. 1992. Relaxed Arakawa-Schubert. A parameterization of moist convection for general circulation models. Monthly Weather Review 120: 978-1002.

N. Takayabu, Y., and M. Kimoto. 2008. Diurnal march of rainfall simulated in a T106 AGCM and dependence on cumulus schemes. Journal of the

Meteorological Society of Japan. Ser. II 86: 163-173.
NarendraBabu, A., J. Nee, and K. K. Kumar. 2010. Seasonal and diurnal variation of convective available potential energy (CAPE) using COSMIC/FORMOSAT‐3 observations over the tropics. Journal of Geophysical Research: Atmospheres (1984‐2012) 115.
Neggers, R., A. Siebesma, G. Lenderink, and A. Holtslag. 2004. An evaluation of mass flux closures for diurnal cycles of shallow cumulus. Monthly weather review 132: 2525-2538.
Neggers, R. A., M. Köhler, and A. C. Beljaars. 2009. A dual mass flux framework for boundary layer convection. Part I: Transport. Journal of the Atmospheric Sciences 66: 1465-1487.
Nesbitt, S. W., and E. J. Zipser. 2003. The diurnal cycle of rainfall and convective intensity according to three years of TRMM measurements. Journal of Climate 16: 1456-1475.
Pan, D. M., and D. D. Randall. 1998. A cumulus parameterization with a prognostic closure. Quarterly Journal of the Royal Meteorological Society 124: 949-981.
Petch, J. 2006. Sensitivity studies of developing convection in a cloud‐resolving model. Quarterly Journal of the Royal Meteorological Society 132: 345-358.
Petch, J., P. Blossey, and C. Bretherton. 2008. Differences in the lower troposphere in two‐and three‐dimensional cloud‐resolving model simulations of deep convection. Quarterly Journal of the Royal Meteorological Society 134: 1941-1946.
Ridout, J. A., and C. A. Reynolds. 1998. Western Pacific Warm Pool Region Sensitivity to Convective Triggering byBoundary Layer Thermals in the NOGAPS Atmospheric GCM. Journal of climate 11: 1553-1573.
Schumacher, C., and R. A. Houze Jr. 2003.Stratiform Rain in the Tropics as Seen by the TRMM Precipitation Radar*. Journal of Climate 16: 1739-1756.
Scinocca, J. F., and N. A. McFarlane. 2004. The variability of modeled tropical precipitation. Journal of the atmospheric sciences 61: 1993-2015.
Sobel, A. H., S. E. Yuter, C. S. Bretherton, and G. N. Kiladis. 2004. Large-Scale Meteorology and Deep Convection during TRMM KWAJEX*. Monthly weather review 132: 422-444.
Sui, C., K. Lau, Y. Takayabu, and D. Short. 1997. Diurnal variations in tropical oceanic cumulus convection during TOGA COARE. Journal of the atmospheric sciences 54: 639-655.

Sun, Y., S. Solomon, A. Dai, and R. W. Portmann. 2006. How often does it rain? Journal of Climate 19: 916-934.

Tao, W.-K., J. Simpson, D. Baker, S. Braun, M.-D.Chou, B. Ferrier, D. Johnson, A. Khain, S. Lang, and B. Lynn. 2003. Microphysics, radiation and surface processes in the Goddard Cumulus Ensemble (GCE) model. Meteorology and Atmospheric Physics 82: 97-137.

Tiedtke, M. 1984. The effect of penetrative cumulus convection on the large-scale flow in a general circulation model.BeiträgezurPhysik der Atmosphäre 57: 216-239.

Tokioka, T. 1988. The equatorial 30-60 day oscillation and the Arakawa-Schubert penetrative cumulus parameterization. J. Meteor. Soc. Japan 66: 883-901.

Wang, W., and M. E. Schlesinger. 1999. The dependence on convection parameterization of the tropical intraseasonal oscillation simulated by the UIUC 11-layer atmospheric GCM. Journal of Climate 12: 1423-1457.

Webster, P. J., and R. Lukas. 1992. TOGA COARE: The coupled ocean-atmosphere response experiment. Bulletin of the American Meteorological Society 73: 1377-1416.

Weisman, M. L. 1993. The genesis of severe, long-lived bow echoes. Journal of the atmospheric sciences 50.

Weisman, M. L., and R. Rotunno. 2004. "A theory for strong long-lived squall lines" revisited. Journal of the atmospheric sciences 61: 361-382.

Weisman, M. L., J. B. Klemp, and R. Rotunno. 1988. Structure and evolution of numerically simulated squall lines. Journal of the atmospheric sciences 45: 1990-2013.

Witek, M. L., J. Teixeira, and G. Matheou. 2011. An integrated TKE-based eddy diffusivity/mass flux boundary layer closure for the dry convective boundary layer. Journal of the atmospheric sciences 68: 1526-1540.

Woolnough, S., J. Slingo, and B. Hoskins. 2004. The diurnal cycle of convection and atmospheric tides in an aquaplanet GCM. Journal of the atmospheric sciences 61: 2559-2573.

Wu, C.-H., and H.-H.Hsu. 2009. Topographic Influence on the MJO in the Maritime Continent. Journal of Climate 22: 5433-5448.

Xavier, P. K. 2012. Intraseasonal convective moistening in CMIP3 Models. Journal of Climate 25: 2569.

Xie, S., and M. Zhang. 2000. Impact of the convection triggering function on single‐column model simulations. Journal of Geophysical Research:

Atmospheres (1984–2012) 105: 14983-14996.

Xie, S., M. Zhang, J. S. Boyle, R. T. Cederwall, G. L. Potter, and W. Lin. 2004. Impact of a revised convective triggering mechanism on Community Atmosphere Model, version 2, simulations: Results from short‐range weather forecasts. Journal of Geophysical Research: Atmospheres (1984–2012) 109.

Yang, Z., and R. W. Arritt. 2002. Tests of a perturbed physics ensemble approach for regional climate modeling. Journal of Climate 15: 2881-2896.

Zhang, G. J., and H. Wang. 2006. Toward mitigating the double ITCZ problem in NCAR CCSM3. Geophysical Research Letters 33.

Zhang, G. J., and X. Song. 2010. Convection parameterization, tropical Pacific double ITCZ, and upper-ocean biases in the NCAR CCSM3. Part II: Coupled feedback and the role of ocean heat transport. Journal of Climate 23: 800-812.

Zhu, H., H. Hendon, and C. Jakob. 2009. Convection in a parameterized and superparameterized model and its role in the representation of the MJO. Journal of the atmospheric sciences 66: 2796-2811.

국 문 초 록

기후모형의 강수모의 특성을 개선하기 위하여 구름물리과정이 도입된 50km 수평해상도를 가진 모형을 개발하였다. 기존의 기후모형은 관측과 비교하여 약한 강수를 많이 모의하고 호우를 적게 모의하는 한계점이 있다. 이는 적운대류강수가 너무 자주 일어나기 때문이며 이를 억제하기 위하여 방아쇠 함수와 구름질량속 추정방법이 도입되었다. 개선된 모형은 기존의 모형보다 약한 강수를 적게, 호우를 상대적으로 많이 모의하는것으로 나타났으나 여전히 200 mm day-1 이상의 극한 강수는 모의하지 못하는것으로 나타났다. 호우와 극한 강수를 보다 향상시키기 위하여 적운대류모수화과정을 제거한 결과 호우강수모의가 향상되었지만 여전히 극한 강수는 모의를 못하는 것으로 나타났다. 너무 단순화된 강수과정이 원인이 될수있다. 이를 명확히 이해하기 위하여 구름분해능모형의 모의 결과가 이용되었다. 강수과정에 대한 수지분석을 통해 약한강수는 구름물에서 강수로의 부착현상으로 대부분 만들어지는데 반해, 호우는 여기에 구름물의 우박으로의 부착현상으로 인해 증가된 우박의 해동으로 인해 발생되는것으로 나타났다. 즉, 호우를 생성하기 위해서는 우박을 만드는 차가운 구름 과정과 구름물을 만드는 따뜻한 구름과정이 동시에 필요한 것으로 나타났으며, 이러한 과정은 현재 기후모형에는 포함되어있지 않다.

구름분해능 모형의 구름 미세물리과정이 기후모형의 강수과정대신에

삽입되었다. 새로 개발된 모형의 강수패턴은 기존기후모형과 비슷하게 나타났으나, 강수량은 적게나타났으며 이는 구름미세물리과정의 해상도종속성 때문이다. 응결과정, 부착과정, 그리고 우박 하강속도공식을 개선하여 강수량은 관측과 비슷하게 증가시켰다. 또한, 구름물이 하층에서 과다모의되는 경향이 있으며, 이는 연직속도가 작아 하층의 수분이 상층으로 공급되지 못했기 때문이며, 확산타입의 층운 대류모수화과정을 도입하여 하층의 수분 모의를 개선하였다. 구름미세물리과정을 도입한 기후모형은 약한 강수를 적게, 호우를 많이 모의하고 있으며 그 빈도는관측과 매우 유사하게 나타났다. 더불어 이모형은 계산적으로 매우 효율적으로 설계되었다.

주요어 :
기후모델링, 적운 모수화, 구름미세물리과정, 호우

학생번호 : 2006-30794